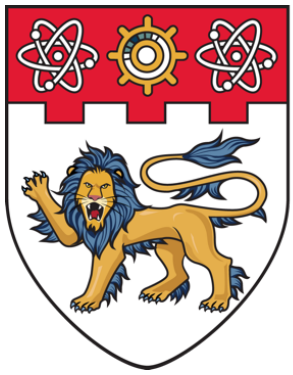

NANYANG TECHNOLOGICAL UNIVERSITY
SINGAPORE

# DEGRADATION STUDY OF EPOXY-BASED INSULATION MATERIALS AND DURABILITY IMPROVEMENT

**DENG YUHENG**

**SCHOOL OF MATERIALS SCIENCE AND ENGINEERING**

**2025**

# DEGRADATION STUDY OF EPOXY-BASED INSULATION MATERIALS AND DURABILITY IMPROVEMENT

**DENG YUHENG**

SCHOOL OF MATERIALS SCIENCE AND ENGINEERING

A thesis submitted to the Nanyang Technological University
in partial fulfilment of the requirement for the degree of
Doctor of Philosophy

**2025**

## Statement of Originality

I hereby certify that the work embodied in this thesis is the result of original research, is free of plagiarised materials, and has not been submitted for a higher degree to any other University or Institution.


10th Jan 2025

. . . . . .

Date

. . . . . .

DENG YUHENG

## Supervisor Declaration Statement

I have reviewed the content and presentation style of this thesis and declare it is free of plagiarism and of sufficient grammatical clarity to be examined. To the best of my knowledge, the research and writing are those of the candidate except as acknowledged in the Author Attribution Statement. I confirm that the investigations were conducted in accord with the ethics policies and integrity standards of Nanyang Technological University and that the research data are presented honestly and without prejudice.

10th Jan 2025

. . . . . .

Date

. . . . . .

Prof Chen Zhong

# Authorship Attribution Statement

This thesis contains material from 4 paper(s) published in the following peer-reviewed journal(s) / from papers accepted at conferences in which I am listed as an author.

Chapter 4 is published as Y. Deng, Q. Wang, J. Ma, J. T. Oh, Z. Chen. The combined impact of voids and thermal aging on the mechanical reliability of epoxy resin evaluated by statistical analysis. *Polymer Degradation and Stability*. 2023. vol. 215, 110455. DOI: 10.1016/j.polymdegradstab.2023.110455.

and Y. Deng, Q. Wang, J. Ma, Y. Yang, M. Yap, W. K. Chern, J. T. Oh, Z. Chen. The impact of thermal aging on mechanical and electrical properties of epoxy/amine resin. *2023 International Symposium on Electrical Insulating Materials (ISEIM 2023)*. Shimane, Japan, 2023. DOI: 10.23919/ISEIM60444.2023.10329098.

The contributions of the co-authors are as follows:

- Prof Chen and Prof Oh provided the initial project direction and acquired funding.
- I prepared the manuscript drafts. The manuscript was revised by Prof Chen and Dr Wang.
- I co-designed the study with Prof Chen and performed all the laboratory work at the School of Materials Science and Engineering and SP Group - NTU joint lab at the School of Electrical and Electronic Engineering. I also analyzed the data.
- All microscopy, including sample preparation, was conducted by me in the Facility for Analysis, Characterization, Testing and Simulation.
- Dr. Wang contributed to the simulation study.
- Dr Ma assisted in the sample preparation.
- Dr. Yang and Mr. Yap assisted in electrical testing.
- Mr. Chern assisted in resource acquirement for electrical testing.

Chapter 5 is published as Y. Deng, Q. Wang, Z. Pan, Z. Lv, W. K. Chern, J. T. Oh, Z. Chen. Unravelling the role of filler surface wettability in long-term mechanical and dielectric properties of epoxy resin composites under hygrothermal aging. *Journal of Colloid and Interface Science*. 2025. vol. 682, pp. 50-59. DOI: 10.1016/j.jcis.2024.11.186.

The contributions of the co-authors are as follows:

- Prof Chen and Prof Oh provided the initial project direction and acquired funding.
- I prepared the manuscript drafts. The manuscript was revised by Prof Chen, Dr Wang and Prof Lv.
- I co-designed the study with Prof Chen and performed all the laboratory work at the School of Materials Science and Engineering and SP Group - NTU joint lab at the School of Electrical and Electronic Engineering. I also analyzed the data.
- All microscopy, including sample preparation, was conducted by me in the Facility for Analysis, Characterization, Testing and Simulation.
- Dr. Wang contributed to the simulation study.
- Mr. Pan assisted in electrical testing.
- Mr. Chern assisted in resource acquirement for electrical testing.

Chapter 6 is published as Y. Deng, Y. W. Wong, L. K. Y. Teh, Q. Wang, W. Sun, W. K. Chern, J. T. Oh, Z. Chen. Optimizing dielectric, mechanical, and thermal properties of epoxy resin through molecular design for multifunctional performance. *Materials Horizons*. 2025. 12, 1323-1333. DOI: 10.1039/d4mh01414f.

The contributions of the co-authors are as follows:

- Prof Chen and Prof Oh provided the initial project direction and acquired funding.
- I prepared the manuscript drafts. The manuscript was revised by Prof Chen and Dr Wang.
- I co-designed the study with Prof Chen and Dr. Sun, and performed all the laboratory work at the School of Materials Science and Engineering and SP Group

- NTU joint lab at the School of Electrical and Electronic Engineering with assistance from Ms. Wong and Ms. Teh. I also analyzed the data.

- All microscopy, including sample preparation, was conducted by me in the Facility for Analysis, Characterization, Testing and Simulation.
- Mr. Chern assisted in resource acquirement for electrical testing.

10th Jan 2025

Deng Yuheng

. . . . . .

Date

. . . . . .

DENG YUHENG

## Abstract

Epoxy-based insulation materials are widely employed in electrical power systems due to their good dielectric and mechanical properties, as well as their cost-effectiveness. However, their long-term performance is often compromised by degradation from thermal, electrical, and mechanical stresses, particularly in high-density power applications. This thesis investigates the degradation mechanisms and presents strategies to enhance the durability of epoxy-based insulation materials, aiming to improve their reliability under demanding operational conditions. Specifically, the study addresses three interconnected topics: 1) assessing the role of voids in pure epoxy resin degradation, 2) examining the impact of interfacial voids on the reliability of epoxy composites, and 3) exploring molecular modification as a strategy for durability enhancement.

First, the effects of voids and thermal aging on the mechanical reliability of epoxy resin are analyzed using Weibull statistical methods, revealing that voids significantly increase the scattering in strength, thereby threatening long-term reliability. Thermal aging introduces heterogeneous degradation from surface to core, with oxidation and molecular chain scission contributing to diminished mechanical stability. This study underscores that controlling void content during manufacturing is essential for maintaining structural integrity over extended service periods.

Building on this foundation, the second part of the study investigates epoxy composites, which offer potential performance improvements but are limited by interfacial defects that can weaken the long-term reliability. To understand the impact of interface conditions on long-term properties, hydrophilic and hydrophobic fillers were incorporated into epoxy resin and subjected to hygrothermal aging. Results indicate that hydrophilic fillers enhance interfacial bonding, improving mechanical robustness and dielectric properties, while hydrophobic fillers, though moisture-repellent, show reduced long-term reliability due to weaker matrix adhesion. These findings emphasize the need to optimize filler-matrix interactions for balanced electrical and mechanical performance.

The third topic investigates molecular modification as an innovative approach to improve durability without relying on fillers, which could potentially overcome the limitations by filler addition such as interfacial defects and dispersion challenges. By incorporating specific functional groups into the epoxy structure, this study achieves significant enhancements in mechanical, dielectric, and thermal performance. These molecular modifications increase cross-linking density and introduce deep charge traps, thereby strengthening both dielectric reliability and mechanical resilience. This approach provides a molecular-level alternative for fortifying epoxy resins, expanding the spectrum of applicable durability improvement strategies.

In summary, this thesis advances the understanding of defect-induced degradation in epoxy-based insulation materials and demonstrates the potential of molecular modifications for enhancing durability. By integrating theoretical insights with practical solutions, this work contributes to the development of robust, high-performance insulation materials, supporting more reliable and cost-effective power systems capable of meeting future operational demands.

## Lay Summary

Epoxy-based insulation materials are essential in electrical systems, where they protect equipment from electrical faults and help prevent system failures. These materials are widely used due to their good insulation properties, mechanical strength, and cost-effectiveness. However, over time, these insulation materials degrade when exposed to high temperatures, electrical stress, and environmental moisture, which can reduce their effectiveness and reliability. This research investigates the causes of degradation in epoxy-based insulation materials and explores strategies to enhance their durability, supporting the reliability of power systems in demanding conditions.

One major factor impacting the lifespan of insulation materials is the presence of voids, which are unavoidable during manufacturing. These voids act as weak points both mechanically and electrically leading to early damage of the equipment. To address this, the study examines how controlling void content in epoxy resin can help reduce material failure.

Additionally, this research explores epoxy resin composites, which can improve insulation performance but are often limited by issues at the connection between filler particles and the resin. To understand these effects, fillers with water-attracting (hydrophilic) and water-repellent (hydrophobic) surfaces were added to the resin and subjected to long-term heat and humid aging. Hydrophilic fillers created stronger bonds with the resin, showing greater stability over time, while hydrophobic fillers, despite resisting moisture on its own, displayed weaker long-term reliability in composite due to poorer bonding. These findings emphasize the importance of optimizing filler-resin compatibility for durable composite performance.

The study also introduces a novel approach to enhance insulation durability through molecular modification, which strengthens the epoxy structure without relying on addition of fillers. By introducing specific functional groups into the molecular framework of epoxy

resin, the material gains improved resistance to thermal, electrical, and mechanical stresses. This approach avoids common issues such as poor dispersion or interfacial defects associated with fillers, while still achieving superior durability in challenging applications.

In summary, this study provides new insights into how epoxy-based insulation materials degrade and presents innovative solutions to extend their service life. These findings have the potential to make electrical power systems more reliable and efficient, reducing maintenance costs and enhancing safety, while supporting infrastructure advancements needed to meet future energy demands.

## Acknowledgements

This dissertation would not have been possible without funding from the Funding Agency Ministry of Education of Singapore, and SP Group, the Energy Market Authority of Singapore, under its Energy Programme (EMA-EP010-SNJL-002).

I am deeply grateful to my project supervisor Professor Chen Zhong for his continual guidance and support. His immense knowledge and patient guidance helped me navigate many challenges. My sincere thank also goes to my co-supervisor Assoc Prof. Oh Joo Tien for his generous support and advice.

My appreciation extends to the staff of the SP-NTU Joint Lab: Dr. Wang Qi, Dr. Ma Jielin, Dr. Sun Weifeng, Dr. Yang Yan, Mr. Wen Kwang Chern, Mr. Malvern Yap, Mr. Pan Zhiyu and Mr. Kavirajan Kalaiselvam for their daily assistance and encouragement.

I would also like to express my gratitude to my seniors, Dr. Sun Ye and Dr. Hernandez Muralles Mario Arturo, for their support and the warm welcome when I joined the group, and to my labmates Wei Lan, Li Jun, Liu Shuming, Wang Pengyu, Yin Xiaoli and Feng Min for their assistance and friendship.

I am particularly grateful to the staff of MSE and FACTS for providing essential facilities and training me to operate instruments and interpret results accurately.

I am fortunate to have received the guidance of Professor Lv Zepeng from Xi’an Jiaotong University, who generously shared his expertise in dielectric studies with me.

Finally, I am deeply grateful to my family for their unwavering love and support. Their constant encouragement has been my strength through every challenge.

## Table of Contents

# Table Captions

## Figure Captions

## Abbreviations

| | |
|---|---|
| AC | Allyl chloroacetate |
| ACF | 2-Amino-5-chloro-2’-fluorobenzophenone |
| ATR | Attenuated Total Reflectance |
| BEI | Backscatter Electron Images |
| BSEs | Backscattered Electrons |
| DMA | Dynamic Mechanical Analysis |
| EDX | Energy Dispersive X-ray Spectroscopy |
| EP | Epoxy resin |
| *f* | Functionality |
| FESEM | Field Emission Scanning Electron Microscope |
| FTIR | Fourier Transform Infrared Spectroscopy |
| GIS | Gas-insulated high-voltage switchgear |
| HB | Hydrophobic |
| HP | Hydrophilic |
| IEC | International Electrotechnical Commission |
| MA | Maleic anhydride |
| OM | Optical Microscopy |
| PD | Partial Discharge |
| RCP | Random Copolymer |
| SEs | Secondary Electrons |
| SEM | Scanning Electron Microscopy |
| $T_g$ | Glass Transition Temperature |
| UV-Vis | Ultraviolet–Visible Spectroscopy |
| XLPE | Crosslinked polyethylene |

# Chapter 1

# Introduction

*This chapter provides the overall research plan for the reliability study of polymeric insulating materials and the improvement of their durability. The background of polymeric insulations is briefly introduced, followed by the hypothesis and objectives of this research. Finally, the expected outcomes and challenges are discussed.*

## 1.1 Hypothesis/Problem Statement

Epoxy-based insulation materials are widely used in electrical power systems for their strong dielectric ability, mechanical durability, and cost-effectiveness. However, in harsh conditions, these materials degrade over time due to thermal, electrical, and environmental stresses. This degradation weakens their insulation performance, leading to potential equipment failures and safety concerns. Thus, the aim of this study is to enhance system reliability by understanding the degradation mechanisms of insulation materials and developing strategies to improve material durability, ultimately contributing to more robust performance in high-demand electrical applications.

Defects are easily introduced in epoxy-based insulation materials. In pure epoxy resin, voids formed during manufacturing can act as stress concentration sites, accelerating material failure. In composite resins, fillers are added to enhance properties, but interfacial defects between fillers and the epoxy matrix can compromise stability. A more accurate evaluation of these effects on the long-term reliability of material is needed to deepen the understanding of degradation mechanisms. Additionally, strategies that enhance material performance while avoiding interfacial issues in composites must be developed.

Thus, this thesis tests the hypothesis that:

1. *A more precise evaluation of void and thermal aging impacts on long-term reliability of epoxy resin can be achieved by applying statistical analysis to a large number of specimens with varying void content and subjecting them to accelerated thermal aging.*

2. *The accuracy of understanding interfacial defect impacts on long-term performance of epoxy resin composites can be improved by analyzing how filler with different surface wettability affects the mechanical and dielectric properties under hygrothermal aging.*

3. *Enhancing epoxy resin performance through molecular modification can be achieved by introducing polar, bulky groups and crosslinking sites to increase breakdown strength, reduce dielectric loss, and improve thermal and mechanical stability.*

These hypotheses address both a critical understanding of degradation mechanism and improvement strategies, providing a foundation for enhancing the performance and reliability of epoxy insulation materials in challenging electrical applications.

## 1.2 Objectives and Scope

The present research focuses on improving the reliability and durability of epoxy-based insulation materials for electrical applications by investigating their degradation mechanisms and exploring performance enhancement strategies. This study specifically examines the impact of manufacturing-induced voids in epoxy resin, interfacial integrity in composites, and molecular modifications aiming at improving the mechanical, dielectric, and thermal performance and long-term stability. These insights aim to address the increasing demands for robust insulation in high-power-density environments.

The specific objectives of this research are:

- Evaluate the aging mechanism and impact of voids on reliability of epoxy resin through accelerated thermal aging tests and statistical analysis.
- Investigate effects of the filler-matric interface in epoxy composites on long-term stability of material by incorporating fillers with varying surface wettability.
- Develop molecular modification techniques to improve dielectric durability, mechanical properties, and thermal resistance.

## 1.3 Dissertation Overview

This thesis investigates the degradation mechanisms and develops strategies to enhance the durability and reliability of epoxy-based insulation materials for electrical applications.

*Chapter 1* outlines the research focus, presenting the rationale, objectives, and scope of the research.

*Chapter 2* reviews literature on degradation mechanisms in epoxy-based insulation materials, concentrating on the impacts of voids and filler-matrix interactions. This chapter also examines various strategies, especially on molecular modification, in improving the performance and longevity of epoxy resins in electrical applications.

*Chapter 3* describes the experimental methods used in this study, including sample preparation, statistical analysis, and various testing and characterization techniques.

*Chapter 4* quantitatively evaluates the impacts of thermal aging and voids on the long-term performance of pure epoxy resin, demonstrating how void content and thermal aging influence the mechanical reliability. This chapter also reveals the heterogeneous degradation mechanism driven by oxygen diffusion.

*Chapter 5* investigates the influence of filler surface properties on interfacial bonding in epoxy resin composites, focusing on how different surface wettability affects material stability under hygrothermal conditions.

*Chapter 6* explores molecular modifications designed to enhance epoxy resin properties, assessing how targeted structural changes applied through a simple procedure with ultra-low modifier dosage can simultaneously improve dielectric, mechanical, and thermal performance.

*Chapter 7* concludes the thesis, summarizing key findings and proposing future research directions to further enhance the durability and reliability of epoxy insulation materials for electrical applications.

# Chapter 2

# Literature Review

*This chapter presents a review of the current research on epoxy-based insulation materials, focusing on their degradation mechanisms and strategies for durability enhancement. It begins with an overview of the properties of epoxy resins and their significance in electrical applications, followed by a detailed discussion of their degradation mechanisms. The chapter then explores the integration of fillers as a strategy for improving various properties while addressing the challenges posed by interfacial defects, as well as the role of the interface between filler and polymer. Furthermore, it highlights molecular modification as a promising approach for enhancing the durability of epoxy resins. Finally, the implications of these findings for the reliability and durability of insulating materials are discussed, outlining research gaps that require further investigation.*

## 2.1 Overview

### 2.1.1 Polymeric Insulating Materials

Polymeric materials play an essential role in the electrical power system as the insulating materials due to their good dielectric and mechanical properties. Epoxy resins are widely used as insulators or insulator housings in gas-insulated switchgear (GIS) for high-voltage systems [1]. The insulation performance can be reinforced by introducing fillers to obtain better thermal, dielectric and mechanical performances [2]. Crosslinked polyethylene (XLPE) [3], [4], [5], and polypropylene[6] are usually used as the cables in the power transmission system due to their good thermal and mechanical qualities. Recently a random copolymer (RCP) and its composites, which show extraordinary electrical property, are also applied as cable materials [6]. A dielectric polymeric film such as polypropylene with metal deposited is used as the capacitor in electrical transmission systems [7], [8]. Polyester films and laminates with thermosetting adhesives are employed in motors and transformers [9].

As the insulation material, its mechanical strength, dielectric strength and aging resistance are important and need to be carefully evaluated to provide useful information for the power industry [10], [11].

### 2.1.2 Application of Epoxy Resins in Electrical System

Epoxy resin, also called polyepoxides, are a family of thermosetting polymers which contain epoxide groups. It has a wide range of applications and especially plays an important role as an engineering material due to its excellent mechanical, electrically insulating and thermal properties in combination with its low price [12].

Epoxy resins have a wide range of applications in daily life. They are widely used as protective coatings for various industries [13]. They are also employed as the matrix material in the aerospace industry with reinforcement by fibres [14]. Besides this, They

can improve efficiency and reduce the cost of many manufacturing processes by replacing traditional materials like wood and metal as machine tooling beds [15].

Moreover, due to their good electrical and mechanical properties, they also play an essential role in the electrical power system as part of the insulators, generators, motors, transformers, winding condenser bushings and wire coatings [16]. Cooperated with mica papers and metals, epoxy resins are widely employed in operation equipment manufacturers to make the stator coil ground wall and random-wound stator insulation system [9], [17]. They can be coated on paper and used as the bushing of the winding condenser [16].

### 2.1.3 Chemistry of Epoxy Resin

Epoxy resins are thermosets with high molecular weight, in which 2 or more oxirane rings or epoxy groups can be observed [18], [19]. They can be produced by polymerizing epoxides with low molecular weight using suitable crosslinking agents [20]. These 2 components are introduced in detail in the following sections.

#### 2.1.3.1 Uncured Epoxy Resins

Epoxides represent a series of chemicals consisting of a 3-membered ring including an oxygen atom bonded to 2 carbon atoms [21]. A typical example is illustrated in **Figure 2.1**.

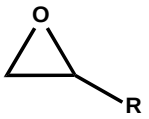


**Figure 2.1** Molecular structure of an epoxide [22].

Based on the functionality, they can be classified into 2 types. Difunctional epoxides (functionality $f = 2$) are commonly employed in a traditional application, such as the matrix of composites. Multifunctional epoxy resins ($f > 2$) display higher $T_g$ than difunctional

epoxides due to their denser crosslinking networks, which can be used under severe conditions [20].

### 2.1.3.2 Curing Agent

Curing agents can solidify the epoxy resin solution by crosslinking them to form a thermosetting network. There are various combinations of epoxy resin and coupling agents, which give a diversity of performances of epoxy resin and reach different requirements in various applications [23], [24], [25], [26]. Phenol, anhydrides, polyamides and amines including aliphatics, cycloaliphatics, and aromatics are commercially used as curing agents for the manufacture of epoxy resin [13], [27]. Normally, more than 2 reactive functional groups ($f > 2$) are required in the curing agents to enable the crosslinking effects.

### 2.1.3.3 Curing Reaction

With curing agents, fluid epoxy resins develop the network structure and become solid epoxy resin, which is the so-called curing process of epoxy resin. Epoxides can react with different types of curing agents to gain molecular weight as illustrated in **Figure 2.2**.

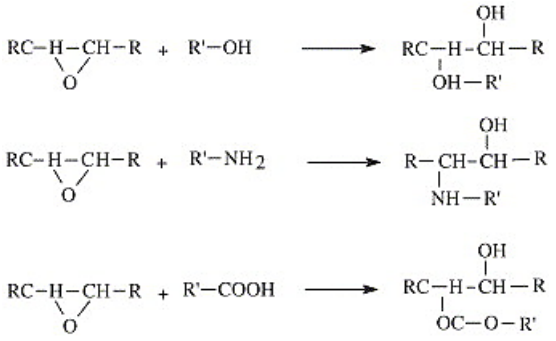


**Figure 2.2** Reactions between epoxides and curing agents with different functional groups. Reproduced with permission from [28].

The whole curing process has 2 specific stages: gelation and vitrification. During gelation, the molecules grow larger and larger, forming the rubber-like system. With the

development of the network structure, the molecular weight of the polymer increases further due to continued crosslinking and the material undergoes a transition from a rubber to a glass. This is the vitrification stage, in which the $T_g$ of the polymer increases above the reaction temperature, resulting in the hindrance of the movement of molecules. With a higher temperature, the molecules become movable again and a higher conversion can be reached, which is denoted as post-curing of epoxy resin [29].

### 2.1.4 Degradation in Epoxy Resin

The electrical insulation materials will degrade under electrical, thermal, mechanical, and environmental stresses, leading to the final breakdown of the insulation system. The degradation, or aging process is complicated and usually caused by multiple stresses [30]. Thus, it is important to investigate the mechanisms of aging and evaluate the degradation of the system carefully to provide useful information during life prediction.

#### 2.1.4.1 Thermal Aging

When used in electronic devices and electrical equipment, polymeric materials are required to withstand high voltage and high heat flux [31], [32]. Excessive heat is easily accumulated during service and causes increasingly severe thermal aging, limiting the service life of the apparatus [33], [34]. Under thermal stress, chemical and physical changes occur in the polymers, causing a change in molecular structure, resulting in a change in final performances [35], [36]. Different stages of the aging process of thermosets were revealed: the mechanical property is enhanced at the beginning due to post-crosslinking and then decreased because of the chain scission, accompanied by oxidation of active groups [37], [38], [39]. Interestingly, different aging behaviors were observed in the sample core and skin [36], [40]: Oxidation and molecular chain rearrangement occurred in the skin, accompanied by a reduction in the free volume fraction, while these changes were not detected in the core. However, the increase in flexural modulus and the reduction in break strain indicate an enhanced cross-linkage of the bulk. This finding is in contradiction with the previous results, and further investigation is required for greater clarity. Furthermore,

the brittleness and degree of scatter in the strengths increased over the aging time [36], [41], indicating increased mechanical scattering, emphasizing the need for further analysis to accurately determine the impact of such fluctuations on reliability. Given this background, it is crucial to evaluate the thermal aging behavior of epoxy resin, especially its effect on mechanical reliability, and reveal the principles behind it. Such a study could provide useful information for material design as well as lifetime prediction for practical usage.

#### 2.1.4.2 Electrical Aging and Breakdown

Electrical reliability is also very important for insulating materials. When an electrical breakdown occurs, it is irreversible and causes a breakdown channel in the polymeric materials [42], leading to the final breakdown of the whole system. Thus, it is necessary to identify the mechanism of electrical breakdown and improve its dielectric reliability.

**1) Electrical tree**

Electrical treeing is the main reason for the electrical breakdown of polymeric insulations due to the degradation of materials under high electric fields [43], [44]. Numerous literatures have discussed the electrical treeing in polymeric insulations. The electrical tree is normally initiated by contaminations or defects, e.g., voids in materials [45]. Electrical stress is concentrated in these areas and microtubes occur. With the existence of partial discharge, the microchannels propagate and form branch structures that cause the final breakdown of the whole material [46]. Ibrahim et al. suggested that there are 5 stages of electrical treeing: initiation, fast-forward tree growth, fine tree growth, darkening fine tree channels, and reverse tree growth [47].

Chen et al. illustrated 2 typical shapes of electrical tree growths in XLPE with a tip to counter electrode distance at 1 mm, as shown in **Figure 2.3** and **Figure 2.4** [48]. The shape of the electrical tree is severely dependent on the voltage applied. Bush trees are likely to occur when the electrical field is high.

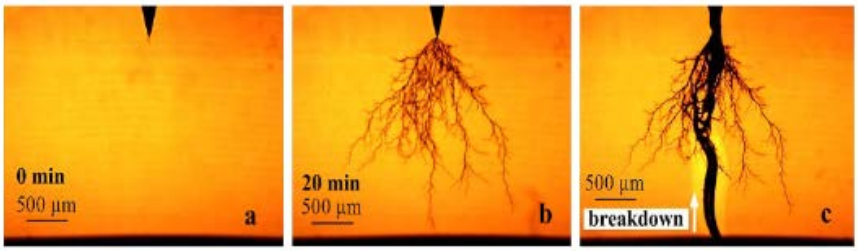


**Figure 2.3** Branch trees grown in XLPE at 11 kV [48]. *No permission is required for thesis purposes.*

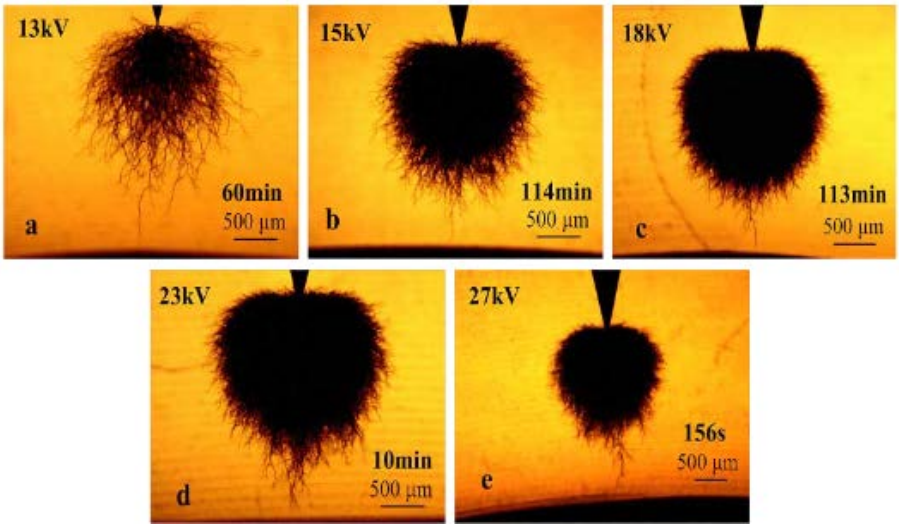


**Figure 2.4** Bush trees grown in XLPE at 13, 15, 18, 23 and 27 kV [48]. *No permission is required for thesis purposes.*

### 2) Partial discharge

During electrical treeing, partial discharge signals can be observed. It is widely considered as the energy source of electrical tree growth. The patterns of partial discharges were found to be in good correlation with different phases of the electrical treeing, as shown in **Figure 2.5** [47]. Thus, partial discharge is suitable for monitoring the electrical degradation of polymeric insulation materials[49].

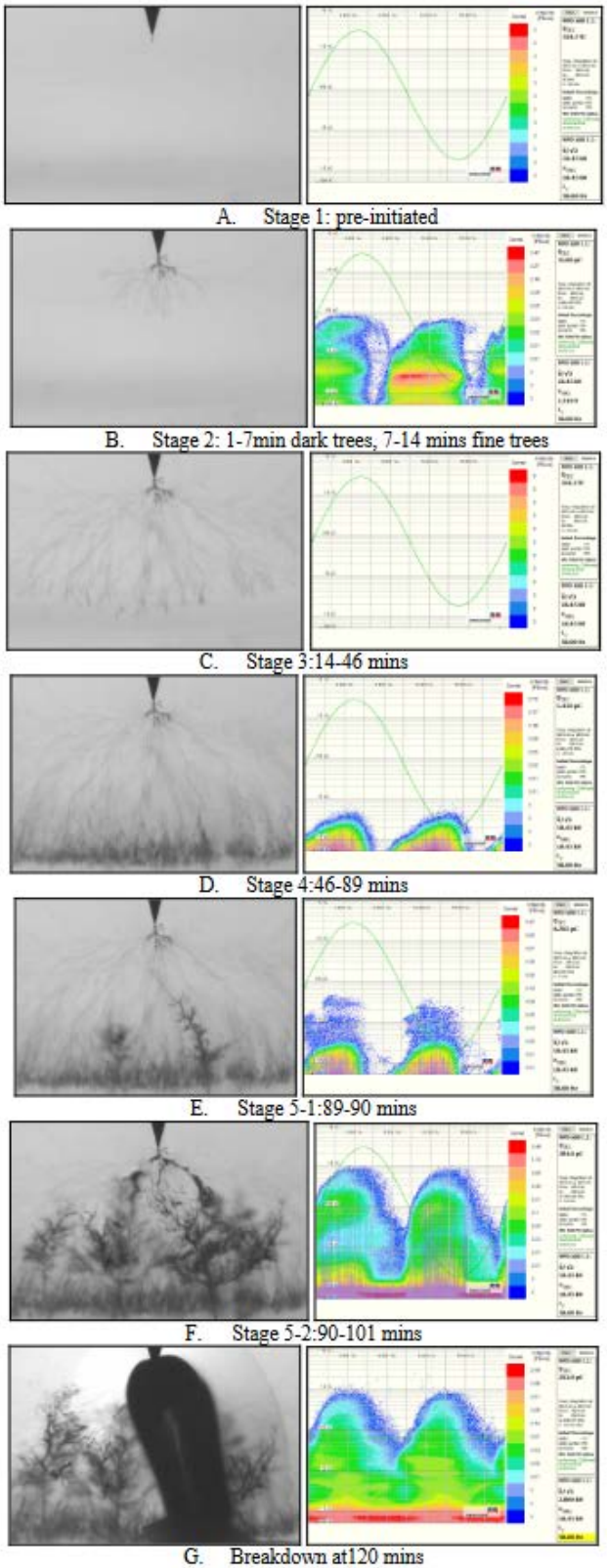


**Figure 2.5** Images of different stages of electrical treeing and corresponding partial discharge patterns [47]. *No permission is required for thesis purposes.*

Two types of typical partial discharge patterns were observed in the electrical tree: 1) wing-like and 2) turtle-like as shown in **Figure 2.6** [76]. Wing-like patterns represent the partial discharges in long channels of the tree, while turtle-like patterns occur when a short branch is growing.

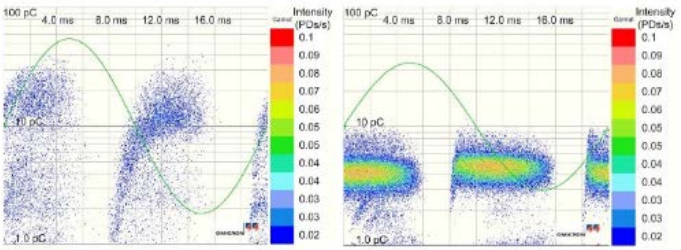


**Figure 2.6** Partial discharge patterns observed in electrical treeing [50]. *No permission is required for thesis purposes.*

### 3) Space charge accumulation

Space charge accumulation, resulting from the charge injection, represents the local concentration of electrical overstresses. With the accumulation of space charge, the distortion of the electric field occurs, which has impacts on the final breakdown of insulators [51], [52]. Accordingly, suppression of space charge accumulation can improve the reliability of insulating materials [53].

## 2.1.5 Impact of Defects on Reliability

Thermoset polymers are widely used as structural materials. A deep understanding of how to resist and support the loads is necessary, and their long-term mechanical behaviour, especially with the existence of voids should be understood and described as accurate as possible. On the other hand, the brittle nature of the thermosets poses a challenge to the description of the mechanical strength of this group of materials.

#### 2.1.5.1 Voids in Epoxy Resin

During the manufacturing process, air can be easily introduced and trapped in the epoxy resin solution because of its high viscosity. The application of fillers in the epoxy matrix also leads to the appearance of voids, which is a common concern in polymer composites, especially for layered materials [54], [55], [56], [57]. The presence of defects would affect the mechanical properties of thermosets like epoxy resin due to their brittleness [58]. The localized flaws can lead to the entire failure of the material. Therefore, it is important to investigate the impact of voids on the mechanical performance of the epoxy resin.

#### 2.1.5.2 Brittleness of Epoxy Resin

Brittleness is one of the mechanical features of materials. Materials which are easily broken or cracked are classified as brittle materials. This type of materials shows limited amount of energy adsorption before failure occurs, which is indicated by little plastic deformation before fracture. Most inorganic non-metallic materials, such as ceramics and glass, show brittleness.

Brittleness is common in thermosets like epoxy resin, which is the major factor in their mechanical failure [35], [59], [60], [61]. Due to the fast growth of cracks in a brittle material, the mechanical behaviour of brittle materials is not as straightforward as ductile materials, presenting a fluctuating failure strength in thermosets [58]. This means the measured strength of the materials with the same composition and processing conditions might have a large scatter among samples prepared under the same conditions. This scatter can be explained by Griffith's theory: the fracture is initiated by the most severe defect in the brittle material, which is always different in each testing sample. This uncertainty causes uncertainty when describing the mechanical properties by the mean value of the measured strength, which is the most commonly used design parameter for the strengths of materials. Thus, a more accurate statistical analysis method is more appropriate to describe the mechanical property of epoxy resin. More efforts are required to accurately characterize the mechanical performance of epoxy resin [58], particularly when it contains

pre-existing flaws and is expected to sustain long-term service stresses (mechanical, thermal, electrical).

#### 2.1.5.3 Evaluation of Mechanical Properties of Epoxy Resin

The mechanical properties of epoxy resin, including Young's modulus, tensile strength, elongation at failure, and fracture toughness, serve as key indicators of its overall mechanical performance. In particular, tensile strength is often used by designers when developing load-bearing structures and components. Therefore, accurately characterizing these mechanical properties is essential for industrial applications. Mechanical testing, which provides valuable insights into the properties of materials, is a crucial method in material design and processing. Tensile testing is commonly used to measure the mechanical property of the bulk material, which is sensitive to the presence of defects, especially for brittle materials.

The stress-strain curve, which reveals the mechanical response of materials, can be produced by tensile testing. Stress is the force applied per unit area which results in the deformation, while a strain is defined as the amount of the deformation in the direction of stress applied divided by initial dimensions. The stress-strain curves for different types of materials are illustrated in **Figure 2.7** [62]. The brittleness of materials can be obviously identified in the obtained stress-strain curve.

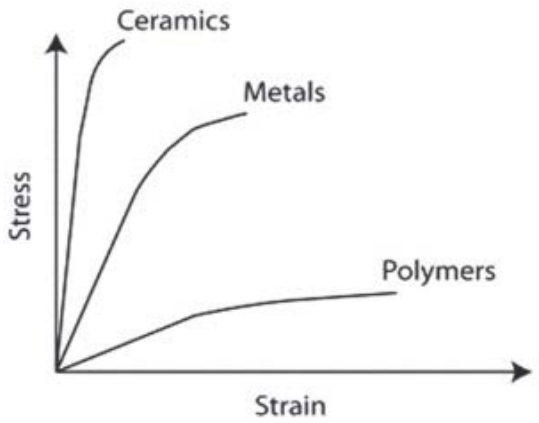


**Figure 2.7** The stress-strain curves for different types of materials [62]. *Open access, no permission is required.*

The standard method used for the tensile strength of polymers is ASTM D638 with a bone-like sample shape. Normally, the tensile strength is obtained by simply averaging several results of several test samples in the group [63], [64], [65]. However, due to the brittleness of the material, the variance between the measured data is quite large, indicating the inaccuracy of this method [41], [66], [67]. Therefore, a more reliable analysis should be introduced. Since epoxy resin shows high brittleness, the method to characterize the mechanical behaviour of brittle materials should be considered.

#### 2.1.5.4 Weibull analysis for mechanical behaviour

The Weibull distribution was developed in the 1950's and is widely used to describe the mechanical performance of brittle materials like ceramics [68]. Since epoxy resin shows brittleness in the mechanical testing, Weibull distribution should be an appropriate tool to describe the mechanical strength of this type of materials.

**1) The concept of Weibull distribution**

The theory behind the Weibull distribution is that the failure of a chain is caused by the failure of the critical link of the chain (the weakest link). This distribution can be expressed as follows [69]:

$$P = 1 - \exp\left[-\left(\frac{\sigma - \sigma_u}{\sigma_0}\right)^m\right] \quad \text{(Equation 2.1)}$$

where *P* indicates the cumulative fracture probability of the samples under a stress σ. $\sigma_0$ is the scale parameter, and *m* is the Weibull modulus, which illustrates the extent of scatter of the breakdown strength. $\sigma_u$ is a threshold, which indicates the possibility of failure is 0 if the stress is lower than $\sigma_u$. Generally, this threshold is regarded as 0 due to the nature of the brittle material. Consequently, *Equation 2.1* can be simplified as a 2-parameter function as shown in Equation 2.2 [70].

$$P = 1 - \exp\left[-\left(\frac{\sigma}{\sigma_0}\right)^m\right] \quad \text{(Equation 2.2)}$$

This function is widely used to describe the fracture strength of brittle materials. From a large quantity of measured data, these 2 parameters in this function can be calculated, which are characteristics of materials. Since the principle of this theory is widely applicable, it can also be applied to characterize other properties, like hardness or even electrical breakdown strength [71], [72], [73] and so on.

To consider the impact of defects, the parameter representing volume defect density with the unit of $m^{-3}$ is introduced. The whole material is divided into very tiny parts, each with a volume of dV and a defect density of $\rho$. Thus, the probability of failure can be written as:

$$P = 1 - \exp\left[-\int_V \left(\frac{\sigma}{\sigma_0}\right)^m \rho dV\right] \quad \text{(Equation 2.3)}$$

Assuming the homogeneity of the material and uniform distribution of defects, this equation can be simplified as:

$$P = 1 - \exp\left[-\left(\frac{\sigma}{\sigma_0}\right)^m \rho V\right] \quad \text{(Equation 2.4)}$$

Rearranging Equation 2.4, a linear curve can be obtained:

$$ln\left[ln\left(\frac{1}{1-P}\right)\right] = \ln(\rho V) + m\, ln\frac{\sigma}{\sigma_0} \quad \text{(Equation 2.5)}$$

$ln\frac{\sigma}{\sigma_0}$ and $ln\left[ln\left(\frac{1}{1-P}\right)\right]$ can be obtained by curve-fitting from experimental data. By plotting this curve, $m$ as the slope and $\ln(\rho V)$ as the intercept can be obtained. Since the volume $V$ can be measured, defects density $\rho$ can be calculated.

**2) Weibull analysis in mechanical characterizations of ceramics**

Numerous research is related to the application of Weibull distribution in the mechanical characterization of brittle materials, especially ceramics. The strength reliabilities of ceramics with various applications can be accurately evaluated by Weibull distribution [74], [75], [76], [77]. Besides this, this Weibull analysis was also employed to describe other mechanical natures of ceramics like fatigue and crack growth [78], elastic modulus and hardness [79], [80], and fracture toughness [81]. The impact of porosity on the mechanical behaviour of ceramics was also studied by Weibull analysis[82]. It is proved that the increase of porosity can cause a reduction in Weibull modulus and strength.

**3) Weibull analysis used in epoxy thermosets**

As discussed before, Weibull analysis has been commonly used in the characterization of ceramics, indicating its accuracy in describing the mechanical behaviour of brittle materials. Therefore, it has the potential to be employed in the mechanical characterization of thermosets like epoxy resin to provide accurate mechanical information for the industry. However, few reports apply this theory to describe the mechanical behaviour of epoxy

resin, and most of them do not focus on the impact of porosity on thermosets.

Among the limited reports, Barbero applied this theory to analyze the variability of the mechanical performance of composites and proposed a novel 3-parameter Weibull distribution [83]. Naresh used a 2-parameter Weibull function to investigate the mechanical reliability of the laminates with epoxy/glass and epoxy/carbon [84]. In their opinion, Weibull analysis can provide useful information on the scattered mechanical behaviour caused by inhomogeneity and brittleness.

### 2.1.6 Epoxy Resin Composites

Insulating materials in electrical systems require excellent electrical resistance combined with long-term thermal and mechanical reliability during service. Research efforts to enhance the performance of polymeric insulating materials under aging conditions have grown steadily, with particular focus on various improvement strategies. Among these approaches, the incorporation of micro- and nano-sized inorganic oxides into epoxy resin has been extensively studied for decades. This strategy has demonstrated significant improvements in the electrical, thermal, and mechanical properties of insulation systems.

#### 2.1.6.1 Selected Properties Summary of Epoxy Resin and Fillers

To better understand the electrical and thermal properties of polymer composites, **Table 2.1** provides an overview of key characteristics for epoxy resin and commonly used fillers. This includes properties such as permittivity, bandgap, and thermal conductivity, which are essential for evaluating and optimizing the performance of these materials in various applications.

**Table 2.1** Key characteristics for epoxy resin and fillers

| Name | Relative permittivity | Breakdown strength $E_b$ (α) [kV mm$^{-1}$] | Thermal conductivity [W m$^{-1}$ K$^{-1}$] | Band gap [eV] |
|---|---|---|---|---|

| | | | | |
|---|---|---|---|---|
| **Epoxy resin** | **4** ($10^{-1}$-$10^{5}$ Hz, 20-60℃) [85]<br>**4** ($4x10^{2}$-$10^{6}$ Hz) [86]<br>**3.6** ($10^{-2}$-$10^{7}$ Hz, -20-80℃) [87] | **182±5** (50Hz AC, 70μm film, D149) [85]<br>**52.3** (50Hz AC, 1mm, D149) [86]<br>**288** (DC, 60μm film) [88] | **0.168** [89]<br>**0.166** [90] | \ |
| **$SiO_2$ (Amorphous)** | **2.3-3.8** (1kHz) [87], [91] | **1000** [92] | **1** (200℃) [93] | **9.0** [94]<br>**8** [92] |
| **BN (h-BN)** | **3.29-4.97** (1layer-bulk, in-plane/out-of-plane, multi-frequency) [95] | **1200** [96] | **602-751** (1-3layer, RT) [97]<br>**220-420** [98] | **6.08** [99] |
| **AlN** | **8.8**[87]<br>**2.3-3.8** (1kHz) [91] | **50-68** (AC)<br>**84-151** (DC) [100] | **30** [93] | **6.2** [101] |
| **SiC** | **6.52-10.03** [102] | **300** [103] | **42** [93]<br>**120** [104] | **3.2-3.3** (4H-SiC)<br>**2.4** (3C-SiC) [105] |
| **$TiO_2$ (Rutile)** | **86-170** [102] | **4** [106] | **8.5** (bulk)<br>**0.40–0.84** (nanotube) [107] | **3.03** [108] |
| **$TiO_2$ (Anatase)** | **22.7-45.1** [109] | | | **3.20** [108] |
| **$Al_2O_3$ (Corundum)** | **11** [87]<br>**9** (1kHz) [91] | **9** [110]<br>**16.9** (AC) [111] | **25** [93] | **8.3** [112] |
| **$Al_2O_3$ (Amorphous)** | | | | **3.64 ± 0.04** [113]<br>**~3.2** [114] |
| **MgO** | **9.7** [87]<br>**3.9** [115] | \ | **41** [93] | **7.77** [116] |
| **$BaTiO_3$** | **4000** (25℃), **2000** (120℃) [91] | \ | **2.65** [117] | **2.53-3.08** (various size NP) [118] |

#### 2.1.6.2 Improvement in dielectric properties

The application of micro- and nano-composites in insulating systems is an increasingly popular topic recently. This compositing strategy is effective to improve the electrical properties of material, such lower dielectric loss, stronger dielectric breakdown strength and higher resistivity.

**1) Dielectric Constant and Loss**

Through integration of fillers, the dielectric constant of epoxy-based composites can be tailored to values either higher or lower than those of neat epoxy resin. The increase of the dielectric constant can be mainly attributed to the higher intrinsic relative permittivity of fillers compared to epoxy resin and the presence of inclusions such as moisture on the nanoparticle surfaces. Conversely, decreases in dielectric constant are generally attributed to fillers with lower intrinsic dielectric constant compared to epoxy resin, along with restricted polymer chain mobility in the interfacial region between the fillers and the epoxy matrix [119].

In addition to the intrinsic properties of fillers, the dielectric constant is highly sensitive to filler size. Microparticles commonly increase the dielectric constant of epoxy resin composites [86], [120]. Nanoparticles such as $Al_2O_3$, MgO, AlN [87] and $TiO_2$ [86], [120], [121] tend to decrease dielectric constant at low concentrations but increase it above that of pure epoxy resin when added in higher amounts. However, the increase in dielectric constant with a high concentration of nanoparticles remains lower than the increase observed with an equivalent concentration of microparticles [86], [120], [121]. In nanocomposites, the particle size of the nanoparticles has an even greater influence on dielectric constant than their intrinsic properties. Smaller nanoparticles lead to a more pronounced reduction in dielectric constant, even when compared to larger nanoparticles with lower intrinsic dielectric constant.

Another factor impacting dielectric constant is the shape of the fillers. For instance, epoxy resin with $TiO_2$ nanowires exhibits a higher dielectric constant compared to composites with $TiO_2$ particles at the same loading [90]. The specific area of nanowires is smaller than the nanoparticles (39.8 and 82.6 $m^2 g^{-1}$, respectively). This smaller interfacial area leads to the increase in the dielectric constant.

The concentration of nanoparticles affects dielectric constant in two distinct ways as loading increases. Initially, dielectric constant tends to decrease with a small amount of nanoparticles added. However, dielectric constant increases when the filler amount surpasses a certain threshold. The first reason is that the nanoparticles tend to agglomerate when the amount is high, thereby decreasing the interfacial area and the amount of restricted polar groups. Secondly, the nanoparticles which have a higher intrinsic dielectric constant than epoxy resin start to contribute to the dielectric constant of the composite since the particles occupy a significant volume fraction, thereby increasing the dielectric constant of the composite [86], [120], [122].

The addition of microparticles generally increases the dielectric loss [86], [120], which causes more localized heat and accelerated aging. However, the introduction of nanoparticles can decrease the dielectric loss when the added amount is low. For $TiO_2$, a decrease in dielectric loss was observed in 1 wt.% dosage, while an increase in that was found with a higher dosage at 5 wt.%.

**2) Dielectric Breakdown Strength**

The dielectric breakdown strength is a vital parameter when determining the insulation properties of the material. According to the model proposed by Tanaka [123], bound and bonded layers are much more resistant to partial discharge than the loose layer and polymer matrix. During the electrical treeing, micro- and nano-particles can act as barriers against tree growth, resulting in the improvement of electrical reliability [124], [125], as shown in **Figure 2.8** [126]. These particles also introduce numerous deep traps capable of capturing injected charges and suppressing space charge accumulation. Various inorganic particles

are employed as fillers in insulating materials to improve their breakdown strength. The researcher has reported that the DC breakdown strength of composites with $SiO_2$ is higher than $Al_2O_3$ and followed by AlN [127].

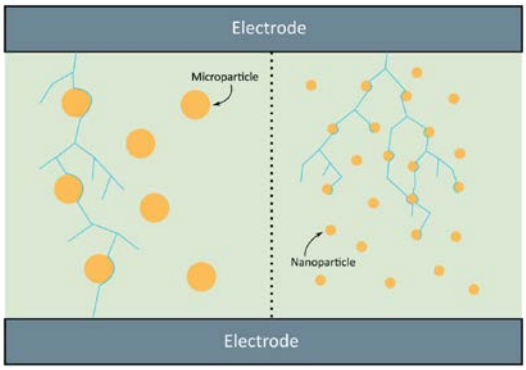


**Figure 2.8** Electrical tree growth in micro- and nano-composites [126]. *Open access, no permission is required.*

However, the addition of particles can also introduce defects such as voids at the interface between particles and the polymer matrix, which may accelerate electrical tree growth and decrease the breakdown strength. Moreover, the presence of fillers can lead to a mismatch between the filler and polymer matrix, causing electric distortion and potentially degrading critical properties such as breakdown strength, dielectric loss, and electrical resistivity [128]. Therefore, the electrical properties of epoxy-based composites depend heavily on the interfacial condition between fillers and the polymer matrix.

#### 2.1.6.3 Improvement in Thermal Properties

High-voltage electrical systems generate substantial heat, which poses a significant challenge for epoxy-based insulation materials due to their inherent low thermal conductivity [31], [32], [129] that accelerates thermal aging [33]. The resulting thermal stress triggers degradation mechanisms including molecular chain breakage, structural reorganization, and oxidative processes [37], [38], [39], ultimately compromising the material performance and system reliability. The incorporation of $SiO_2$ into the epoxy resin is a cost-effective strategy to improve heat resistance. Research has demonstrated notable

improvements, with one study showing that a 4 wt% $SiO_2$ addition resulted in a 12°C elevation in glass transition temperature ($T_g$) [130].

Improving the thermal conductivity by incorporating inorganic particles [131], [132] is also a commonly used strategy to obtain a reliable performance of the insulation system. Oxides such as $SiO_2$ [133], nitrides such as BN, AlN nanoparticles, are reported to be effective to improve the thermal conductivity of epoxy resin due to their high intrinsic thermal conductivity [134], [135]. Besides the thermal behaviour of fillers, the size and morphology of fillers also affect the final thermal conductivity of composites [136]. Composites with micro fillers usually show higher thermal conductivity than those with nanofillers. Kochtov attributed this effect to the more phonon scattering on the larger surface area of nanoparticles [89]. The fillers with higher aspect ratios, such as nanowires, can increase the thermal conductivity of composites more efficiently [90]. A longer nanowire is more beneficial for heat transfer than spherical nanoparticles as they form thermally conductive channels. In addition, a good interaction between filler and matrix, which can be obtained by modifying the surface of the filler, decreases the interfacial thermal resistance and reduces defects like voids. Ultimately, it results in the reduction of phonon scattering and improved thermal conductivity [137].

#### 2.1.6.4 Mechanical Enhancement

Extensive research highlights that nano- and micro-composites often exhibit superior mechanical properties compared to pure polymers. These enhancements are commonly observed in stiffness, strength, and toughness due to the reinforcing effects of the fillers [138], [139], [140], [141]. For instance, Becker et al. [142] reported a 20% increase in modulus in resin systems with a 10% concentration of organoclay, attributing the improved stiffness to the presence of exfoliated high-aspect-ratio platelets. This reinforcement mechanism arises from shear deformation and efficient stress transfer within the platelet particles. Similarly, Chan et al. [143] found that adding just 5 wt.% of nanoclay increased the composite's Young's modulus and tensile strength by 34% and 25%, respectively, compared to the unfilled polymer.

### 2.1.7 Interface Between Filler and Polymer Matrix

The interface between the filler and polymer matrix plays a crucial role in the composite's properties. The molecules and dipoles in the interface layer close to particle can be restricted, causing the enhancement in mechanical properties and reduction in polarization [122]. In addition, deep traps are developed in the interface layer, improving the dielectric durability [123]. The impact of interface is more significant in nano composites than micro composites, due to the higher interfacial volume brought by smaller particle, as shown in **Figure 2.9** [144]. However, poor interaction can lead to electric distortion and potentially degrade critical properties such as dielectric breakdown strength, dielectric constant/loss [128], [145], [146], toughness and mechanical strength [147]. Therefore, a deep understanding of the interactions between fillers and matrices is essential for optimizing the performance and functionality of particulate-filled polymers.

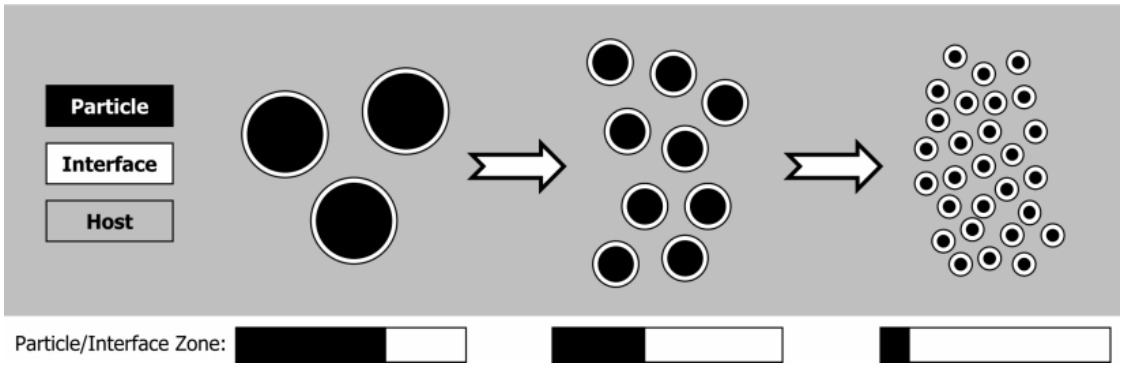


**Figure 2.9** Change of ratio between particle and interface volume as a function of particle size [144]. *No permission is required for thesis purposes.*

#### 2.1.7.1 Multi-core model for nanocomposites

Tanaka et al. [123] proposed a multi-core model to reveal the interaction between filler and polymer matrix, as shown in **Figure 2.10**. There are 3 layers:

1) The first layer (inner bonded layer): Polymer chains are chemically bonded to the particle surface by coupling agents. This layer only exists when coupling agents are used.
2) The second layer (bond layer): Polymer chains strongly interact with the first layer. The mobility of polymers is restricted in this layer.
3) The third layer (loose layer): Polymer chains weakly interact with the second layer.

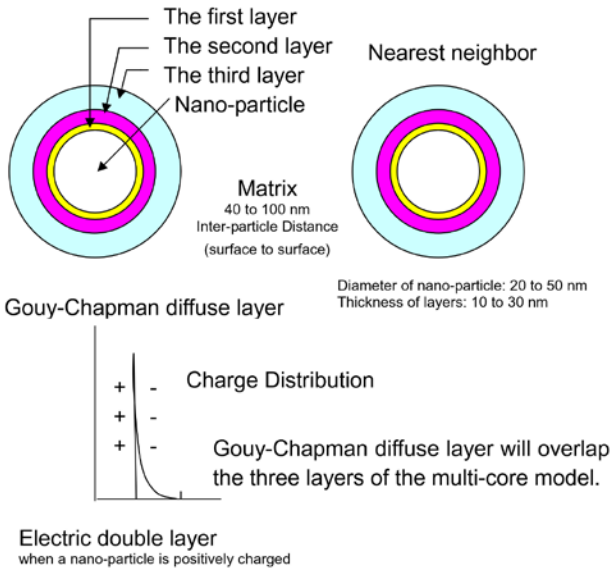


**Figure 2.10** Multi-core model for nano-particle-polymer interfaces [123]. *No permission is required for thesis purposes.*

### 2.1.7.2 Impact of Interfacial Area on Electrical Properties

#### 1) Dielectric Constant and Loss

The interface between fillers and polymer matrix shows a great impact on the electrical performance of the composites [148]. Kochetov [87] and Tanaka [123] proposed the interfacial region as the “third phase”. In this region, there are immobilized polymer chains, and polar groups in these chains are less able to follow changes in the applied external electric field, resulting in a decrease in dielectric constant and loss. With surface-modified nanoparticles which can improve the interface bonding, the dielectric loss in composites is

even lower than that in composites without surface modification on particles [85], [88]. The thickness of this interface is independent of the filler size. Nanoparticles have a higher surface area than microparticles, resulting in a larger third phase. Thus, more polar groups are restricted, causing a decrease in relative permittivity [122]. However, the presence of voids between fillers and matrix due to poor interaction may act as the weak point during usage, which should be avoided [149], [150].

**2) Dielectric Breakdown**

The dielectric breakdown strength of epoxy-based composites depends heavily on the interfacial condition between fillers and the polymer matrix. The deep carrier traps can be introduced in the first and second interface layers, improving the dielectric durability [123] by charge trapping mechanism. Besides, the ligands with electron-withdrawing groups or π-conjugated ligands in some surface modifier could act as the electron traps [88], [151], increasing the breakdown strength effectively. Higher DC breakdown strength can be observed in composites with smaller filler sizes due to its larger interfacial area [144]. However, the addition of particles can also introduce defects and voids at the interfacial area, which may accelerate electrical tree growth and decrease breakdown strength.

#### 2.1.7.3 Impact of Interfacial Area on Other Properties

The enhanced mechanical properties of these composites can be attributed to two main factors: effective interfacial bonding and proper dispersion of fillers. Strong interfacial adhesion allows efficient load transfer between the polymer matrix and fillers, while well-dispersed fillers increase the surface area over which this reinforcement occurs, leading to greater resistance to crack propagation. For example, a propagating crack interacts with numerous nanoparticles rather than bypassing large microparticles, which requires more energy and improves toughness [152].

However, if the interface or dispersion is inadequate, these benefits may not be realized, and the composite's properties may be compromised. Rong et al. [153] demonstrated that

poor dispersion and inhomogeneous filler distribution can significantly reduce performance, particularly in wear resistance. Therefore, the advantages of nanocomposites hinge critically on achieving optimal interfacial interactions and uniform filler dispersion within the polymer matrix.

Interfacial condition is also important for thermal properties. There is no obvious trend in $T_g$ when $TiO_2$ nanoparticles were introduced, but after surface treatment on particles, the $T_g$ increased. Lizundia [154] attributed the increase in $T_g$ to the improved dispersion of nanoparticles in the polymer matrix due to surface modification. However, Zhao [155] and Yeung [85] observed a decrease in $T_g$ when the surface modification was applied to the particles.

#### 2.1.7.4 Factors Weakening Performance

As discussed above, a dense interface between the filler and polymer matrix is essential to achieving multiple performance improvements. However, imperfections at the interface are often unavoidable in practical applications, potentially leading to adverse effects on the performance.

**1) Interfacial Defects**

Interfacial defects between the filler and polymer matrix brought by micro and nano fillers are inevitable, severely weakening electrical and mechanical performance. These defects act as sites for stress concentration and potential paths for breakdown under electrical stress. Furthermore, such imperfections can reduce the efficiency of load transfer and create regions where electrical charges may accumulate, increasing the risk of partial discharge and ultimately reducing the breakdown strength of the composite.

**2) Dispersion Issue**

Uniform dispersion of fillers within the polymer matrix is crucial to ensure consistent performance across the composite material. Poor dispersion leads to agglomeration of filler particles, creating localized regions with different dielectric and thermal properties than the surrounding matrix. These agglomerates can serve as points of weakness where electrical or mechanical failure may initiate, thus reducing the reliability and longevity of the material. Techniques such as surface modification of fillers or the use of surfactants are often employed to improve dispersion, although they also add complexity to the manufacturing process.

**3) Amount of Fillers**

Although fillers can significantly enhance the breakdown strength of insulating materials, there is a practical limit to the filler concentration due to increased processing chanllenges, particularly in nanocomposites. As filler concentration increases, voids and other imperfections are more likely to form, and nanoparticles tend to absorb moisture due to their high surface area. This absorbed moisture can further degrade electrical insulation properties, leading to a significant reduction in breakdown strength when filler content becomes excessive [149].

### 2.1.8 Surface Wettability and Interface

#### 2.1.8.1 Concept of Wettability

Surface wettability is a critical property that describes how a liquid interacts with a solid surface, quantified by the contact angle (CA) formed between the liquid droplet and the surface. A lower contact angle indicates a hydrophilic surface ($\theta < 90°$), which readily attracts water and allows it to spread, while a higher contact angle signifies a hydrophobic surface ($\theta > 90°$), which repels water. Specifically, surfaces with a contact angle less than 10° are considered extremely hydrophilic, whereas those exceeding 150° are classified as extremely hydrophobic [156].

The water contact angle (WCA) serves as a quantitative measure of this wettability, with lower values correlating with increased hydrophilicity and higher values indicating hydrophobicity [157]. The chemical composition of the surface determines its polarity and surface energy, which are critical in defining the WCA [158]. In addition, the surface roughness also has impact on the measured WCA of material, as shown in the Wenzel model:

$$\cos\theta_w = R\cos\theta_0 \qquad \text{(Equation 2.6)}$$

In this equation, $\theta_w$ is the measured contact angle, while $\theta_0$ is the contact angle on a flat surface, and $R$ is the surface roughness factor, defined as the ratio of the actual surface area in contact to its projection on a flat plane, which is always greater than or equal to 1. When $\theta_0$ is below 90°, increasing roughness factor results in a lower measured contact angle $\theta_w$; conversely, if $\theta_0$ is above 90°, the measured contact angle $\theta_w$ increases with higher $R$. This roughness factor amplifies the effect of the chemical properties, further influencing the measured wettability.

#### 2.1.8.2 Impact of Filler Wettability on Interface in Composites

The surface wettability of fillers plays a crucial role in determining the interface between the filler and polymer matrix. Suitable wettability allows the polymer to spread and adhere more uniformly across the filler surface, minimizing interfacial defects and improving dispersion, which in turn improve the interfacial adhesion within the composite materials [159]. This strong adhesion is vital for overall performance of the composites [123], [160]. Consequently, optimizing filler surface wettability is essential for achieving superior composite material performance, as it directly correlates with the effectiveness of the interaction between filler and polymer matrix.

#### 2.1.8.3 Hydrophilicity and Hydrophobicity of Fillers

As discussed in Section **2.1.6**, the incorporation of oxides particles into epoxy resin system is effective to improve multiple performance including dielectric, mechanical and thermal properties. However, a challenge remains in that the hydrophilicity of oxides, resulting from the abundant surface hydroxyl groups, and the nature of small particles, might increase water uptake [161]. Water uptake severely impacts adhesion between fillers and epoxy resin matrix, leading to significant changes in material properties [162]. Consequently, some researchers have explored methods to modify particle surfaces from hydrophilic to hydrophobic. Xu et al. successfully grafted hexadecyltrimethoxysilane onto nano-$SiO_2$ surfaces, increasing the water contact angle (WCA) from 25.8° to 170.9° [161]. Dichlorodimethylsilane and fluoro-silane have also proven effective in imparting hydrophobicity to $SiO_2$, with WCAs of 155° [163] and 167° [164], respectively.

As mentioned in section **2.1.8.2**, the interface between the filler and polymer matrix plays a crucial role in the composite's properties. Although hydrophobic particles are expected to reduce water uptake, the compatibility between these hydrophobic fillers and hydrophilic epoxy resin remains questionable [162], rendering long-term performance of the composites unpredictable.

### 2.1.9 Performance Enhancement by Molecular Modification

While integrating nano and micro fillers into polymer matrix offers significant benefits, it also presents challenges such as interfacial defects and dispersion issues, as discussed in section **2.1.7.4**. To address these challenges, molecular modification serves as an alternative strategy that focuses on directly altering the molecular structure of the polymers themselves. This section will explore how molecular-level modification can improve inherent properties such as thermal stability, mechanical strength, dielectric ability and overall functionality, presenting a fresh perspective beyond conventional nanofiller strategies.

#### 2.1.9.1 Mechanical Enhancement

Improving the toughness of EP is another active area of research, aimed at enhancing the ability of these materials to deform plastically and resist crack propagation. Misaki et al. [165] investigated the fracture properties of p,p'-diaminodiphenyl methane-cured EP modified with various aromatic and aliphatic glycidyl compounds. Their findings revealed that while most of these compounds promoted an increase in fracture toughness, the heat resistance of the modified EP was compromised to some extent by the incorporation of glycidyl compounds. Additionally, they observed an inverse relationship between cross-linked density of the resins and their impact strength and fracture toughness. Remarkably, the addition of 10 wt% of a terpolymer resulted in a substantial (140%) increase in the fracture toughness of the modified EP.

#### 2.1.9.2 Thermal Enhancement

The effects of modifications on the thermal stability of EP have been extensively studied. Lin and Pearce [166], [167] investigated the thermal properties of DGEBA-DGEBF and DGEBA-DGEPP copolymers. Their findings revealed that the DGEBA-DGEBF copolymer exhibited superior heat and flame resistance compared to the DGEBA-DGEPP copolymer, attributable to its higher aromatic ring content. Fourier-transform infrared (FTIR) data suggested that the possible degradation mechanisms for these EP involve the Wieland rearrangement, Claisen rearrangement, and Norrish-type reactions. Chen et al. prepared five different EPs cured with TMB (trimethoxy boroxine) and DDS (diaminodiphenylsulfone) hardeners [168]. The results indicated that polymers with high aromaticity and/or cyclic ring structures in the chain backbone generally exhibited enhanced heat resistance. Furthermore, the morphology and structure of organosilicon polymer-modified EP were investigated by incorporating an organosilicon polymer (denoted as ETOP) as a modifier to blend with bisphenol A-type EP [169]. The study demonstrated that the cross-linked epoxy-rich matrix possessed a higher glass transition temperature ($T_g$) than pure EP at higher ETOP content. This observation was attributed to the participation of epoxide groups on ETOP molecules in the cross-linking reaction of the matrix, thereby increasing the cross-link density and enhancing the $T_g$.

#### 2.1.9.3 Electrical Enhancement

While extensive research efforts have been dedicated to modifying EP to improve their thermal and mechanical properties, relatively few studies are focused on enhancing their dielectric characteristics. With the rapid development in energy storage and conversion, flexible electronics, smart sensing, and 5G/6G communication, there is an urgent need for EP with tailorable dielectric properties [128]. Some research demonstrates that the introduction of polar groups in polyethylene and PVDF enhances the dielectric breakdown strength, which can be attributed to the formation of deep traps that capture charges [170], [171]. Meanwhile, the existence of bulky groups benefits the reduction of dielectric constants [172]. Given these findings, it is essential to investigate how molecular modification strategies can be applied specifically to epoxy resin to improve its multi-functional performance.

### 2.1.10 Other Improving Strategies

In addition to incorporating micro and nano inorganic oxides into epoxy resin, and modifying epoxy resin at molecular level, there are some other strategies to improve the performance of epoxy resin. It is reported that low-density polyethylene (LDPE) with graphene exhibits good thermal stability and reliable dielectric performance due to the strong ability of graphene to capture electrons [173], [174]. The addition of rubber nanoparticles in epoxy resin also increases the toughness and heat resistance [175]. Based on the concept that oriented molecular chains could benefit thermal conductivity, solution-shearing and liquid crystallization technologies are employed to get high thermal conductivity polymers [31], [176].

## 2.2 Summary and Research Gaps

This literature review underscores the critical need to deepen understanding of the degradation mechanisms in epoxy-based insulation materials, as well as to develop strategies for improving their durability. Such insights are essential for enhancing the

reliability of both these materials and the equipment that depends on them. A comprehensive exploration of degradation processes, paired with durability enhancement strategies, is vital for creating effective solutions to prevent potential failures.

As demonstrated in this literature review, understanding how defects impact the long-term performance of pure epoxy resins is crucial for gaining insight into their degradation behavior. Randomly distributed voids within the resin can weaken structural integrity and lead to premature failures, highlighting the importance of statistical tools like Weibull distribution to quantify the influence of voids on material reliability. This understanding is critical for guiding improvements in design and manufacturing practices.

Beyond pure epoxy resin, the addition of inorganic oxide fillers presents a promising approach for enhancing material performance. However, filler integration introduces its own challenges, as interfacial defects can significantly weaken material reliability. Filler surface wettability plays a crucial role. Adequate wettability fosters strong interfacial adhesion, which reduces void-related weaknesses and improves durability. Nevertheless, the hydrophilic nature of oxides may increase water uptake, which could undermine long-term stability. This complex correlation underlines the need to understand how filler surface wettability influences the performance of epoxy composites over time.

Given the challenges of interfacial defects and agglomeration in filler integration, molecular design offers a promising alternative for enhancing durability. Modifying the molecular structure of epoxy resins can improve multiple properties without the interfacial issues common to filler-based strategies. However, limited research has been done in epoxy resins, especially for electrical enhancement, highlighting the need for further study on how tailored structures can enhance dielectric performance. This holistic approach aims to boost the reliability of insulating materials, ultimately reducing the risk of failures.

# Chapter 3

# Experimental Methodology

*This chapter explains the synthesis of epoxy resin specimens. Materials characterization and testing methods are also described. The rationales for material and methodology selection are explained.*

## 3.1 Rationale for selection

The rationales for selecting the pure epoxy/amine resin curing system ARALDITE® LY 5052 / ARADUR® 5052 CH are its good workability, transparent appearance and simple formula. This system requires a relatively low curing temperature, while its viscosity remains low at the beginning of the curing process, showing good workability. After curing, the transparent appearance makes it easy to visually detect defects and observe the electrical treeing phenomenon using an optical microscope. Additionally, the simple formula is suitable for understanding its chemical reactions and investigating the effects of improvement strategies, such as molecular modification and compositing with ceramic particles.

Accelerated aging tests under harsh environments are used to evaluate the long-term performance of the materials and investigate their degradation mechanisms. The mechanical, electrical, and thermal properties of the epoxy resins and their composites are measured, providing valuable insights into the durability of insulating materials. The morphology and chemical structure are also examined to reveal the mechanisms behind the observed material behavior.

## 3.2 Materials and Processing

The epoxy resin sample is prepared by the two components system: resin solution (ARALDITE® LY 5052) and hardener (ARADUR® 5052 CH).

The uncured epoxy resin solution ARALDITE® LY 5052 used in this study consists of a large amount of ether. The composition is illustrated in **Table 3.1**. The concentration is provided by the supplier and is shown as a range due to the protection of confidentiality. The chemical structure of the chemicals is shown in **Figure 3.1**.

**Table 3.1** Ingredients of uncured epoxy resin solution ARALDITE® LY 5052

| Ingredient name | CAS number | Molecular formulation | Concentration |
|---|---|---|---|
| Phenol, polymer with formaldehyde, glycidyl ether | 28064-14-4 | $(C_6H_6O)_x \cdot (CH_2O)_x \cdot (C_3H_6O_2)_x$ | 60-100% |
| butanedioldiglycidyl ether | 2425-79-8 | $C_{10}H_{18}O_4$ | 30-60% |

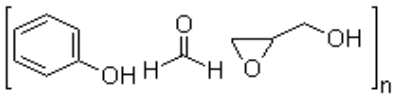

Phenol, polymer with formaldehyde, glycidyl ether

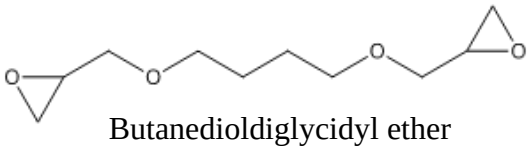

Butanedioldiglycidyl ether

**Figure 3.1** Molecular structure of ingredients in uncured epoxy resin ARALDITE® LY 5052 [177], [178].

The hardener used in this study is ARADUR® 5052 CH provided by Huntsman. It mainly contains di- and polyamines collaborated with a few phenols and acids. For each amine group, there are 2 reactive functional groups. Therefore, the di- and polyamines applied as the hardener here has an $f \geq 4$, indicating their great crosslinking ability. The ingredients with rough concentrations provided by the product safety data sheet are listed in **Table 3.2** and their molecular structures are illustrated in **Figure 3.2**.

**Table 3.2** Ingredients in hardener ARADUR® 5052 CH

| Ingredient name | CAS number | Molecular formulation | Concentration |
|---|---|---|---|
| Cycloaliphatic polyamine | 6864-37-5 | $C_{15}H_{30}N_2$ | 30-60% |

| | | | |
|---|---|---|---|
| Isophorone diamine | 2855-13-2 | $C_{10}H_{22}N_2$ | 30-60% |
| 2,4,6-tris(dimethylaminomethyl)phenol | 90-72-2 | $C_{15}H_{27}N_3O$ | 1-3% |
| Salicylic acid | 69-72-7 | $C_7H_6O_3$ | 1-3% |

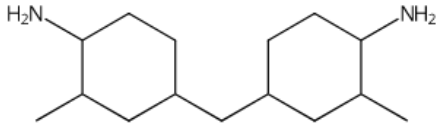


Cycloaliphatic polyamine

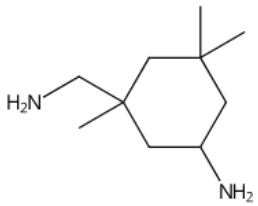


Isophorone diamine

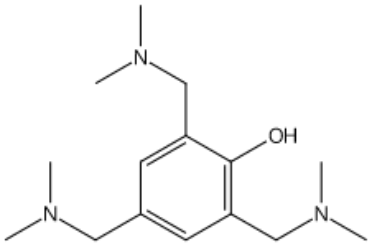


2,4,6-tris(dimethylaminomethyl)phenol

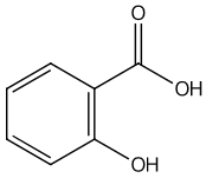


Salicylic acid

**Figure 3.2** Molecular structure of ingredients in ARADUR® 5052 CH [179], [180], [181], [182].

The composition of the epoxy resin solution used in this study is 2 kinds of ether and the hardener mainly consists of various diamines as mentioned in the previous sections. The main curing reaction occurs between ethers and amines as illustrated in **Figure 3.3**. There are 3 steps in this crosslinking reaction as described here [27], [29], [183]:

1) Epoxy group + primary amine group → secondary amine
2) Epoxy group + secondary amine group → tertiary amine
3) Etherification

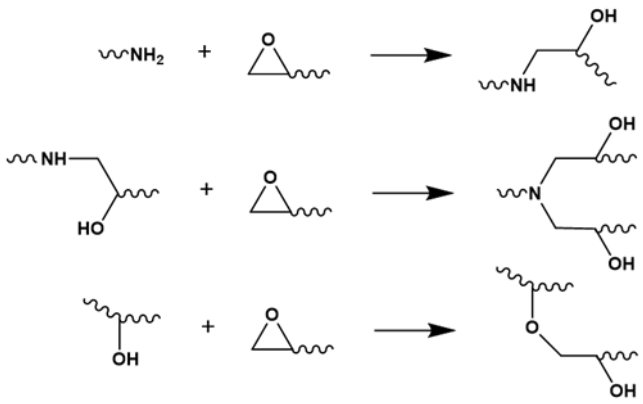


**Figure 3.3** Main reaction between epoxy resin and hardener used in this study.

Epoxy/amine resin specimens were prepared by mixing the uncured EP solution with the amine-containing hardener at a fixed weight ratio of 1:0.38. A Thinky Mixer ARE-310 was utilized for planetary mixing at 2000 rpm and centrifugal defoaming at 2200 rpm. Then the mixture was poured into a mold with various shapes. Various types of molds were used for manufacturing test specimens with different dimensions:

1) Silicone mold setup for bone, rectangular and small circle specimens

   Silicone replica molds were used to prepare specimens in bone shape (for tensile tests), rectangular shape (for FTIR, DMA tests), and small circle shape (for thermal conductivity tests). These molds were made by hand-mixing the PDMS solution and hardener in a 1:1 ratio. The mixture was placed in a vacuum chamber to remove trapped air. Metal bars with standard specimen shapes were fixed to a petri dish, and the mixture was poured into the dish, followed by vacuum degassing again. Afterward, the petri dish with the mixture and metal bars was placed in an oven at 60°C for 2 hours. Once cured, the silicone mold was released and placed in the oven at 200°C for 1 hour to remove any moisture. After cooling to room temperature, the molds were stored in a dry box. The silicone mold with different shape of cavities can be seen in **Figure 3.4**.

**Figure 3.4** Silicone molds with different shape of cavities.

To use the molds, the mixed epoxy resin and hardener were poured directly into the cavities. A release cloth made of Teflon was placed over the liquid, and the entire mold was pressed with a heavy metal block. The resin mixture was cured at room temperature for 24 hours, followed by post-curing at 100°C for 4 hours. The specimens were then stored in a dry box at 40% relative humidity.

The advantages of this mold are its low cost and the ease of removing the resin from the mold. However, a drawback is that it tends to expand during the heating process and may deform after multiple uses. Therefore, regular replacement of the molds is necessary to ensure consistent sample dimensions. Additionally, this mold is not suitable for manufacturing thin film and large disk specimens due to its tendency to expand during heating, so other methods are used for those specimens.

2) Stainless-steel mold setup for thin film and disk specimens

The stainless-steel mold was used to prepare disk and thin film specimens for electrical tests. The detailed setup for this preparation is explained as follows: thin stainless-steel boards were coated with release agent 770 NC to prevent cured samples from adhering to the boards. The whole setup of this mold can be seen in **Figure 3.5**. A Mylar film (A) with a thickness of 0.1 mm was placed on top of a stainless-steel board. A steel

ring (for disk specimens) or a gasket made of Mylar film (for thin film specimens) was then placed on top of Mylar film (A). Next, the uncured epoxy resin solution was poured into the mold, followed by the placement of another Mylar film (B) on top of the resin. A heavy metal block was placed on top of the setup. The curing process was the same as described in the silicone mold section. Due to the stable shape of the stainless-steel mold during heating, the specimen shapes were consistent, and their thicknesses were uniform.

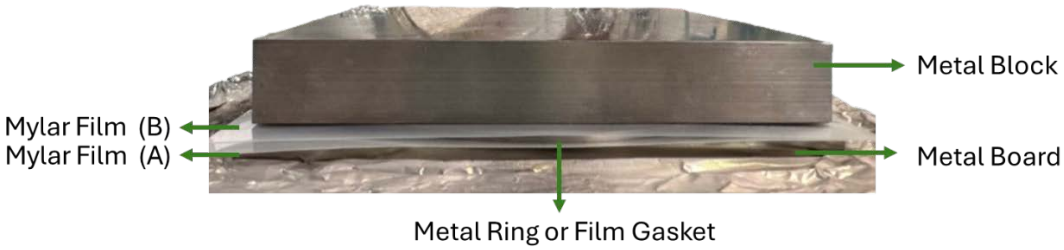


**Figure 3.5** The mold setting for preparing disk and film specimens.

## 3.3 Characterization

The theory of characterization method used in this research is described in the following sections.

### 3.3.1 Scanning Electron Microscopy (SEM) and Energy Dispersive X-Ray Spectroscopy (EDX)

The resolution of microscopy is limited by the wavelength of the illumination. The electron has a shorter wavelength than light, indicating a higher resolution. To increase the magnification of the microscope, an electron beam generated by the electron gun is selected as the source.

When the focused electron beam with high energy interacts with the specimen, various signals like secondary electrons (SEs), backscattered electrons (BSEs) and X-rays are produced as shown in **Figure 3.6**. With relatively low energy of incident electron beam,

SEs are generated from the collision between the incoming electrons and the outer shell electrons of specimens, which are loosely bonded. Since the energy is low, only SEs generated near the surface can escape and be detected as the SEs signal. Thus, the secondary electron microscope (SEM) is usually used to reveal the topographic information of materials. When the high-energy electron beam interacts with the specimen, characteristic X-rays are produced, forming the basis of Energy Dispersive X-ray Spectroscopy (EDX). As incoming electrons displace inner-shell electrons from atoms, the resulting energy difference is released as X-rays. These X-rays have specific energies unique to each element, allowing EDX to detect and identify the elemental composition of the specimen. This technique is often combined with SEM, enabling both surface imaging and compositional analysis, making it ideal for identifying the distribution of elements in materials.

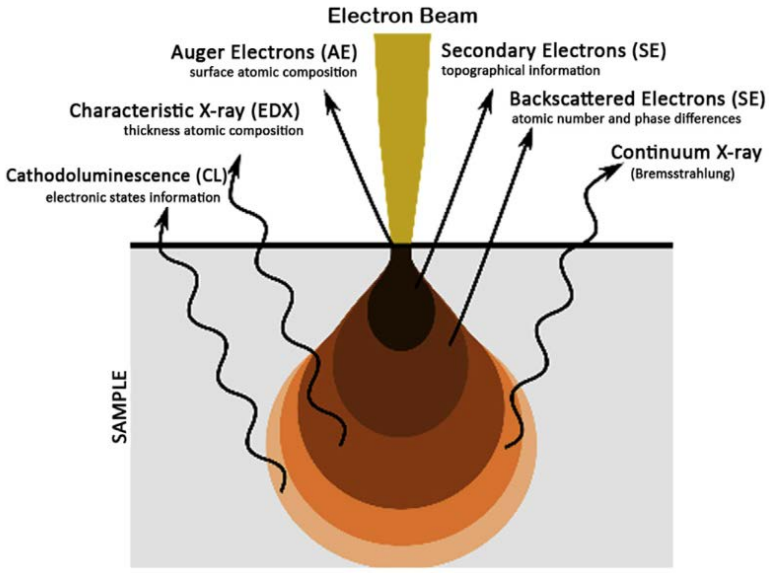


**Figure 3.6** Signals generated by the interaction between the electron beam and specimen [184]. *No permission is required for thesis purposes.*

In this study, SEM and EDX were used to observe the fracture surfaces of specimens after tensile failure to reveal the mechanical failure mechanisms and the element distribution. A JEOL JSM 7800F Prime, equipped with an Oxford Ultim Max EDS detector, was used for this analysis. Various accelerating voltages, ranging from 1.5 to 10 kV, were employed

depending on the observation purpose. Since the specimen is non-conductive, platinum was sputtered onto the surface in combination with conductive tape to prevent charge accumulation and enhance image quality.

### 3.3.2 Optical Microscopy

Optical microscopy is a technology with long history using visible light and a series of lenses to observe small features to get precise measurements. A camera is installed to capture the optical microscope images. Various illumination techniques are explored and applied in optical microscopy. For bright field illumination, the image contrast comes from the absorbance of light in the sample. While for dark field illumination, the contrast is generated from the light scattered by the sample.

By observing the specimen at multiple focuses, a 3D structure can also be generated. And more features of the specimen can be concluded in one image by combining images taken by multi-focuses. Also, the optical microscope can scan the whole sample surface and merge all images to get a large image with detailed characteristics.

In this study, DSX1000 digital microscope was used to observe the structure of specimen and electrical tree growth. Bright-field and mixed illuminations were employed to generate images. OLYMPUS Stream image analysis software was used to process the image. Before this observation, samples are slightly ground and polished to improve the quality of images.

### 3.3.3 Fourier Transform Infrared Spectroscopy (FTIR)

Fourier transform infrared spectroscopy (FTIR) is widely used for the characterization of organic compounds. The principle of this technology is that the molecules absorb frequencies that are characteristic of their chemical bonds. When the molecule absorbs infrared light, it changes from a ground vibrational state to an excited vibrational state. As a result, the dipole moment of the molecule changes with the expansion and contraction of the bond. The energy required for this phenomenon is characteristic to the molecules,

indicating the unique frequencies of light which can be absorbed. Thus, the molecular structure of materials can be detected qualitatively even quantitatively by comparing its absorption peak to the database.

For liquid and powder samples, the pellet consisting of samples and KBr powder is prepared for testing. The infrared beam goes through the pellet and is collected by the detector on the other side. For solid samples, the attenuated total reflection (ATR) is required, which can measure the samples in a simple and non-destructive way. The path of the infrared beam in ATR-FTIR is shown in **Figure 3.7**.

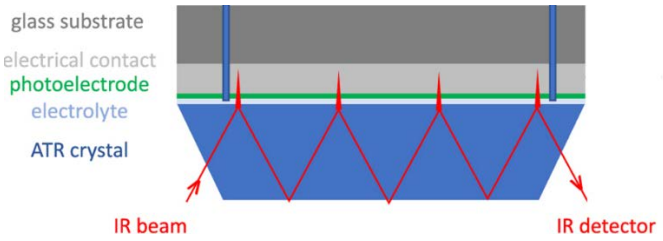


**Figure 3.7** Schematic of ATR technology [185]. *Open Access, no permission is required.*

### 3.3.4 Electrical Properties

The electrical performance of the polymeric materials was evaluated to assess their insulating properties and overall reliability in electrical equipment Key factors such as dielectric constant, dielectric loss, volume resistivity, and dielectric breakdown strength were considered, as these characteristics directly impact the ability to prevent electrical breakdown and withstand operational stresses. In addition, electrical tree growth was characterized to reveal the failure mechanism.

#### 3.3.4.1 Dielectric Spectroscopy

In this study, dielectric spectroscopy was conducted using a Megger IDAX 300 to examine the dielectric constant and dielectric loss of the specimens over a frequency range of 1 mHz to 1000 Hz under ambient conditions. This technique provides insights into the polarization

mechanisms of the material. The investigation is based on IEC 62631 test standard [186]. Uniform disk samples with a radius at 10 cm and thickness at 2 mm were used in this testing. The samples were carefully positioned between the electrodes to ensure reliable measurements. The guarded electrodes system was used with a guarding ring. This guarding system effectively mitigates stray effect, thus no further correction is required. The setup of specimen and electrodes is illustrated in **Figure 3.8**.

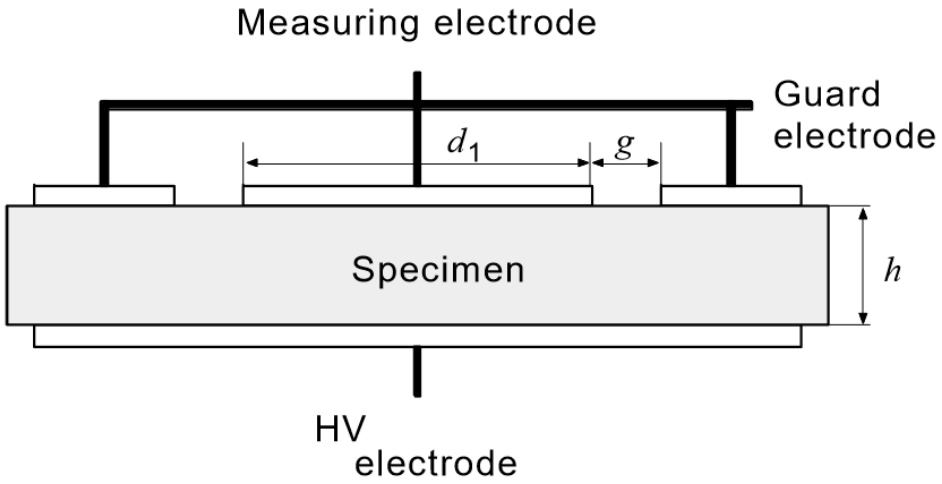


**Figure 3.8** Cylindrical electrode with guard ring for disk specimen [186].

### 3.3.4.2 Volume Resistivity

Resistivity is one of the most important insulating properties for the power system. A Keithley 6517B Electrometer was employed to measure the volume resistivity. The same specimen and electrode system used in the dielectric spectroscopy were utilized for this resistivity analysis. This measurement is based on IEC 62631 test standard [186].

### 3.3.4.3 Electrical Tree Growth

The formation and growth of electrical trees represent a primary failure mechanism in high-voltage insulation systems. The experimental setup and the specimen used in this test are illustrated in **Figure 3.9**. A needle was embedded in the epoxy resin and connected to the high voltage source. The ground electrode was placed to the opposite

surface of the specimen. Silve paste was applied to that surface to improve the conductivity. The whole assembly was immersed in silicone oil to prevent surface flashover. The 50 Hz AC high voltage supply (Hipotronics 700 Series) was employed. Step voltage starting from 9 kV and up to 23 kV was used to initiate the tree growth. After initiation, 15 kV was applied for tree propagation. An optical microscope equipped with a digital camera was used to monitor and record the tree development process.

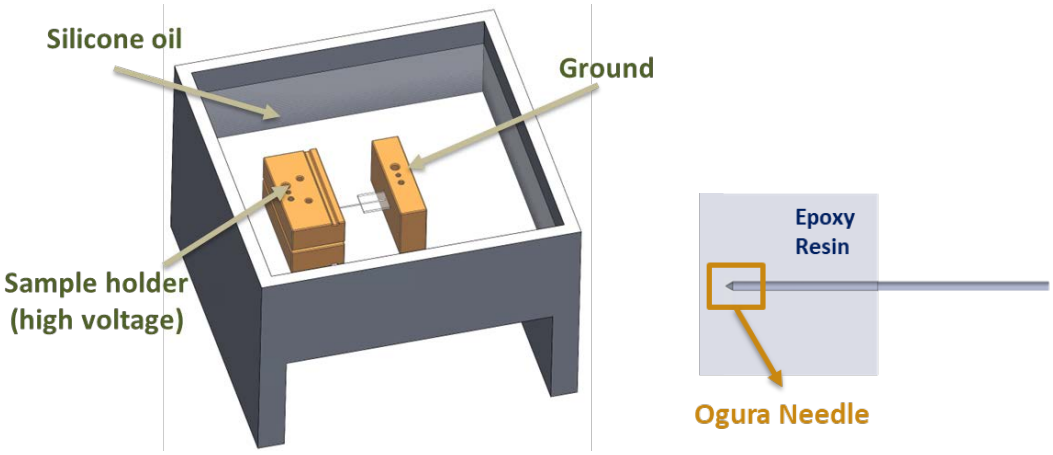


**Figure 3.9** The experimental setup and specimen embedded with needle for dielectric tree growth testing.

### 3.3.4.4 Dielectric Breakdown Strength

The dielectric breakdown strength was measured using thin film specimens of 200 μm thickness, placed between cylindrical electrodes and immersed in silicone oil, as illustrated in **Figure 3.10**. The test setup utilized the same high-voltage source as the electrical tree growth experiments, following ASTM D149 standard procedures [187]. A preliminary test with a constant voltage increasing rate of 0.5 kV/s was performed to establish testing parameters. Based on these results, the initial voltage was set at 50% of the short-time breakdown voltage. The step-stress method was then implemented, applying 1 kV increments at 20-second intervals until breakdown occurred.

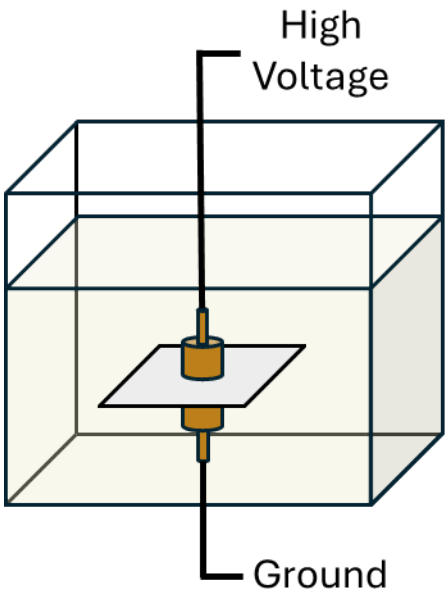


**Figure 3.10** Experimental setup for AC dielectric breakdown test.

Statistical analysis of at least 10 breakdown events was conducted using a two-parameter Weibull distribution, as shown in Equation 3.1. $F$ denotes the probability of failure at a given electrical stress. $E$ is the measured breakdown strength. $\alpha$ is the scale parameter, and $\beta$ is the shape parameter. The characteristic breakdown strength was determined at 63.2% failure probability.

$$F(E;\alpha,\beta) = 1 - \exp\left\{-\left(\frac{E}{\alpha}\right)^{\beta}\right\} \qquad (Equation\ 3.1)$$

### 3.3.5 Mechanical Properties

The tensile properties was tested based on ASTM D638 test standard [188]. The dog-bone-shaped test samples with a thickness of 2.5 mm, a width of 3.18 mm, and a gauge length of 7.62 mm were used.The detailed dimension of the specimen is illustrated in **Figure 3.11** and **Table 3.3**. The tensile test was conducted by a universal testing machine (Instron 5567) or a Shimadzu AGS-X mechanical tester. The strain rate, which indicates the rate of motion of the grips during the test, was set as 1 mm/min. Tensile strength and Young's modulus

were measured by this test. The hardness was measured using a MITECH MH180 Leeb Hardness Tester.

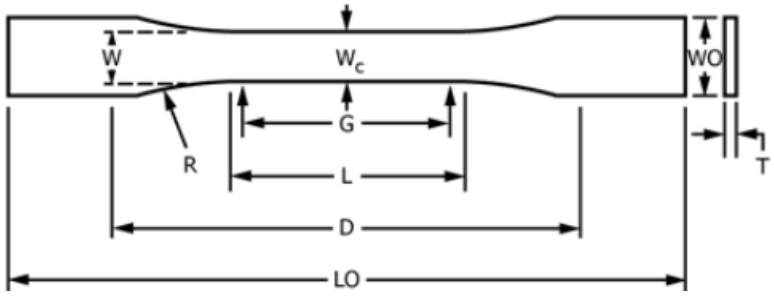


**Figure 3.11** Drawing of tensile testing samples.

**Table 3.3** Dimensions of tensile testing samples

| **Dimensions (see drawing)** | Specimen dimensions (mm) |
|---|---|
| W—Width of the narrow section | 3.18 |
| L—Length of the narrow section | 9.53 |
| WO—Width overall | 9.53 |
| LO—Length overall | 63.5 |
| G—Gage length | 7.62 |
| D—Distance between grips | 25.4 |
| R—Radius of fillet | 12.7 |

### 3.3.1 Accelerated Degradation Tests

Accelerated degradation tests were conducted under two distinct conditions to evaluate long-term material stability. One is the thermal aging test without humidity control based on the standard IEC 60505 [30] using an oven with a stable temperature of 105 ℃. The selection of this temperature was according to the recommendation that the test temperature should be below the $T_g$ measured by DMA, which is 135 ℃ for the epoxy samples in the

current study. The relative humidity under 24℃ in the lab is 60%, the relative humidity in the 105℃ oven is calculated as 1.44%. Another one is hygrothermal aging performed in an environmental chamber under combined conditions of 95°C and 95% relative humidity for a duration of 1200 hours.

# Chapter 4

## Effects of Voids and Thermal Aging on The Mechanical and Dielectric Property of Epoxy Resin

*This chapter explores combined impact of voids and thermal aging on epoxy properties. Specimens with varying void content are thermally aged at 105°C for up to 1000 hours, and tensile strength, dielectric behavior, and molecular composition are analyzed using tensile tests, SEM, ATR-FTIR, and UV-Vis spectrometry. Thermal aging induces chain scission, oxidation, and surface chemical inhomogeneity, while the core remains less affected. Voids serve as stress concentrators, initiating cracks and reducing tensile strength. A defect density parameter ρ, is integrated into Weibull analysis to quantify the synergistic effects of voids and aging, revealing notable strength reduction and increased data variability with higher ρ. These findings underscore the importance of addressing void and aging effects through Weibull analysis for reliable epoxy-based material design.*

---

*This section is published substantially in Polymer Degradation and Stability, Sep 2023. https://doi.org/10.1016/j.polymdegradstab.2023.110455. No written permission is necessary for thesis purpose, Copyright 2023 Elsevier.

and published substantially in 2023 International Symposium on Electrical Insulating Materials (ISEIM), Sep 2023. https://doi.org/10.23919/ISEIM60444.2023.10329098. No written permission is necessary for thesis purpose, Copyright 2023 The Institute of Electrical Engineers of Japan.

## 4.1 Introduction

The employment of polymeric materials in advanced electronic devices and electrical power systems as insulators, capacitors, and energy storage apparatus, has gained increasing attention recently [31], [189], [190], [191], [192], [193], [194]. Epoxy resin, which presents high resistance against chemical corrosion, adequate dielectric ability, good workability and low cost, are one of the polymers widely used in these fields [16], [86], [127], [195], [196].

When used in electronic devices and electrical equipment, polymeric materials are required to withstand high voltage and high heat flux [31], [32]. The excessive heat is easily accumulated and causes the increasingly severe thermal aging, limiting the service life of the apparatus [33], [34]. Recently, numerous researchers have reported the solutions by introducing fillers with high thermal conductivity and forming heat transfer networks [197], [198], [199], [200], [201]. However, only a few literatures have been devoted to exploring the thermal aging phenomenon of polymers [202], [203], even though it remains fundamental in epoxy materials and composites. Different stages of the aging process of thermosets were revealed: the mechanical property is enhanced at the beginning due to post-crosslinking and then decreased because of the chain scission, accompanied by oxidation of active groups [37], [38], [39]. Interestingly, different aging behaviors were observed in the sample core and skin [36], [40]. However, the increase in flexural modulus and the reduction in break strain indicate an enhanced cross-linkage of the bulk. This finding is in contradiction with the previous results, and further investigation is required for greater clarity. Furthermore, the brittleness and degree of scatter in the strengths increased over the aging time [36], [41], indicating increased mechanical scattering, emphasizing the need for further analysis to accurately determine the impact of such fluctuations on reliability. Given this background, it is crucial to evaluate the thermal aging behavior of epoxy resin and reveal the principles behind it. Such a study could provide useful information for material design as well as lifetime prediction for practical usage.

In addition to thermal challenges, the inherent brittleness of epoxy resin [58] and unavoidable voids [57] introduced during the manufacturing process further limit its mechanical reliability, affecting its reliability and limiting its application. Numerous researchers have proposed effective approaches to improve brittleness by incorporating micro- or nano-sized fillers [204], [205], [206], [207]. However, there is still a lack of discussion on the topic of void defects within the material. The randomly distributed voids are air bubbles that are inevitably introduced during the molding process due to the high viscosity of the solution [55], [57]. Some researchers have established the method to detect and analyze void defects [208], [209], studied the factors affecting void formation during the liquid molding process, and proposed some models as well as solutions [55], [210], [211], [212], [213]. As mechanical stresses are always concentrated near localized defects like voids, defects act as the initiation point of failure [58], [214], resulting in a decrease in the mechanical properties of the material, such as reduced strength [55], [209] with increased standard deviation [215]. These adverse effects will ultimately affect the mechanical performance and reliability of the equipment using the materials. Thus, it is essential to understand the impact of voids on the mechanical property of the material. However, little attention has been paid to the quantitative impact of voids on the reliability of epoxy resin, which is crucial for evaluating its quality in practical applications [215].

Given this background, void defects and thermal aging emerge as key factors that increase variability in the mechanical properties of epoxy resin, ultimately diminishing its reliability. Thus, studying the combined adverse effects of void defects and thermal aging, as well as uncovering the underlying aging mechanisms, is essential for designing more durable and reliable epoxy-based materials.

To evaluate these effects more precisely on mechanical reliability, it is necessary to employ statistical analysis on the mechanical data of a large number of specimens, which provides more information than simply averaging the data of a few samples. Weibull distribution, a well-known statistical model, as reviewed in 2.1.5.4, has the potential to describe the failure strength and evaluate the reliability of epoxy resin with voids and/or after thermal aging. Employing Weibull distribution is expected to improve the accuracy when

describing the mechanical reliability of epoxy resin under practical conditions and provide more accurate information to the industry.

Herein, this study aims to investigate the combined effects of void defects and thermal aging on the mechanical reliability of epoxy resin. Specimens in large quantity are prepared and thermally aged. Tensile measurement, electrical characterization, SEM, finite element simulation and FTIR are employed in this research. Statistical analysis is employed to improve the accuracy of the mechanical property evaluation. The outcomes of this research are expected to yield significant insights that could aid material refinement and facilitate precise lifetime prediction.

## 4.2 Experimental details

### 4.2.1 Materials

Epoxy resin solution (ARALDITE® LY 5052) and hardener (ARADUR® 5052 CH) was provided by Huntsman Advanced Materials Americas LLC. Details of their compositions are given in Chapter 3. The two-component silicone rubber (RTV-2) was obtained from Shenzhen Rongxingda Polymer Material Co., Ltd.

### 4.2.2 Synthesis of epoxy resin with different void content

Epoxy resin specimens with different levels of voids were prepared by mixing the epoxy and hardener at a fixed ratio of 1:0.38 via different mixing methods, as shown in **Table 4.1**.

**Table 4.1** Mixing procedure for epoxy resin specimens with a different void content

| Group | Planetary mixing | Centrifugal defoaming | Vacuum degassing | Manual mixing |
|---|---|---|---|---|
| **L**- expected low void content | Yes | Yes | Yes | No |

| | | | | |
|---|---|---|---|---|
| **H**- expected high void content | Yes | No | No | Yes |

The mixture was poured into a silicone mold for curing. The mold was pressed by a metal block to ensure an even sample surface. Teflon cloth was placed between the mold and metal block to enable release of cured samples after curing. The epoxy resin was cured at room temperature for 24 hours and then post-cured at 100℃ for 4 hours. DMA was then used to measure the $T_g$ of epoxy resin, which is 135℃. Then the specimens were ground with sandpaper and stored in a dry box with a relative humidity of 52%.

### 4.2.3 Characterizations

#### 4.2.3.1 Void Detection

To obtain the void distribution of the sample surface, the optical images of the sample surface were obtained by the DSX1000 digital microscope. Specifically, 3 rectangular specimens of each group were randomly selected. Bright-field and mixed illumination were used in the measurement. The samples were slightly ground and polished to get a smooth surface for high-quality imaging. Then the distribution of void defects on the images was statistically analysed by the OLYMPUS by the Stream image analysis software.

#### 4.2.3.2 Thermal Aging

The thermal aging was conducted based on the standard IEC 60505 using an oven with a stable temperature of 105 ℃. The relative humidity at 24℃ in the lab is ~60%, and the relative humidity in the 105 ℃ oven is calculated to be 1.44%.

Tensile specimens with different void content (60 specimens for each group) for statistical analysis were aged for 1000h at 105 ℃ to study the combined effect of voids and thermal aging. Besides, another thermal aging test was conducted for specimens with low void level

under the same environment with different aging time (0 h, 60 h, 120 h, 288 h, 480 h, 576 h, 672 h, 792 h and 984 h) to observe the variation of strength with aging time.

#### 4.2.3.3 Mechanical Characterization

The mechanical properties of epoxy resin were measured using an Instron universal 5567 testing machine based on the ASTM D638 standard. A load cell of 30 kN and a strain rate of 1 mm/min were selected in this test. The testing samples are bone-shaped with a thickness of 2.5 mm, a width of 3.18 mm and a gauge length of 7.62 mm.

#### 4.2.3.4 Dielectric Tree Growth

Electrical tree growth was characterized to reveal the dielectric breakdown mechanism. Silver paste was painted on the bottom surface of the specimen to improve the electrical contact of the sample to the ground electrode. The specimen was immersed in silicone oil during tests to avoid surface charge. A 50 Hz AC dielectric testing system was utilized to provide a voltage source. Step voltage ranging from 9 kV to 23 kV was applied to initiate the electrical tree. Then the specimen was stressed under 15 kV for 10 minutes to get the tree propagation. Leica Emspira 3 digital microscope was equipped to record the in-situ tree growth. Olympus DSX 1000 digital microscope was used to acquire the high-resolution images after tree growth.

#### 4.2.3.5 Chemical Structure Analysis

UV-Vis spectrum obtained by the Shimadzu UV 2700 was analysed to study the chemical change of epoxy resin during thermal aging process. Fourier-transform infrared (FTIR) spectroscopy was used to identify the change of chemical bonds of epoxy resin after the curing and after the thermal aging process. The FTIR MIR/NIR Frontier (Perkin Elmer) machine with and without the attenuated total reflectance (ATR) mode was employed. The light source with a wavelength range of 4000-600 $cm^{-1}$ (with ATR for solid samples) and 4000-500 $cm^{-1}$ (without ATR for liquid samples) with 32 scan accumulations was selected

with a resolution of 4 $cm^{-1}$. The spectra were analyzed by the software Spectrum (PerkinElmer)

#### 4.2.3.6 Fractographic analysis

To understand the morphology of the fracture surface of epoxy resin after tensile failure, a field emission scanning electron microscope (FESEM 7600F) was used with an operating voltage of 5kV. Platinum was coated on the surface of the sample in combination with the use of conductive tapes to obtain high-quality SEM images for this insulation polymer.

#### 4.2.3.7 Weibull Statistical Analysis for The Mechanical Reliability

Large data of tensile strength for Weibull analysis was obtained by mechanical measurement. The nomenclature and description of these specimen groups are listed in **Table 4.2**.

**Table 4.2** Nomenclature and descriptions of specimens for statistical analysis

| Group | Specimen volume | Description |
|---|---|---|
| L | 60 | Low void content, unaged |
| H | 60 | High void content, unaged |
| L-a | 60 | Low void content, 105 ℃ aged for 1000h |
| H-a | 60 | High void content, 105 ℃ aged for 1000h |

## 4.3 Results and Discussion

### 4.3.1 Effect of Voids on Mechanical Properties

#### 4.3.1.1 Characterization of void content

For groups L and H, 3 rectangular samples of each were randomly selected for void detection to obtain reliable results on void size and density. To remain more details,

hundreds of optical microscopic (OM) images with high magnification were captured under mixed lighting condition with the same focal length, and then merged as one image like a puzzle, as shown in **Figure 4.1**.

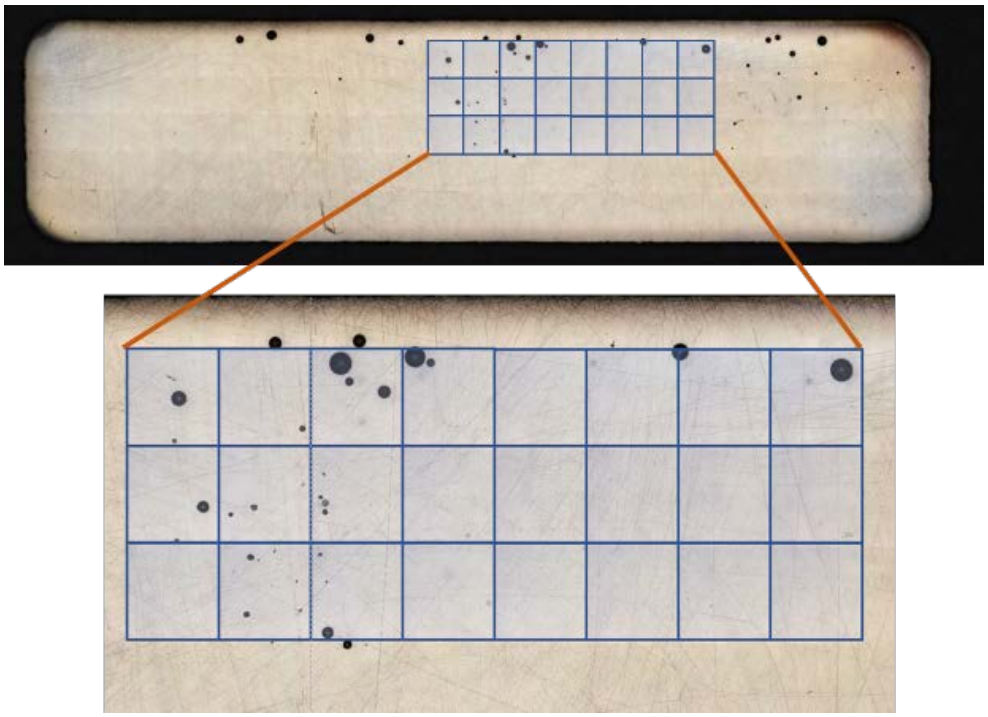

**Figure 4.1** The draft of image combination. Each blue box represents one single image with high magnification.

The merged photos for group L and H are shown in **Figure 4.2(a)** and **Figure 4.2(b)**. There were more densely distributed void defects in H samples than in L samples, illustrating the successful preparation of specimens with different content of void defects. To quantify the void distribution of the sample surface, BF imaging was used to scan the whole sample due to the high contrast and clear illustration of the surface defects. Images taken under high magnification were merged as one image for voids counting. Then the void area was manually classified in the software as shown in **Figure 4.2(c)**. Due to the high resolution and relatively low number of voids, the overlapping of voids was not observed, ensuring the accuracy of the voids distribution analysis.

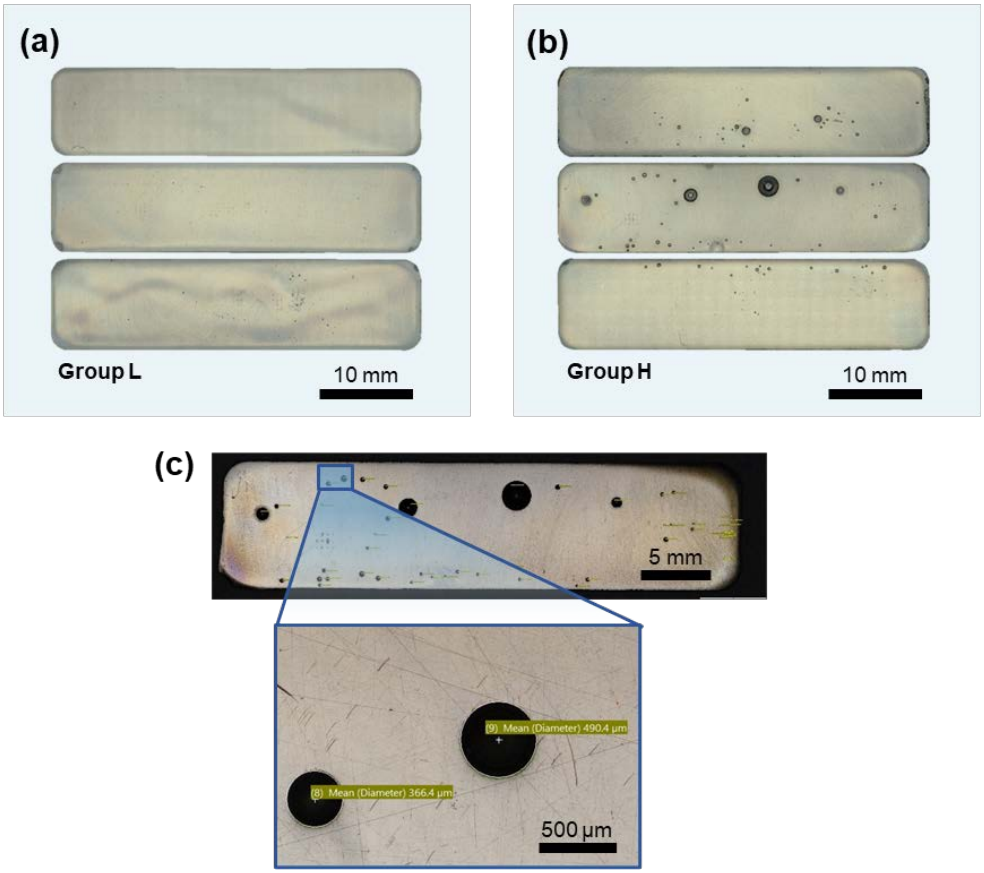


**Figure 4.2** Examples of specimens. **(a, b)** The merged optical images of specimens of group L and H**. (c)** An example of void detecting process.

To obtain an accurate statistical result of the void distribution, the voids of 3 samples were counted and analyzed. The results are shown in **Figure 4.3**. Group L presents fewer total void number, lower void ratio (defined as the total surface area of void over the total sample surface), smaller average size, and narrower size distribution than group H as shown in **Figure 4.3(a)** and **Figure 4.3(b)**. This reveals that conventional hand mixing can easily introduce voids in both the number and size, consequently increasing the void ratio.

The fraction of void area with different sizes on the whole porous area is shown in **Figure 4.3(c)**. For groups L and H, the largest area was respectively contributed by voids with a diameter of 50-100 µm, and above 500 µm. It is notable in group H that even though the number of voids decreases with the size increasing, the void with a diameter larger than

500 μm still provides 61% of the total void area. It can be concluded that voids with larger sizes have a greater impact on the overall porosity of the material [54], which is supposed to affect the reliability of this material during mechanical testing. The specific evaluation number of void level of those samples were counted together and summarized in **Table 4.3**.

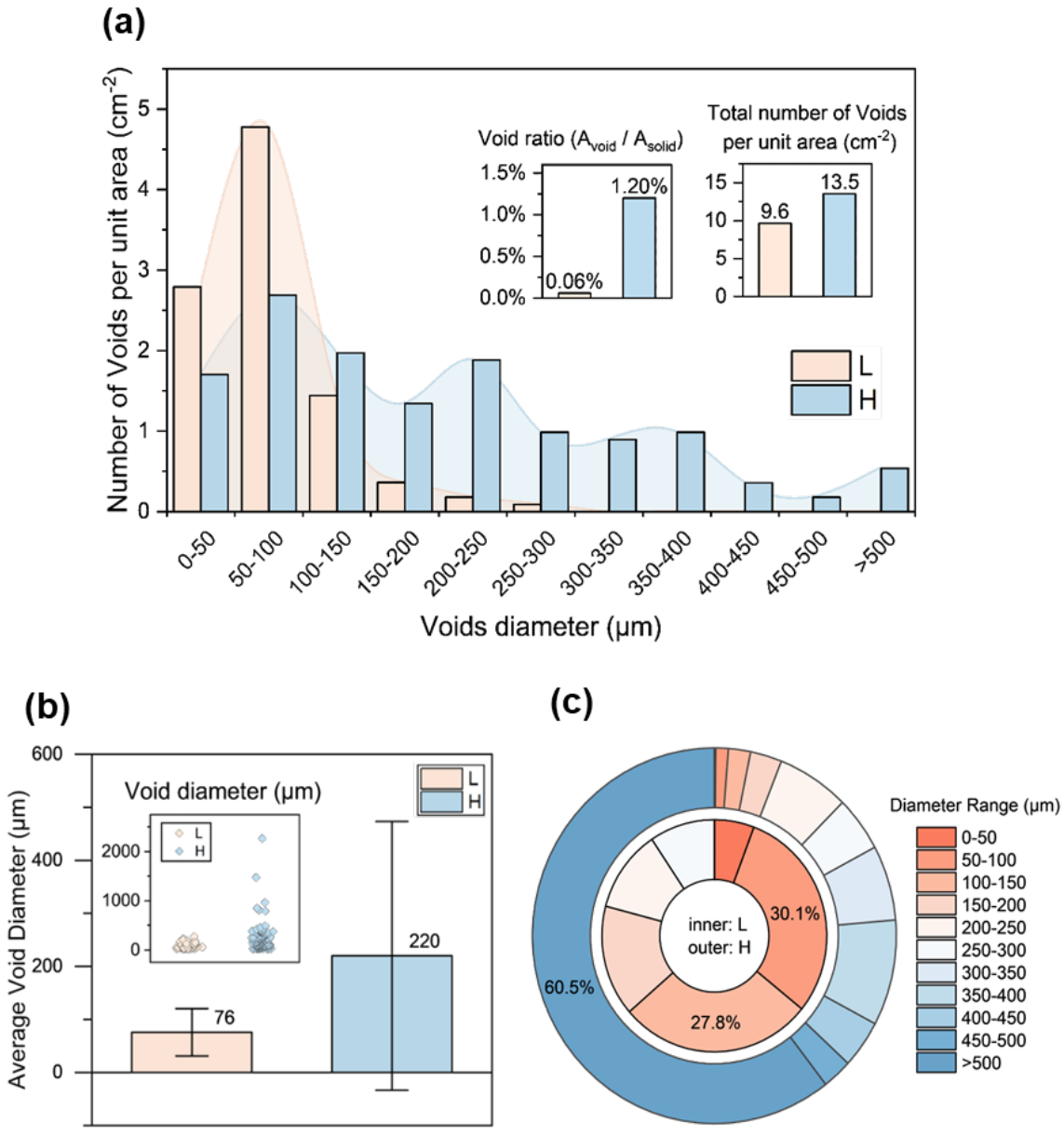

**Figure 4.3** Statistical analysis of voids. **(a)** Void size distribution and void density. **(b)** Average void diameter and column scatter graph of void size. **(c)** The area proportion of void within specific size ranges in total void area**.**

**Table 4.3** Void size and density of different groups

| Group | Voids level | Number of Voids per unit area ($cm^{-2}$) | Void Diameter Range (μm) | Average Diameter (μm) | Fractional area of voids on the surface |
|---|---|---|---|---|---|
| L | low | 9.6 | 19 - 271 | 76 | $5.9 \times 10^{-4}$ |
| H | high | 13.5 | 21 - 2265 | 220 | $1.2 \times 10^{-2}$ |

#### 4.3.1.2 Mechanical Properties for Specimen with Various Void Level

60 specimens for each group were tested by the universal testing machine (Instron 5567) based on the standard ASTM D638. The average strengths of the groups with different void levels are listed in **Table 4.4**.

**Table 4.4** Average strength of groups L and H.

| Group | Voids level | Number of Voids per unit area ($cm^{-2}$) | Average Void Diameter (μm) | Tensile specimen amount | Average strength $\sigma_0$ (MPa) | Standard deviation |
|---|---|---|---|---|---|---|
| L | low | 9.6 | 76 | 60 | 71.1 | 2.65 |
| H | high | 13.5 | 220 | | 65.3 | 8.16 |

The scatter and box chart of tensile strengths of L and H groups are shown in **Figure 4.4(a)**. A higher average strength is observed in L (71.1 MPa) than that of H (65.3 MPa), accompanied by a lower scattering in group L. Based on our test results, high void defect content can slightly reduce the average strength but severely increase the data scattering of epoxy resin.

**Figure 4.4(b)** presents the simulation results on the stress distribution and crack propagation of a specimen containing a void with a radius of 250 μm. The results indicate that a significant stress concentration is generated at the edge of the void, where the crack will be initiated. The first principal stress ($1^{st}$ PS) near the void reaches 80 MPa and causes crack propagation. Finally, a crack through the void crosses the specimen causing the failure of the specimen, which is also observed in the SEM image as illustrated in **Figure 4.4(c,d)**. The average critical value of the $1^{st}$ PS is 40.8 MPa, which is much lower than the average strength, indicating that the material with void defects cannot fully exert its mechanical properties. The fracture surfaces of typical specimens with and without void were observed by SEM to illustrate the fracture mechanism affected by the void defect, as shown in **Figure 4.4(d,e)**. Relative flat fracture sections are observed, indicating the brittleness of the epoxy specimens. Meanwhile, the river-like fracture striations can be observed. For the specimen with void, the fracture striations are generated from the edge of the void, which confirms that the crack is initiated at the edge of the void. The fracture section of the specimen is flatter, accompanied with a higher tensile strength (60.1 MPa) compared to the specimen with the void (39.9 MPa).

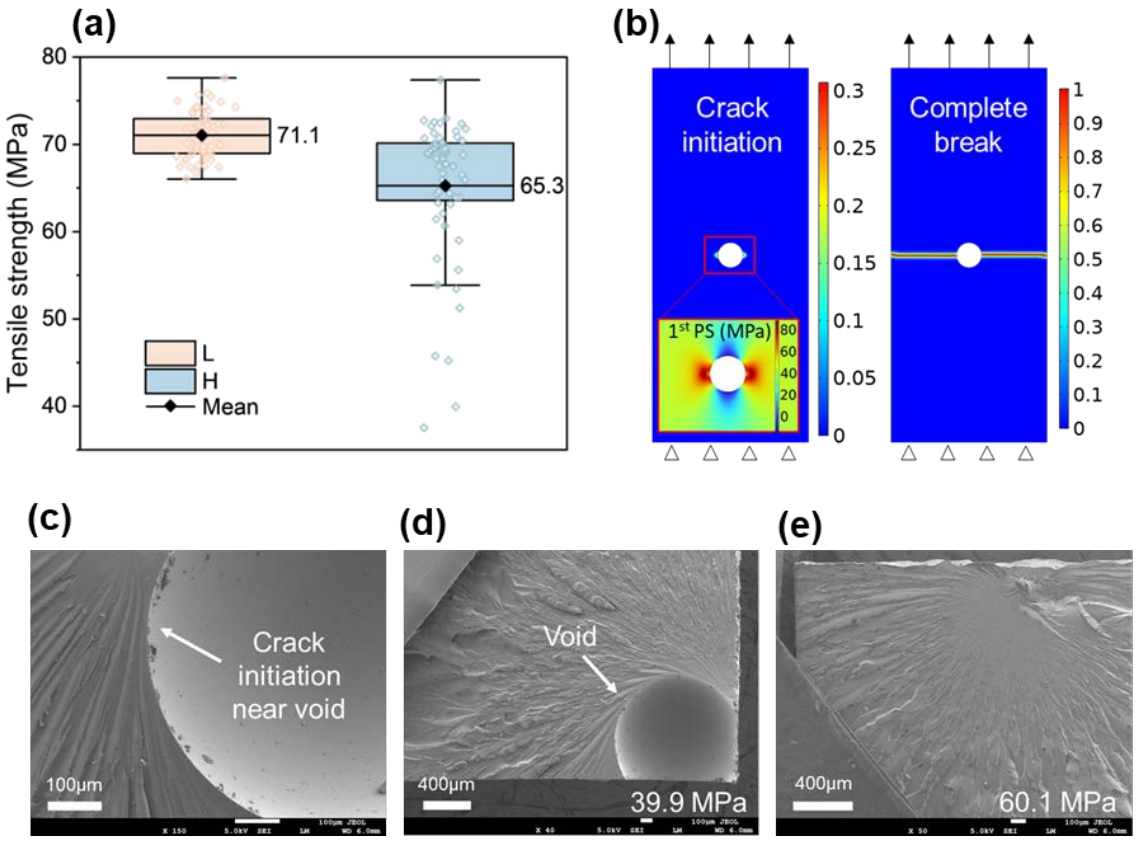


**Figure 4.4** Tensile strength and failure mechanism. **(a)** Scatter and box chart of tensile strengths for L and H. **(b)** Damage phase-field simulation model. **(c)** The magnified SEM image of the void edge. **(d, e)** SEM images of the fracture surface of typical specimens with and without void defect

### 4.3.2 Effect of Thermal Aging

#### 4.3.2.1 Change in Tensile Strength

The change of the failure strength with aging time is plotted in **Figure 4.5**. Two periods can be seen during the aging process [39]: The first one is the increasing period where continued curing occurs. This is because that the epoxy resin is not completely cured after the recommended curing by the supplier. With the continued heating, continued curing at 105 ℃ increases the degree of cross linking and the failure strength reaches 110 % (75 MPa) of the initial failure strength (69 MPa). The aging effect may exist during this period, but the post-curing dominates. After this period (~300 h), the strength starts to decrease,

reaching 41 MPa after 984 h aging. During this period, the effect of thermal aging determines the strength of the material.

With the aging time increasing, the strength of epoxy resin increased at the beginning from 69 MPa to 75 MPa and then decreased to 41 MPa at the end of the tests. A similar peak of failure strength of polyurethane in the aging process is obtained by Tcharkhtchi et al. [39] Two periods can be concluded during the aging process:

- The increasing period: from 0h to 288h.
  The epoxy resin was not completely cured after the recommended curing by the supplier. With the continued heating in the degradation study, its failure strength reached 110% of the initial failure strength due to post-crosslinking under 105 ℃. The aging effect may exist, the post-curing contributed more during this period.

- The decreasing period: from 288h to the end of the test.
  During this period, the strength of epoxy resin decreased from the highest point to 61% of the unaged failure strength finally. The crosslinking of epoxy resin was almost completed before this stage and the effect of thermal aging played a more essential role.

With the fitted curves from data points with decreasing strength as shown in **Figure 4.5**, the failure strength of epoxy resin is predicted to reach 50% when the aging time reaches 1640 h, which can be regarded as the end of the service lifetime of electrical insulators according to IEC 60216-2 standard.

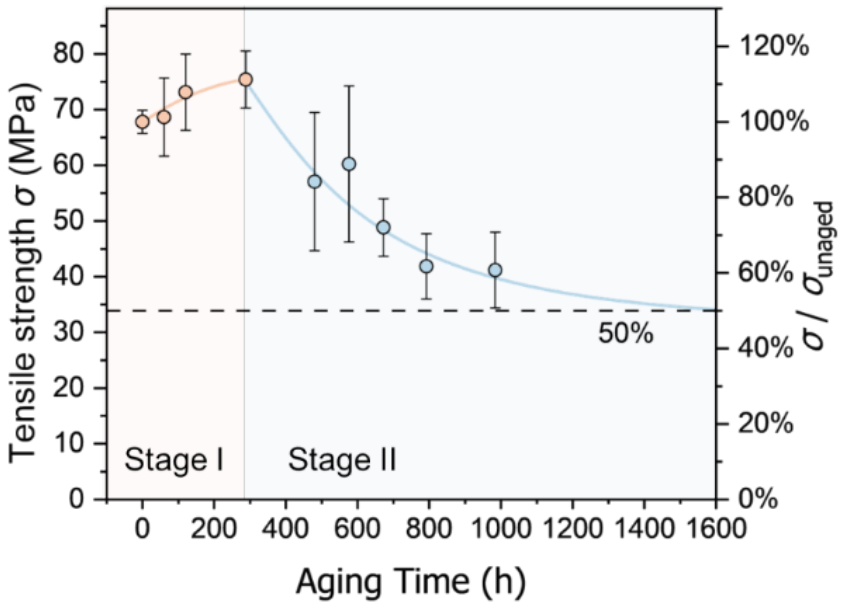


**Figure 4.5** Variation of failure strength with different aging time.

#### 4.3.2.2 Change in Dielectric Performance

The electrical tree was firstly initiated by step increasing voltage and then propagated for another 10 minutes under 15 kV. Examples of electrical trees in unaged and 1000 h-105 ℃-aged epoxy resin after the 10 minutes of propagation are shown in **Figure 4.6**. A branch-like tree forms in the unaged specimen, while a short bush-like tree forms in the aged sample. More specific parameters characterizing the tree growth are summarized in **Table 4.5**. The tree length is defined as the maximum length between the tree tip and the needle tip that is parallel to the electrical field, and the expansion coefficient is the ratio between the longest lengths that are parallel and perpendicular to the electrical field. After thermal aging, the electrical tree initiation voltage becomes higher, and the electrical tree propagated under the same condition becomes shorter but denser, indicating a slower growth rate calculated by the tree length.

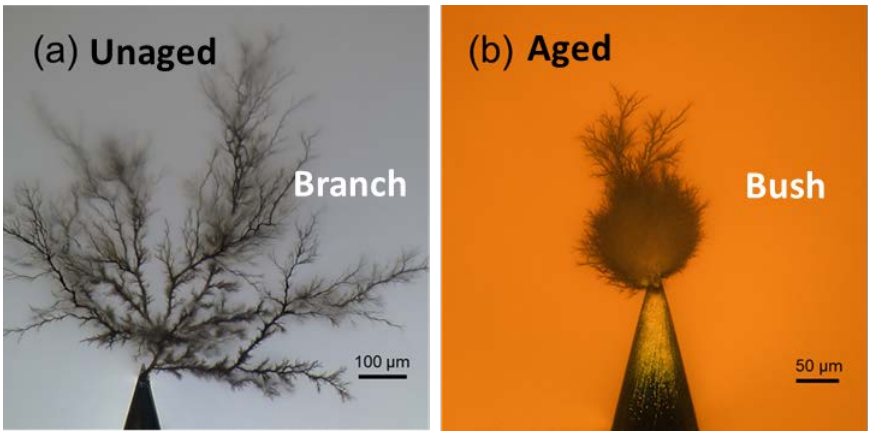


**Figure 4.6** Electrical tree propagated for 10 min under 15 kV. **(a)** Unaged epoxy resin. **(b)** Aged (1000 h, 105 °C) epoxy resin.

**Table 4.5** Electrical Tree Initiation and Propagation for Unaged and Aged Epoxy Resin

| Aging condition | Tree initiation voltage (kV) | Propagated tree length (µm) | Expansion factor | Growth rate (µm/min) |
|---|---|---|---|---|
| Unaged | 14 | 702 | 0.64 | 64.2 |
| Aged | 20 | 242 | 1.52 | 8.17 |

#### 4.3.2.3 Chemical Change

**1) Reaction of Epoxy Resin During Curing**

FTIR was employed to investigate the chemical change of epoxy resin before and after curing. The characteristic peaks, which are similar to the results revealed by other researchers [29], [216], are combined and listed in **Table 4.6**. FTIR spectra of epoxy resin solution, hardener and cured epoxy resin are shown in **Figure 4.7**.

**Table 4.6** Characteristic bands for epoxy resin solution, hardener and cured epoxy resin.

| Band ($cm^{-1}$) | Assignment |
|---|---|
| ≈ 3500 | O-H stretching |
| 3060 | Stretching of C-H of the oxirane ring |
| 2965- 2873 | Stretching C-H of $CH_2$ and CH aromatic and aliphatic |

| | |
|---|---|
| 1713 | C=O |
| 1648 | C=C |
| 1608 | N-H |
| 1509 | Stretching C-C of aromatic |
| 1448 | Deformation C-H of $CH_2$ and $CH_3$ |
| 1368 | Deformation $CH_3$ of C-$(CH_3)_2$ |
| 1107 | aliphatic C-O-C of ethers |
| 1036 | aromatic C-O-C of ethers |
| 915 | Stretching C-O of oxirane group |
| 831 | Stretching C-O-C of oxirane group |
| 772 | Rocking $CH_2$ |

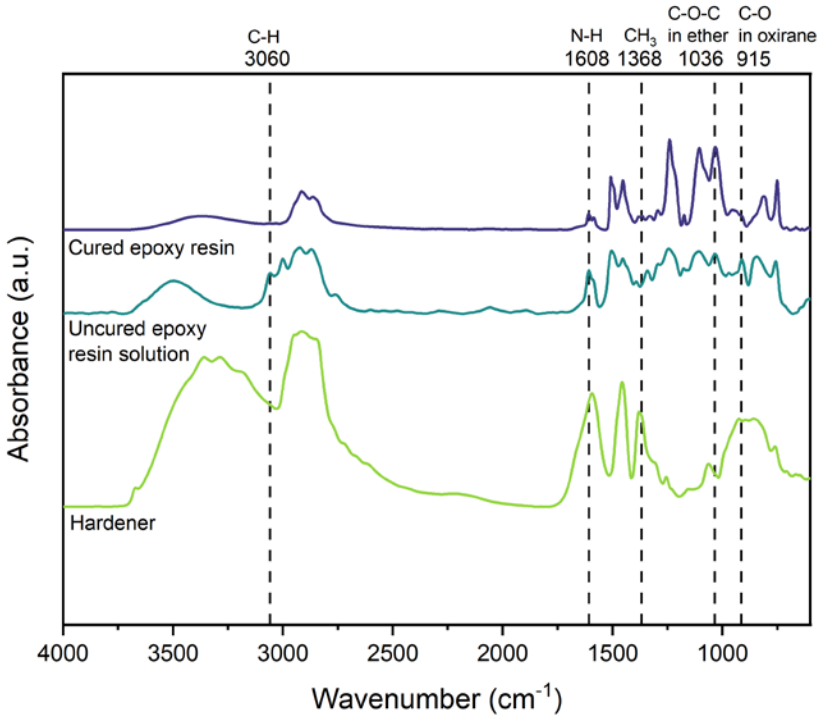


**Figure 4.7** FTIR spectra for uncured/cured epoxy resin and hardener.

The curing reaction has 3 steps as shown in **Figure 4.8**. For the first 2 steps, epoxy concentration is supposed to decrease due to the mechanism of the reaction, and this is observed in the spectra as the decrease of C-O in oxirane at 915 $cm^{-1}$, N-H bond at 1608

$cm^{-1}$ and C-H in oxirane at 3060 $cm^{-1}$. The increase of C-O-C band of ethers at 1036 indicates the crosslinking via etherification, which is step (c). The decrease of $CH_3$ band of $C-(CH_3)_2$, which is usually the end of the molecular chain, also indicates the increment of crosslinking.

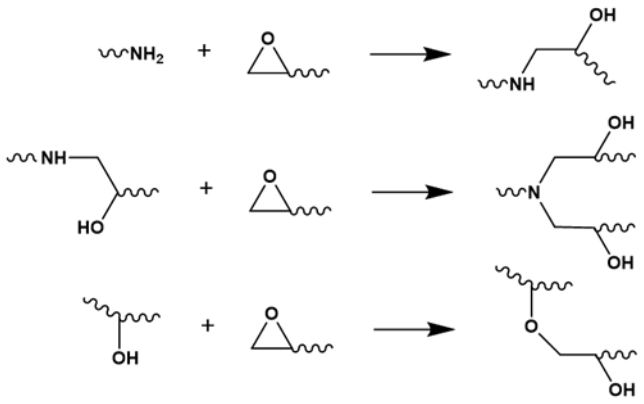


**Figure 4.8** Chemical reactions during curing of epoxy resin.

### 2) Color Change in Aging Process and UV-Vis Results

As discussed before, the mechanical property of epoxy/amine resin is severely weakened by long-term thermal aging, while the impact on electrical properties is relatively small. To further clarify the mechanism, the chemical change of epoxy resin with various thermal aging durations is characterized. As aging time increases, the colour of epoxy resin becomes deeper from light beige to dark brown, as shown in **Figure 4.9**. This color change indicates the chemical change. UV-Vis is used to evaluate the chemical reason for this color change, as shown in **Figure 4.10**. With thermal aging, the absorbance from 350 to 600 nm increases, identifying the formation of quinone methide [217], which leads to the discoloration of epoxy/amine resin.

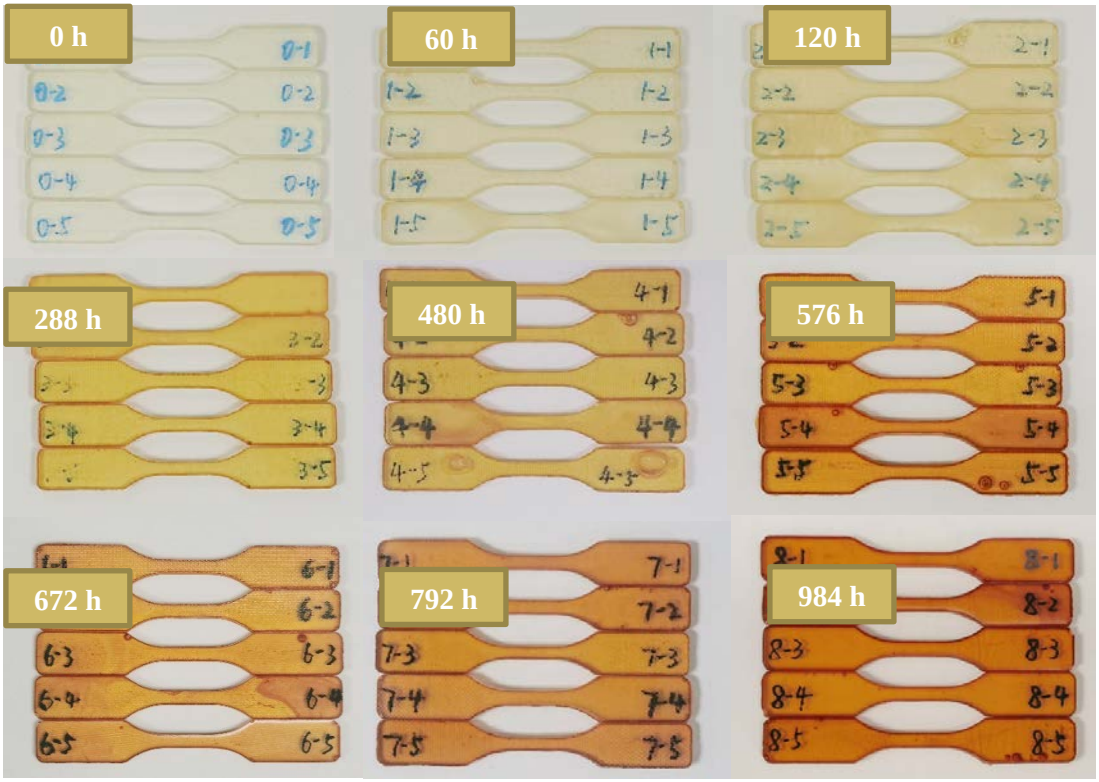


**Figure 4.9** The color change of epoxy resin under 105℃ with different aging time.

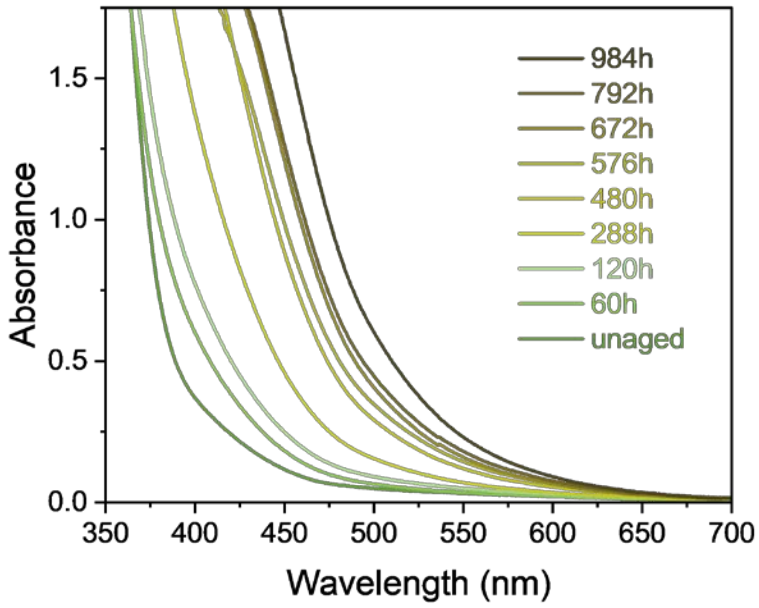


**Figure 4.10** UV-Vis curves for epoxy resin under various aging time durations.

### 3) FTIR Change in Aging Process

ATR-FTIR spectroscopy was utilized to further investigate the chemical change of epoxy resin during thermal aging. As shown in **Figure 4.11(a)**, the intensities of C=O at 1713 $cm^{-1}$, C=C at 1648 $cm^{-1}$ increase with the aging time, indicating the oxidation and chain scission in resin network[29]. However, the peak intensities of aliphatic and aromatic ether bonds (1107 $cm^{-1}$ and 1032 $cm^{-1}$, respectively) rise and subsequently fall, as illustrated in **Figure 4.11(b)**. This peak indicates the formation of ether due to post-curing and the following degradation of the same bond, revealing the initial increase and subsequent decrease of the crosslinking degree, which can explain the peak that occurred in the tensile strength.

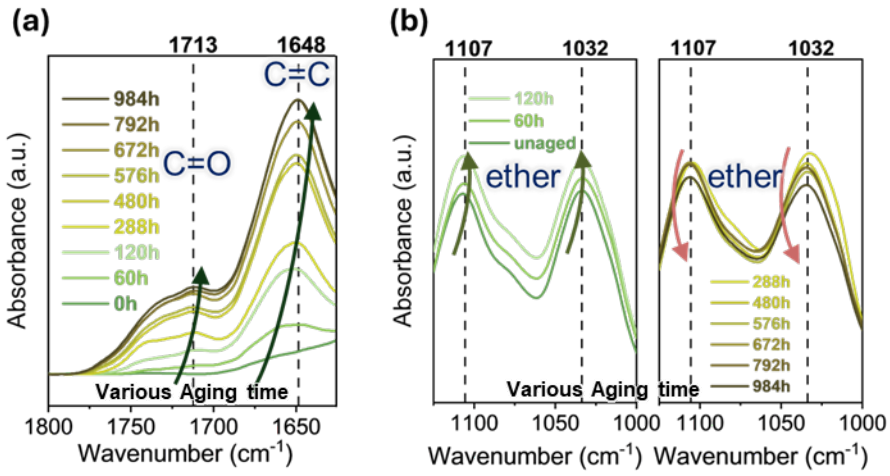


**Figure 4.11** FTIR spectra of epoxy/amine resin thermally aged for various durations, showing chemical bond variations over time. **(a)** Spectra with wavenumber from 1800 $cm^{-1}$ to 1625 $cm^{-1}$. **(b)** Spectra with wavenumber from 1125 $cm^{-1}$ to 1000 $cm^{-1}$.

However, the impact of thermal aging on the electrical tree growth is not the same as that on tensile strength. The tensile strength is highly dependent on the weakest point, especially the ones on the surface, while the electrical tree growth is mainly decided by the core material near the needle tip, which is deeply embedded in the bulk material. Thus, the

different trends exhibited in mechanical strength and electrical performance possibly indicate a heterogeneous degradation in the epoxy/amine resin.

To confirm this hypothesis, the surface layer of the 105°C-984h-aged epoxy resin was successively removed for up to to 0.3 mm in depth, to investigate the chemical structure at these locations, as shown in **Figure 4.12**.

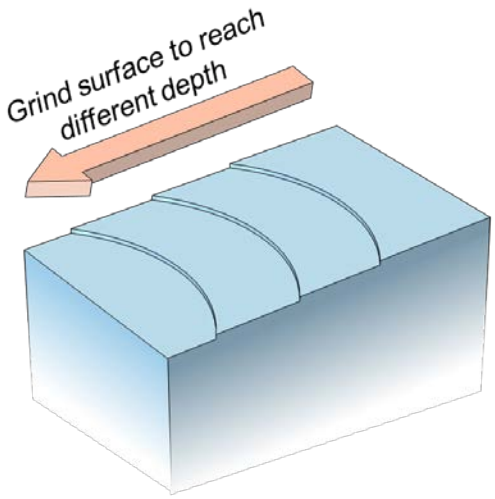


**Figure 4.12** Schematic drawing of surface removal to reach various depths in the specimen.

The corresponding ATR-FTIR results for these layers are illustrated in **Figure 4.13**. As more surface removed, the peak intensities for C=O and C=C consistently drop-down (**Figure 4.13(a)**), revealing a gradual degradation in polymer chains. Notably, in the 0.3 mm depth, the peak intensity of the components is similar to that of the unaged epoxy/amine resin, indicating nearly no degradation in epoxy resin at this depth. The crosslinking degree of epoxy resin can be correlated to the peak intensity of ether at 1107 $cm^{-1}$ and 1103 $cm^{-1}$, as exhibited in **Figure 4.13(b)**. The ascending intensity of the ether bond is observed with thicker surface being removed, and all are higher than the unaged epoxy resin. Thus, the crosslinking degree of the aged epoxy resin is higher than the unaged epoxy resin due to post-curing in the thermal aging process, which can explain the higher tree initiation voltage in the aged specimen.

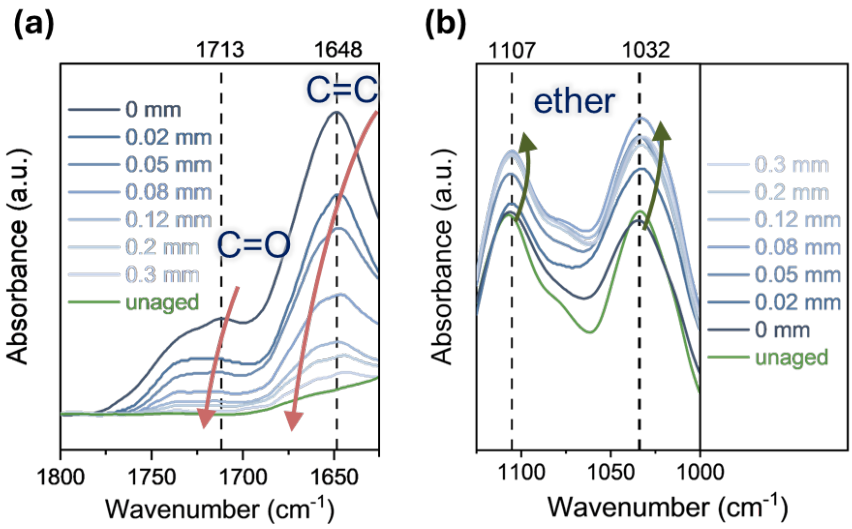


**Figure 4.13** FTIR spectra of epoxy/amine resin thermally aged for 960 hours after sequential surface layer removal, showing depth-dependent chemical changes. **(a)** Spectra with wavenumber from 1800 $cm^{-1}$ to 1625 $cm^{-1}$. **(b)** Spectra with wavenumber from 1125 $cm^{-1}$ to 1000 $cm^{-1}$.

The inhomogeneity in the thermal degradation of epoxy resin is found in this work. The thermal aging process is a combined effect of both post-curing and degradation and is closely related to oxygen and heat diffusion. Even thermal aged for almost 1000 hours, the interior part (more than 0.3 mm to the surface) of epoxy resin still shows no chain scission and even obtains more ether bond

### 4.3.3 Combined Effects of Void Defects and Thermal Aging

#### 4.3.3.1 Results of tensile strength

The tensile strengths of 60 specimens for each group L, H, L-a, and H-a were tested to understand the combined effects of void defects and thermal aging. The preparation method, aging condition and nomenclature can be found in **Table 4.1** and **Table 4.2**. The tensile strengths of the epoxy resin, with different void levels before and after aging, are presented in **Figure 4.14**. More void defects result in lower tensile strength and higher

fluctuation in data, regardless of whether they are measured before or after aging. Meanwhile, thermal aging also causes a severe reduction in tensile strength and an increase in data scatter, as can be seen by comparing L with L-a and H with H-a. Both void defect and thermal aging have significantly affected the mechanical properties of epoxy resin. Furthermore, the combined effect of void and thermal aging is revealed by comparing the results of L and H-a. The average strength of group H-a is merely 45% of that of group L. Additionally, the standard deviation of group H-a is 237% greater than that of group L. This indicates a sharp decrease in the mechanical properties of epoxy resin when void defects and thermal aging simultaneously exist.

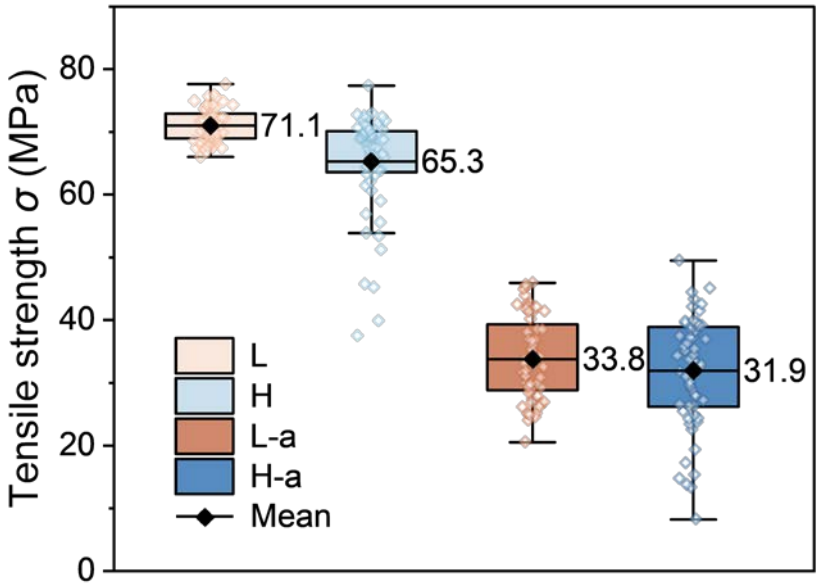


**Figure 4.14** Scatter and box chart of tensile strength of L, H, L-a and H-a.

#### 4.3.3.2 Weibull statistical analysis

Weibull statistical analysis is employed in this study to evaluate the mechanical reliability of epoxy resin affected by the two factors.

The theory behind the Weibull distribution is that the failure of a chain is caused by the failure of the critical link of the chain (the weakest link). The 2-parameter function of the Weibull distribution is shown in Equation 4.1 [70].

$$P = 1 - \exp\left[-\left(\frac{\sigma}{\sigma_0}\right)^m\right] \qquad (Equation\ 4.1)$$

where $P$ indicates the cumulative fracture probability of the samples under a stress $\sigma$. $\sigma_0$ is the scale parameter, and $m$ is the Weibull modulus, which illustrates the scatter extent of the strength.

To describe the impact of the void defect and thermal aging, the parameter $\rho$ representing volume defect density with the unit of $cm^{-3}$ is introduced. The whole material is with a volume of $V$. Thus, the equation can be written as:

$$P = 1 - \exp\left[-\int_V \left(\frac{\sigma}{\sigma_0}\right)^m \rho dV\right] \qquad (Equation\ 4.2)$$

Assume that the defect density is the same in the bulk material tested, the equation becomes:

$$P = 1 - \exp\left[-\left(\frac{\sigma}{\sigma_0}\right)^m \rho V\right] \qquad (Equation\ 4.3)$$

By rearranging this equation, it can be written as:

$$\ln\left[\ln\left(\frac{1}{1-P}\right)\right] = m\ln\sigma + \ln\rho V - m\ln\sigma_0 \qquad (Equation\ 4.4)$$

The above equation presents a linear relationship between $\ln\{\ln[1/(1-P)]\}$ and $\ln\sigma$. In this study, $\sigma_0$ is taken by the average strength and the cumulated probability of failure for $i^{th}$ failed specimen is:

$$P = \frac{i - 0.5}{N} \qquad (Equation\ 4.5)$$

where $N$ is the total number of test specimens and $i$ the sample sequence number when all the test specimens are ranked from the lowest test strength to the highest. Thus, $m$ and $\rho$ can be obtained by plotting $\ln\{\ln[1/(1-P)]\}$ and $\ln\sigma$. The double logarithm curves of L, H, L-a and H-a are plotted in **Figure 4.15(a)**. As shown in this figure, the regression line moves to the left (smaller $\sigma_0$) and becomes flatter (smaller $m$) with the increment of voids and the thermal aging. The lower value of $m$ means a higher degree of scattering of the strength. Thus, voids and thermal aging not only cause the loss in strength, but also increase the fluctuation in mechanical properties. The $m$ observed in the high void content samples (H) is only 26% of that in the low void content samples (L). According to the void distribution analysis discussed in the previous section, group H exhibited a higher void ratio, a greater number of voids, and larger average void size compared to group L. These factors resulted in the significant decrease in the parameter $m$, indicating an increase in data scattering. Meanwhile, thermal aging causes an 81% decrease in $m$ by comparing the results of L and L-a, which reveals that thermal aging will also increase the data scattering. Furthermore, the synergetic effect of voids and thermal aging leads to a significant reduction in $m$, which is merely 11% of the original specimens (L).

The defect density of $\rho$ obtained from the double logarithm curves is illustrated in **Figure 4.15(b)**. The $\rho$ increases with the void content (including void number and size) and the 1000 h thermal aging. With the increment of $\rho$, $m$ and $\sigma_0$ becomes lower, as shown in **Figure 4.15(c)**. This indicates that the high defect density due to voids and thermal aging leads to the loss of strength and increment of data scattering, resulting in poor reliability.

Weibull modulus $m$, average strength $\sigma_0$, defect density parameter $\rho$ and $R^2$ value for the fitted double logarithm curve are summarized in **Table 4.7**. The high $R^2$ value indicating the experimental results are in good agreement with the fitted curve.

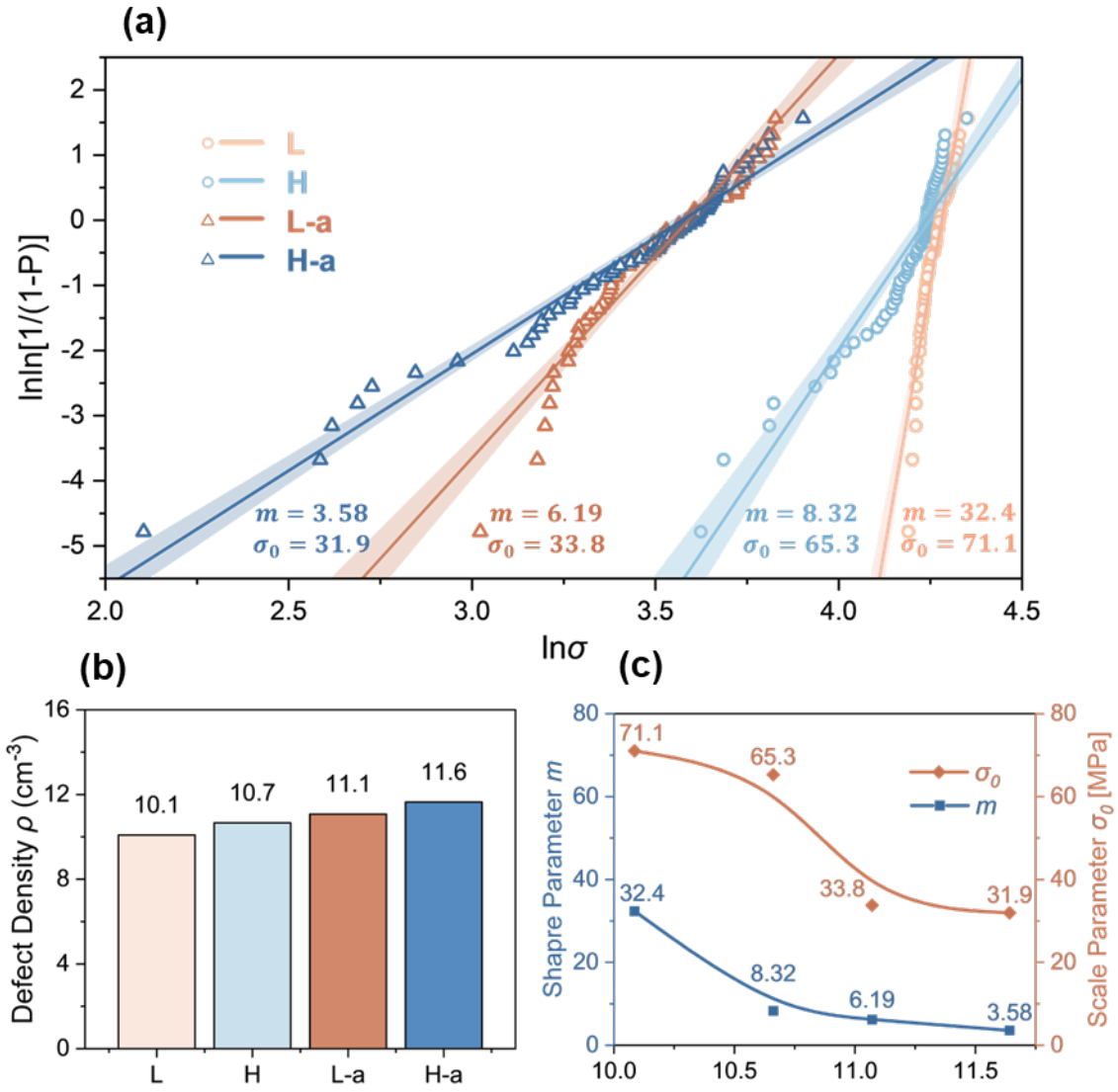


**Figure 4.15** Weibull statistical analysis. **(a)** Weibull plot with shape parameter $m$ and scale parameter $\sigma_0$. **(b)** Defect density parameter $\rho$. **(c)** Relationship between defect density parameter $\rho$ and shape parameter $m$, scale parameter $\sigma_0$.

**Table 4.7** Weibull modulus of groups with different void levels before and after aging.

| Group | Voids level | Aging condition | Weibull modulus *m* | Average strength $\sigma_0$ (MPa) | Defect density parameter $\rho$ | Correlation coefficient ($R^2$) of fitted double logarithm curve |
|---|---|---|---|---|---|---|

| | | | | | | |
|---|---|---|---|---|---|---|
| **L** | low | No aging | 32.4 | 71.1 | 10.1 | 0.90 |
| **L-aged** | | 1000 h, 105 ℃ | 6.2 | 33.8 | 11.1 | 0.93 |
| **H** | high | No aging | 8.3 | 65.3 | 10.7 | 0.90 |
| **H-aged** | | 1000 h, 105 ℃ | 3.6 | 31.9 | 11.6 | 0.97 |

The theoretical probabilities of fracture as a function of tensile strength for groups L, H, L-a and H-a are plotted and compared with the experimental data, as shown in **Figure 4.16(a)**. The distribution moves to the left and becomes wider with the increased void content and after thermal aging, indicating the adverse influence on the mechanical reliability of epoxy resin due to the existence of voids and thermal aging.

To directly illustrate the influence of aging and voids on the mechanical property of epoxy resin, the predicted stresses for low failure probabilities (10%, 1%, 0.01% and 0.0005%) of different groups are indicated in **Figure 4.16(b)** and summarized in **Table 4.8**. Under high-reliability requirements, the theoretical tensile strengths of H, L-a and H-a are reduced compared to L. When 0.0005% failure probability is required, the predicted stress for unaged epoxy resin with low void (L) remains 49.6 MPa. Meanwhile, the predicted stress for the one with high void content (H) is 16.0 MPa, the one after thermal aging (L-a) is 5.06 MPa and the one withstood both two effects (H-a) is merely 1.18 MPa, which is 32%, 10% and 2% of the original strength (L), respectively. However, the average strengths remain relatively high, which are 71.1 MPa, 65.3 MPa, 33.8 MPa and 33.1 MPa for L, H, L-a and H-a, respectively. The results from the Weibull analysis significantly indicate the adverse impact of voids and thermal aging on the mechanical property of epoxy resin, while the influence concluded from simply averaging method is not that severe. Thus, it is important to employ Weibull statistical analysis in the evaluation of the mechanical property of epoxy resin to accurately describe the combined effect of voids and thermal aging when high reliability is required.

It is also notable that the groups processed by the void removal method always show more reliable mechanical properties before and after thermal aging, compared to the groups with

higher void content. For industrial applications, voids should be considered in the lifetime prediction and be effectively removed to obtain a more reliable performance.

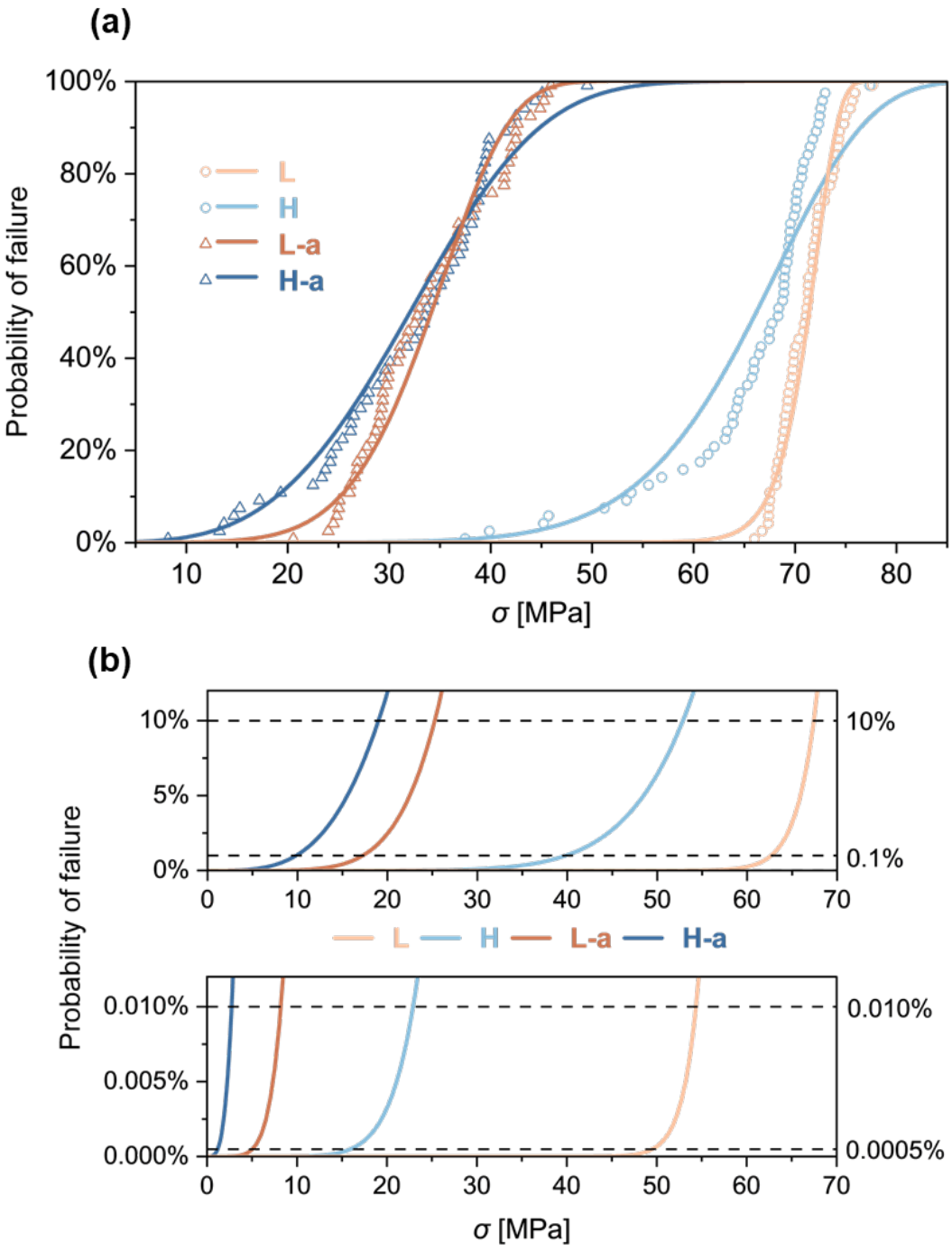


**Figure 4.16** Failure probabilities versus tensile strength. **(a)** Experimental and theoretical failure probabilities for groups L, H, L-a, and H-a, showing good correlation. **(b)** Theoretical failure probabilities of the four groups in the high-reliability region, emphasizing differences under high reliability requirements.

**Table 4.8** Predicted stress at various failure probabilities.

| Group | Defect density parameter $\rho$ ($cm^{-3}$) | Stress for 10% failure $\sigma_{10\%}$ (MPa) | Stress for 1% failure $\sigma_{1\%}$ (MPa) | Stress for 0.01% failure $\sigma_{0.01\%}$ (MPa) | Stress for 0.0005% failure $\sigma_{0.0005\%}$ (MPa) |
|---|---|---|---|---|---|
| L | 10.1 | 67.4 | 62.7 | 54.4 | 49.6 |
| H | 10.7 | 52.9 | 39.9 | 22.9 | 16.0 |
| L-a | 11.1 | 25.3 | 17.3 | 8.21 | 5.06 |
| H-a | 11.6 | 19.0 | 9.87 | 2.72 | 1.18 |

## 4.4 Summary

This chapter presents a detailed study on the effects of void and thermal aging on the mechanical and electrical properties of epoxy resin, combining experimental techniques and statistical analysis to interpret the findings. Data from digital microscopy, FTIR, tensile measurements, and SEM, along with Weibull statistical modeling, provide insight into the degradation mechanisms and the role of defects in impacting epoxy resin performance.

Thermal aging introduces specific changes in both mechanical and electrical properties, with degradation occurring unevenly throughout the material. Initially, thermal aging increases strength due to post-curing crosslinking, but prolonged aging leads to degradation through chain scission, oxidation. Oxygen diffusion controls this aging process, with degradation more severe near the surface. After removing a 0.3 mm-thick surface layer, no degradation was detected in the core even after 1000 hours aging, indicating that degradation proceeds inward from the surface. Further evidence of this inhomogeneity was found in the higher ether bond intensity in the core of aged specimens, suggesting increased crosslinking in the inner layers due to continuously curing. This contributed to higher electrical tree initiation voltage.

The statistical analysis reveals the critical impact of void content and thermal aging on the mechanical reliability of epoxy resin. Voids act as crack initiation sites, reducing tensile

strength and leading to greater variability in performance. As void content increases, the Weibull modulus $m$ decreases significantly (from 32.4 to 8.32), indicating reduced stability in tensile strength. This instability becomes more pronounced when both voids and thermal aging are present, with the Weibull modulus $m$ dropping further to 3.58, demonstrating a compounded adverse effect. A defect density parameter $\rho$ was introduced to quantitively describe the combined effects of voids and thermal aging, where specimens with higher void content and exposure to thermal aging display lower Weibull modulus mmm and characteristic strength $\sigma_0$ reflecting diminished mechanical reliability. Furthermore, with failure probability at 0.0005%, the stresses for specimens with low void content (L), high void content (H), low voids after aging (L-a), and high voids after aging (H-a) varied considerably, as 49.6 MPa, 16 MPa, 5.06 MPa, and 1.18 MPa, respectively. These findings underscore the necessity of Weibull analysis in accurately assessing the mechanical reliability of epoxy resins, particularly when both voids and thermal aging contribute to increased variability.

Overall, this research provides valuable insight into the combined impact of void defects and thermal aging on structural integrity and reliability of epoxy resin, deepening the degradation mechanism understanding, emphasizing the need for effective defect management and employment of statistical analysis in high reliability required material design and application.

# Chapter 5

## Effect of Filler Surface Wettability on Long-Term Mechanical and Dielectric Properties of Epoxy Resin Composites

*Incorporating inorganic oxides into epoxy resin enhances dielectric and mechanical properties, with the filler-matrix interface playing a critical role. However, the impact of interface on long-term performance under harsh conditions remains a key concern. This study explores the effects of filler surface wettability on the durability of EP-$SiO_2$ composites. Micro-sized $SiO_2$ with hydrophilic (HP) and hydrophobic (HB) surfaces are prepared via surface treatment, incorporated into epoxy resin, and subjected to hygrothermal aging at 95°C and 95% humidity for up to 1200 hours. Comprehensive characterizations of wettability, microstructure, mechanical, and dielectric properties reveal that HP- $SiO_2$-EP exhibits superior dispersion, interfacial adhesion, and durability against hygrothermal aging compared to HB- $SiO_2$-EP. This study highlights the role of filler surface wettability in enhancing long-term composite performance, informing the design of durable materials for advanced dielectric applications.*

---

* This section is published substantially in Journal of Colloid and Interface Science, Mar 2025. http://dx.doi.org/10.1016/j.jcis.2024.11.186. 

## 5.1 Introduction

The electrical and electronic industries have experienced rapid advancements in recent years, driving demand for dielectric materials with superior performance characteristics, including tailored dielectric constants, low dielectric loss, high breakdown strength, high thermal conductivity, and reliable long-term performance [218], [127], [219]. Epoxy resin (EP) filled with micro inorganic oxides exhibits enhanced dielectric and thermal properties, strong mechanical support, and ease of handling, making it ideal for various applications in electrical and electronic industries, such as insulation in high-voltage power systems, substrates for printed circuit boards, and compounds for transformers and motors [16], [31], [86], [127], [195], [196]. Nevertheless, the long-term degradation of epoxy composites presents a critical challenge to the reliability of electrical equipment.

The interface between the filler and polymer matrix plays a crucial role in the composite's properties. Poor interaction can lead to electric distortion and potentially degrade critical properties such as dielectric breakdown strength, dielectric constant/loss [128], [145], [146], toughness and mechanical strength [147]. Some research has been devoted to enhancing the interface by modifying the surface condition of fillers. Grafting organic molecules onto fillers has recently gained significant attention, showing improvements in dielectric breakdown, energy storage performance, thermal and mechanical properties of composites due to uniform dispersion and enhanced interface [220], [221]. Zeng et al. used polydopamine and graphene oxide to modify carbon fibers, which increased interfacial shear strength by 69% and tensile strength by 82%, enhancing composite mechanical performance [222]. Sun et al. summarized the use of silane coupling agents to modify multiple filler surfaces, improving interfacial bonding in epoxy composites and enhancing compatibility with the matrix, resulting in better mechanical and thermal properties [223]. Furthermore, silane functionalization of inorganic fillers was shown to effectively tailor the permittivity of the composites [224]. In addition to grafting organic molecules on to filler surface, a method involving liquid-phase sintering was used to increase the hydrophobicity of the MgO surface, leading to a significant increase in the thermal conductivity of the epoxy composite, from 4.5 W/mK to 7.5 W/mK [225]. In general, the

multifunctional properties of composites are enhanced through the surface modification of fillers, which also alters the wettability of the filler surface.

However, the long-term performance of these composites with modified fillers has not been adequately addressed. During the operation of electrical and electronic devices, excessive thermal energy generated by high voltage and heat flux in electrical systems, combined with the low thermal conductivity of EP [31], [32], [129], can accelerate thermal aging [33]. During this process, polymer properties change due to chain scission, rearrangement, and oxidation [37], [38], [39], which will significantly affect the reliability of dielectric materials and potentially compromise equipment performance. Additionally, the incorporation of oxide fillers, which have abundant surface hydroxyl groups and large surface area, might increase water uptake [161], threatening the long-term performance under humid conditions. The long-term performance of composites with different filler wettability, particularly under hygrothermal environments, remains a significant concern for practical applications, yet there is limited discussion in the literature on this issue.

Given these complexities, a critical research gap exists regarding the impact of filler surface wettability on the long-term performance of epoxy composites under intense heat and humid conditions. A systematic evaluation of how filler surface wettability influences interfacial conditions and subsequently impacts long-term properties is urgently needed. Understanding the hygrothermal aging behavior of these composites with different filler wettability will provide essential insights for enhancing product reliability and enabling more accurate lifetime predictions.

To address this gap, this research prepares micro-$SiO_2$ with different surface wettability characteristics and incorporates these particles into EP. The resulting EP-$SiO_2$ composites then undergo hygrothermal aging for up to 1200 hours, with systematic evaluation of their long-term dielectric and mechanical properties. Scanning electron microscopy (SEM) and energy-dispersive X-ray spectroscopy (EDX) are employed to reveal filler dispersion and interfacial characteristics. Finite element simulations on stress distribution and dielectric breakdown are conducted to illustrate the failure mechanism. This comprehensive

investigation aims to elucidate the relationship between filler surface wettability, filler-matrix interfacial properties, and the long-term performance of composites. Interestingly, hydrophobic fillers outperformed hydrophilic fillers in some properties initially, but with aging, the trend was reversed, highlighting notable degradation behavior deserving investigation. The findings offer valuable insights for material design and selection in practical applications, enabling more accurate lifetime predictions and enhancing the design for reliable electrical and electronic devices.

## 5.2 Experimental Details

### 5.2.1 Materials

Epoxy resin solution ARALDITE® LY 5052 and amine hardener ARADUR® 5052 CH were provided by Huntsman Advanced Materials Americas LLC. $SiO_2$ micro-particles with a diameter of 0.5-10 μm and 1H,1H,2H,2H-perfluorodecyltriethoxysilane (FAS) were purchased from Sigma-Aldrich Pte Ltd. Deionized (DI) water was used in the hydrolysis of FAS and the hygrothermal aging process. Methanol was provided by Aik Moh Chemicals Pte Ltd. Silicone oil (XIAMETERTM PMX-561 Transformer Liquid) used in the dielectric tests was supplied by Dow Inc.

### 5.2.2 Sample Preparation

#### 5.2.2.1 Surface Modification of $SiO_2$ Particles

**1) Preparation of Hydrophobic $SiO_2$ (HB-$SiO_2$)**

0.5 mL of FAS was dissolved in methanol with constant magnetic stirring. Then 1.5 mL of DI water was slowly added to the solution to hydrolyze FAS molecules. Next, 1.5 g of $SiO_2$ was dispersed into the solution under magnetic stirring for 2 hours. The mixture was then ultrasonicated for 30 minutes, followed by another 30 minutes of magnetic stirring. Subsequently, the mixture was centrifuged for 10 minutes at 10,000 rpm, and the

precipitate was collected and dried at 110 °C. The obtained HB-$SiO_2$ was stored in a dry cabinet.

**2) Preparation of Hydrophilic $SiO_2$ (HP-$SiO_2$)**

The $SiO_2$ micro-particles were hydrophilic as received. To clean the particle surface, the same process as in the HB-$SiO_2$ preparation was conducted, but without the addition of FAS and DI water. The $SiO_2$ particles were washed with methanol, using magnetic stirring and ultrasonication. The solid was then separated by centrifugation and dried in an oven to remove the methanol. The obtained HP-$SiO_2$ particles were stored in a dry cabinet.

#### 5.2.2.2 Preparation of EP-$SiO_2$ Composites

The epoxy resin consisted of two components: uncured epoxy resin solution and amine hardener. 5 wt% of treated $SiO_2$ particles were mixed with the uncured epoxy resin solution for 30 minutes under sonication followed by 10 minutes of planetary mixing at 2000 rpm (Thinky mixer ARE-310). The amine hardener was then added to the mixture at a ratio of 1:0.38 (uncured epoxy resin: hardener). The mixture was planetary mixed for 5 minutes at 2000 rpm and centrifugally defoamed for 5 minutes at 2200 rpm. The mixture was then gently poured into silicone or steel molds for curing. The liquid was cured at room temperature for 24 hours, followed by a 4-hour high-temperature curing at 100°C. The specimens were then collected and stored in a dry cabinet at 40% relative humidity.

### 5.2.3 Surface Wettability Measurements

#### 5.2.3.1 Water Contact Angle (WCA)

The wetting state of the $SiO_2$ particles was characterized by WCA tests using an OCA 25 (DataPhysics Instruments GmbH). The particles were pressed into a flat pellet. A 10 μL droplet of DI water was placed on the pellet, and the contact angle between the droplet and pellet surface was recorded and measured. For the untreated hydrophilic $SiO_2$, water was

rapidly adsorbed into the porous pellet, making it difficult to measure the static WCA. Thus, the droplet absorption process was recorded, and the dynamic change in WCA over time was analyzed.

#### 5.2.3.2 Sliding Angle

To further validate the hydrophobicity of the HB-$SiO_2$ particles, the sliding angle was measured using the same equipment as in the WCA tests. The sample stage was gradually tilted, and a 15 μL droplet of deionized water was placed on the particle pellets. The minimum angle at which the droplet began to slide off the surface was recorded as the sliding angle, providing additional insight into the water-repellent properties of the modified silica particles.

### 5.2.4 Microstructural Analysis

Morphological analysis and elemental mapping of the fracture surfaces of EP composites were conducted using field emission scanning electron microscopy (SEM) and energy-dispersive X-ray spectroscopy (EDX). A JEOL JSM 7800F Prime microscope, equipped with an Oxford Ultim Max EDS detector, was employed for this purpose. To enhance the image quality of the non-conductive polymer samples, their surfaces were coated with platinum and secured with conductive tapes.

### 5.2.5 Thermal Property Evaluation

Differential Scanning Calorimetry (DSC) tests were conducted using a DSC Q10 from TA Instruments. For testing the curing dynamics, the uncured epoxy resin, hardener, and 5 wt.% of HP- or HB-$SiO_2$ were mixed, and the tests were started within 5 minutes after mixing. The heating rate used was 10°C/min, from 0°C to 250°C, and the heat released during curing was recorded. Two tests are done for same type of specimens, and the curing heat of specimen 1 ($H_1$) and 2 ($H_2$) was confirmed to satisfy the following inequality provided by BS ISO 14322 standard:

$$\frac{|H_1 - H_2|}{(H_1 + H_2)/2} \times 100 \leq 10\% \qquad (Equation\ 5.1)$$

The cured specimens, prepared under the conditions described in material preparation section **5.2.2.2** (cured for 24 hours at room temperature followed by 4 hours at 100°C), were measured by DSC to investigate the curing degree and glass transition temperature ($T_g$). The specimens were heated from 0°C to 250°C at 10°C/min, then cooled at 20°C/min, followed by a second heating cycle to 250°C. The first heating cycle was used to determine if the curing was complete under the given conditions and to remove the thermal history, while the second heating cycle was used to observe the $T_g$.

### 5.2.6 Hygrothermal Degradation Tests

The HP-$SiO_2$-EP and HB-$SiO_2$-EP composites were hydrothermally aged under harsh conditions using an environmental chamber. The aging temperature was 95°C, and the relative humidity was 95%, with aging durations ranging from 0 to 1200 hours. After the required degradation time, the specimens were placed in a dry cabinet at 40% relative humidity for at least 24 hours before testing.

### 5.2.7 Material Characterization

#### 5.2.7.1 Mechanical Properties

Tensile properties were measured using a Shimadzu AGS-X mechanical tester following the ASTM D638 standard. The setup included a 20 kN load cell with a loading rate of 1 mm/min. Test specimens were dog-bone shaped with dimensions of 2.5 mm in thickness, 3.18 mm in width, and 7.62 mm in gauge length. Tensile strength and Young's modulus were obtained from the tensile tests. Five specimens were tested for each time point.

#### 5.2.7.2 Dielectric Breakdown Strength

An AC high voltage tester (Hipotronics 700 Series) was employed to determine the dielectric breakdown strength. Thin film specimens with a thickness of 200 μm were used to minimize the impact of defects. During the breakdown strength tests, specimens were immersed in silicone oil to avoid surface flashover. A step voltage was applied to the films using copper electrodes, with the initial voltage determined by a short-time test with a constant increasing speed. Detailed procedures can be found in ASTM D90. The collected data were analyzed using a two-parameter Weibull distribution, as shown in Equation 5.1, where $F$ denotes the probability of failure at a given electrical stress. $E$ is the measured breakdown strength. $\alpha$ is the scale parameter, and $\beta$ is the shape parameter.

$$F(E;\alpha,\beta) = 1 - \exp\left\{-\left(\frac{E}{\alpha}\right)^{\beta}\right\} \qquad \text{(Equation 5.2)}$$

#### 5.2.7.3 Dielectric Spectroscopy and Volume Resistivity

Dielectric spectra for the HP-$SiO_2$-EP and HB-$SiO_2$-EP composites were obtained using the Megger IDAX 300 to assess the effect of filler surface on the long-term dielectric constant and dielectric loss. A Keithley 6517B Electrometer was used to determine the volume resistivity of high resistivity samples. Uniform plate samples with a thickness of 2 mm and cylindrical electrodes with a guard ring, as recommended by IEC 62631, were used for these investigations.

## 5.3 Results and Discussion

### 5.3.1 Surface Wettability Characterization of $SiO_2$ Particles

The hydrophilicity of HP-$SiO_2$ is demonstrated in **Figure 5.1(a)**, which illustrates the dynamic behaviour of a water droplet over time. The water droplet was rapidly absorbed into the silica pellet within 1.3 seconds. Conversely, the hydrophobicity in HB-$SiO_2$ is evident in **Figure 5.1(b)**, exhibiting a WCA of 152° and a sliding angle of 5°. Due to the surface roughness of the $SiO_2$ pellet, the measured WCA is lower than the actual value on

its continuous solid hydrophilic surface owing to the Wenzel effect, and higher than that on its hydrophobic counterparts owing to the Cassie-Baxter effect [226]. The hydrophobic property is attributed to the FAS chains, which are covalently bonded to the $SiO_2$ surface through silanol head groups. **Figure 5.1(c)** illustrates the chemical reaction in this modification process [227]: FAS undergoes hydrolysis to form silanol groups, which then condense with surface silanol groups on $SiO_2$ particles, forming stable Si-O-Si bonds. This reaction effectively grafts the fluorinated chains onto the silica surface. The resulting hydrophobic layer formed by the fluorine-rich tails is illustrated in **Figure 5.1(d)**. The successful grafting of FAS on silica is confirmed in Fourier-transform infrared spectroscopy (FTIR) analysis, as shown in **Figure 5.2**. According to previous literature [228], the untreated flat silica glass with a roughness of 0.001 μm showed an apparent surface energy of 61.99 $mJ/m^2$. After FAS treatment, the surface energy was reduced to 11.69 $mJ/m^2$ with unchanged roughness, demonstrating the effectiveness of FAS in reducing surface energy. It was reported that the FAS layer is assembled on the substrate surface as a monolayer with an extremely thin thickness [229]. There is hydrogen bonding between the silica surface and epoxy resin in HP-$SiO_2$ due to the presence of Si-OH groups. This hydrogen bonding is weakened when FAS is attached to the surface, leading to a poorer interface.

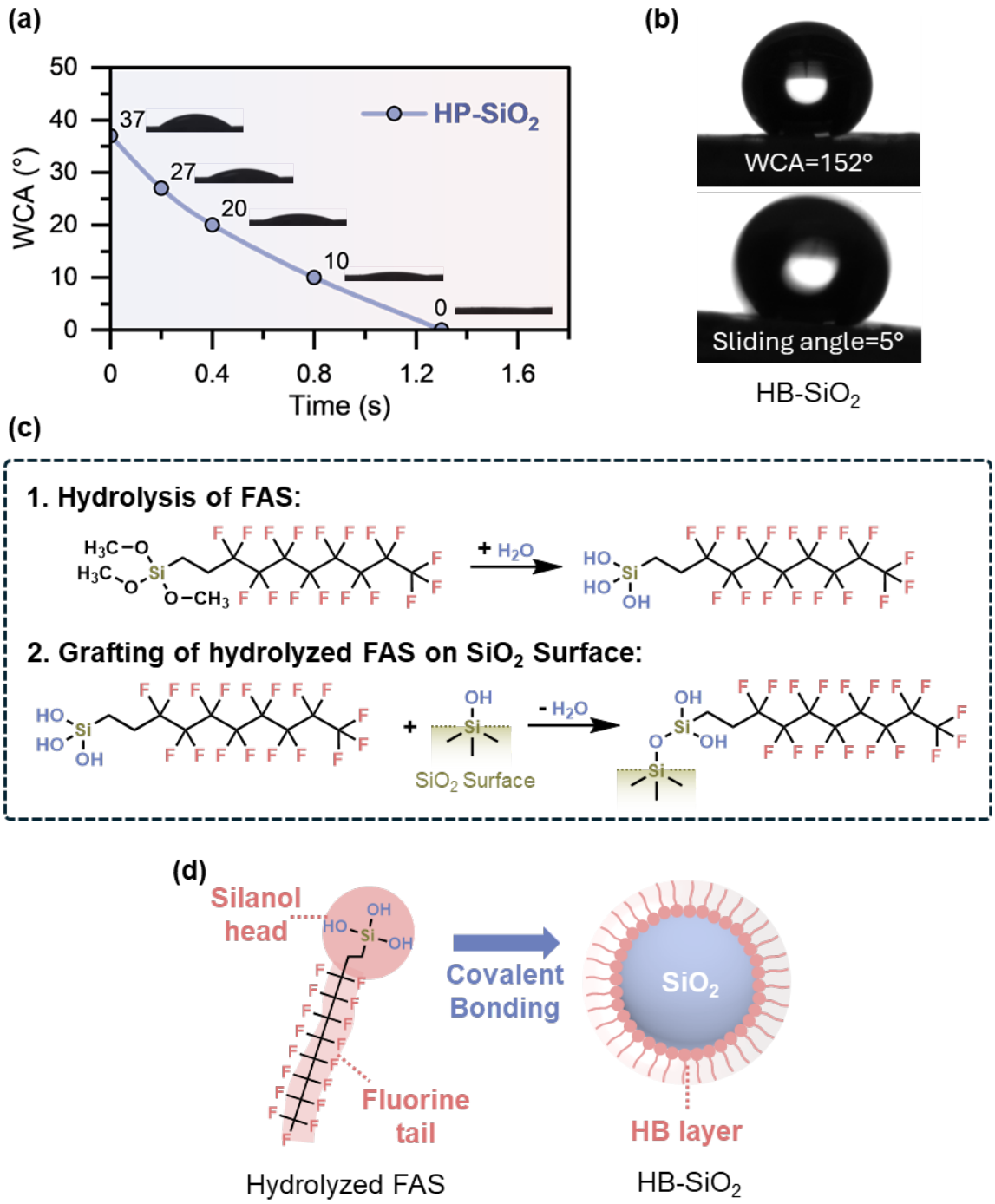


**Figure 5.1** Wettability characteristics of HP-$SiO_2$ and HB-$SiO_2$ pellets. **(a)** Dynamic WCA of HP-$SiO_2$, indicating hydrophilicity. **(b)** WCA and sliding angle of HB-$SiO_2$, showing hydrophobicity. **(c)** Chemical reaction for modifying $SiO_2$ particles to achieve a hydrophobic surface. **(d)** Schematic representation of the hydrophobic layer formation.

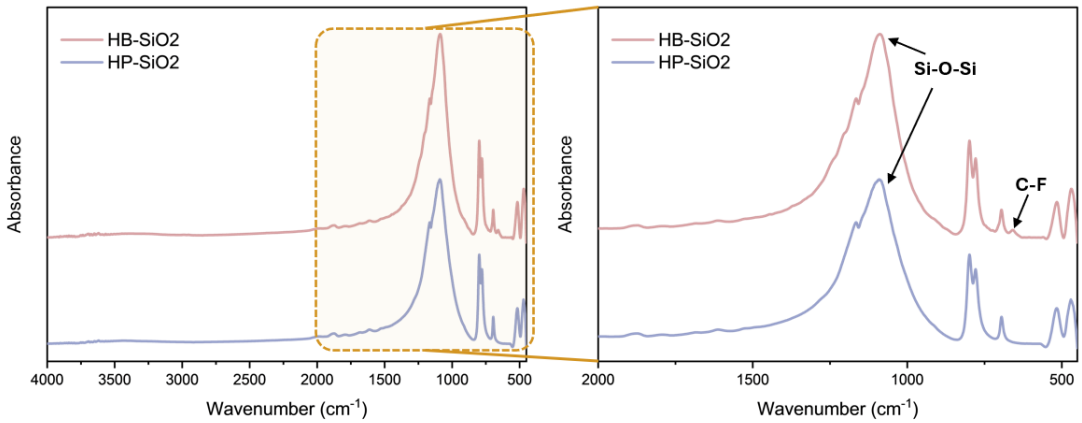


**Figure 5.2** FTIR Results for HP-$SiO_2$ and HB-$SiO_2$, indicating successful grafting of FAS on silica surface.

### 5.3.2 Microstructural Analysis of Modified $SiO_2$ and Derived EP Composites

The morphology and elemental information of both $SiO_2$ particles were characterized using SEM and EDX, as illustrated in **Figure 5.3(a,b)**. The two types of particles exhibit similar sizes ranging from 0.5 to 10 μm. Notably, fluorine is clearly detectable on the HB-$SiO_2$ particles, providing evidence for the successful surface modification via fluoro silane grafting.

The morphological and compositional characteristics of the fractured surfaces of EP composites after the tensile test are presented in **Figure 5.3(c,d)** for HP-$SiO_2$-EP and **Figure 5.3(e-h)** for HB-$SiO_2$-EP. The HP-$SiO_2$ particles maintain their dimensions before compositing and exhibit homogeneous dispersion throughout the matrix. This uniform distribution suggests favorable compatibility between HP-$SiO_2$ and EP. Moreover, the filler-matrix interface appears dense, with no visible voids or discontinuities. In contrast, HB-$SiO_2$-EP composites exhibit noticeable filler agglomeration, showing poor dispersion of HB-$SiO_2$ in epoxy resin system. Micro-voids are observable at the interface between HB-$SiO_2$ particles and EP, suggesting a weak interface between the particles and the matrix.

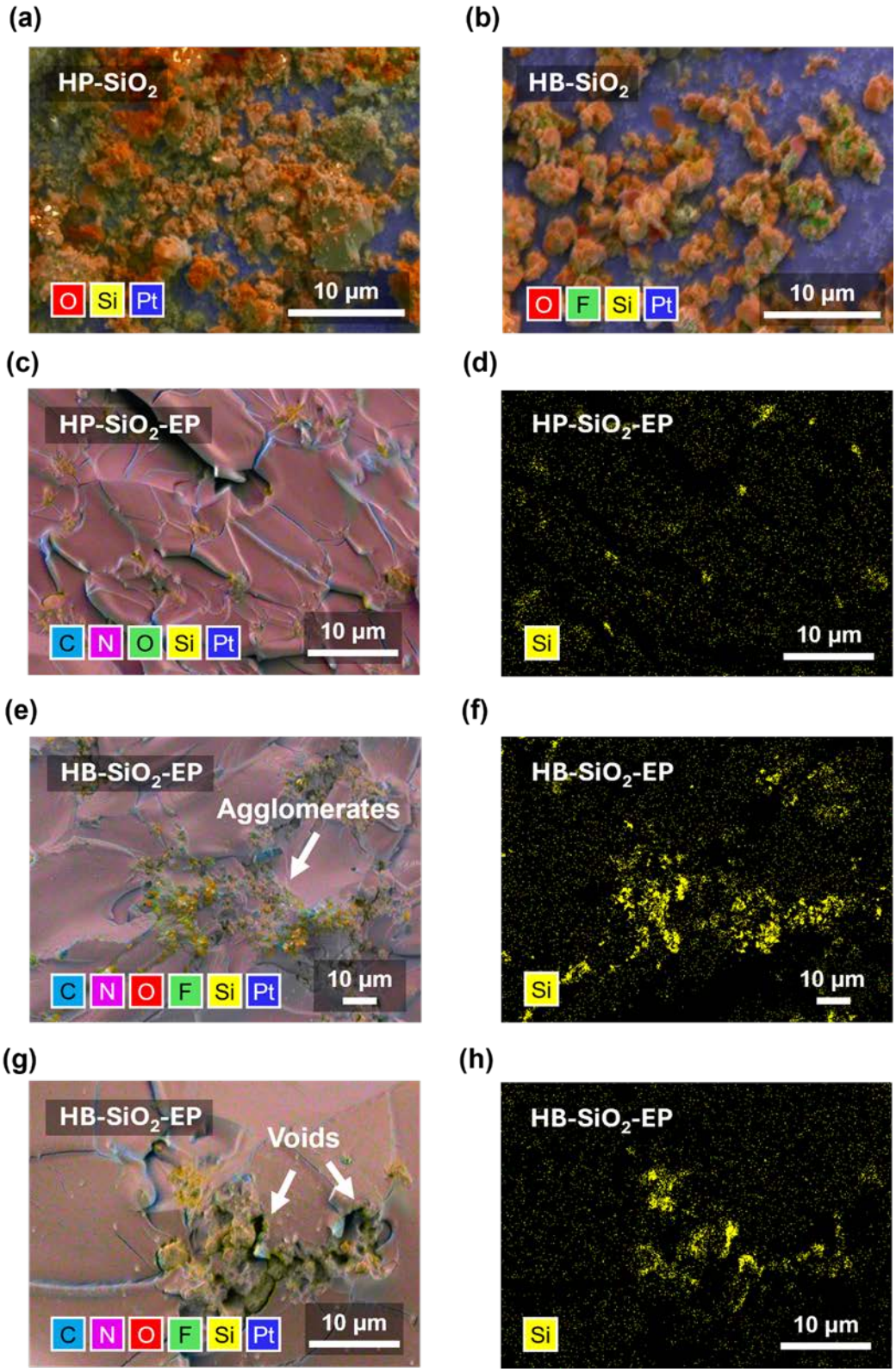


**Figure 5.3** Microstructural analysis of $SiO_2$ particles and their composites. **(a,b)** EDX mapping of $SiO_2$ particles with hydrophilic and hydrophobic surfaces. **(c,d)** EDX mapping of HP-$SiO_2$-EP

composites, showing uniform dispersion. EDX mapping of HB-$SiO_2$-EP composites, illustrating **(e,f)** agglomeration and **(g,h)** interfacial micro voids.

### 5.3.3 Thermal Properties and Curing Dynamics

The curing dynamics and glass transition temperature ($T_g$) were studied using DSC, and the relevant parameters are summarized in **Table 5.1**. For the curing dynamics, the released heat during the curing reaction was recorded as *H*. The results indicate that the addition of $SiO_2$ fillers decreases the exothermic peak area, as the fillers occupy part of the composite's weight, reducing the amount of EP available for curing compared to pure EP. Therefore, the heat calculation was corrected by deducting the weight of the silica. The corrected heat of curing ($H_{corr}$) still shows a decrease after adding silica, suggesting that the incorporation of fillers reduces the crosslinking density of the epoxy resin, possibly due to the hindrance of polymer chain movement caused by the fillers during the curing process [230]. Specifically, the heat of curing for HP-$SiO_2$-EP is slightly lower than that of HB-$SiO_2$-EP, which may be attributed to the more uniform dispersion of HP-$SiO_2$, providing greater hindrance to molecular movement.

No exothermic peaks are observed for the specimens cured under the conditions described in the material preparation section **5.2.2.2**, confirming complete curing for all samples. The corresponding curves are provided in **Figure 5.4**. The $T_g$ values of HP-$SiO_2$-EP, HB-$SiO_2$-EP, and pure epoxy resin composites are similar, indicating that the addition of 5 wt.% $SiO_2$ fillers does not significantly affect the thermal stability of the material.

**Table 5.1** Thermal properties of $SiO_2$-EP composites and pure epoxy resin.

| | Heat of curing *H* (J/g) | Corrected heat of curing $H_{corr}$ (J/g) | Glass transition temperature $T_g$ ($C^o$) |
|---|---|---|---|
| HP-$SiO_2$-EP | 408.3 | 429.8 | 124.7 |
| HB-$SiO_2$-EP | 416.5 | 438.4 | 124.2 |

| | | | |
|---|---|---|---|
| Pure Epoxy Resin | 469.9 | 469.9 | 124.3 |

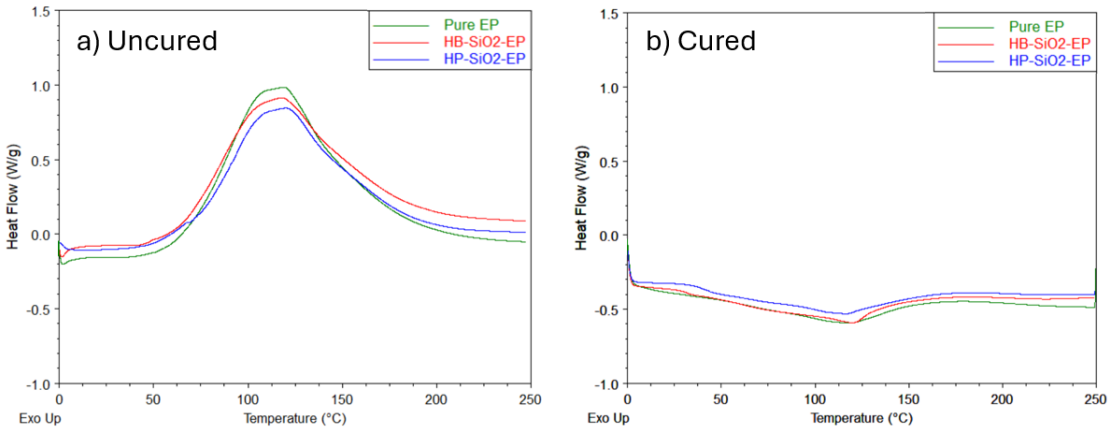


**Figure 5.4** DSC curves for HP-$SiO_2$-EP, HB-$SiO_2$-EP compared to pure epoxy resin. **a)** Uncured specimens to observe the curing reaction heat. **b)** Cured specimens by the given curing conditions to determine the curing degree.

### 5.3.4 Mechanical Properties and Failure Analysis

The mechanical properties of HP-$SiO_2$-EP and HB-$SiO_2$-EP composites were evaluated through tensile tests after various aging durations. Their tensile strength and Young's modulus are illustrated in **Figure 5.5(a,b)**. During the 1200-hour aging period, both EP composites exhibit a marginal decrease in tensile strength, not exceeding 3.3%. This slight degradation can be attributed to polymer chain scission, oxidation, and hydrolysis induced by heat and moisture exposure [231], [232], [233]. At the same time, the Young's modulus of HP-$SiO_2$-EP and HB-$SiO_2$-EP diminishes from 714 ± 21 to 648 ± 34 MPa and from 660 ± 45 to 632 ± 38 MPa, respectively. This reduction in modulus is due to the plasticization effect caused by water absorption, which leads to volumetric swelling of the epoxy resin matrix and increases chain mobility [146], [234].

Notably, HP-$SiO_2$-EP consistently demonstrates superior tensile strength and higher modulus compared to HB-$SiO_2$-EP, both before and after hygrothermal aging. This

enhanced performance under harsh conditions can be attributed to the strong interfacial adhesion between HP-$SiO_2$ and the epoxy resin matrix.

The fracture surfaces of representative specimens before and after 1200 hours of aging were examined by SEM, as shown in **Figure 5.5(c)**. All specimens exhibit river-like patterns and relatively flat surfaces, indicating the brittleness of the material [146]. HP-$SiO_2$-EP displays smoother fracture surfaces compared to HB-$SiO_2$-EP. No significant differences are observed in the fracture surface before and after the hygrothermal aging. Finite element analysis was conducted to compare the stress distributions in HP-$SiO_2$-EP and HB-$SiO_2$-EP under the same unit lateral displacement, as shown in **Figure 5.5(d)**. Arbitrary shaped voids were modelled around the $SiO_2$ fillers in HB-$SiO_2$-EP. The results show that although the uneven stress fields can be observed in both cases, the interfacial defects in HB-$SiO_2$-EP introduce severe stress concentration, with a maximum is 82.2 MPa compared to 17.4 MPa in HP-$SiO_2$-EP. Such stress concentration may cause failure to occur earlier, resulting in the degradation of material performance.

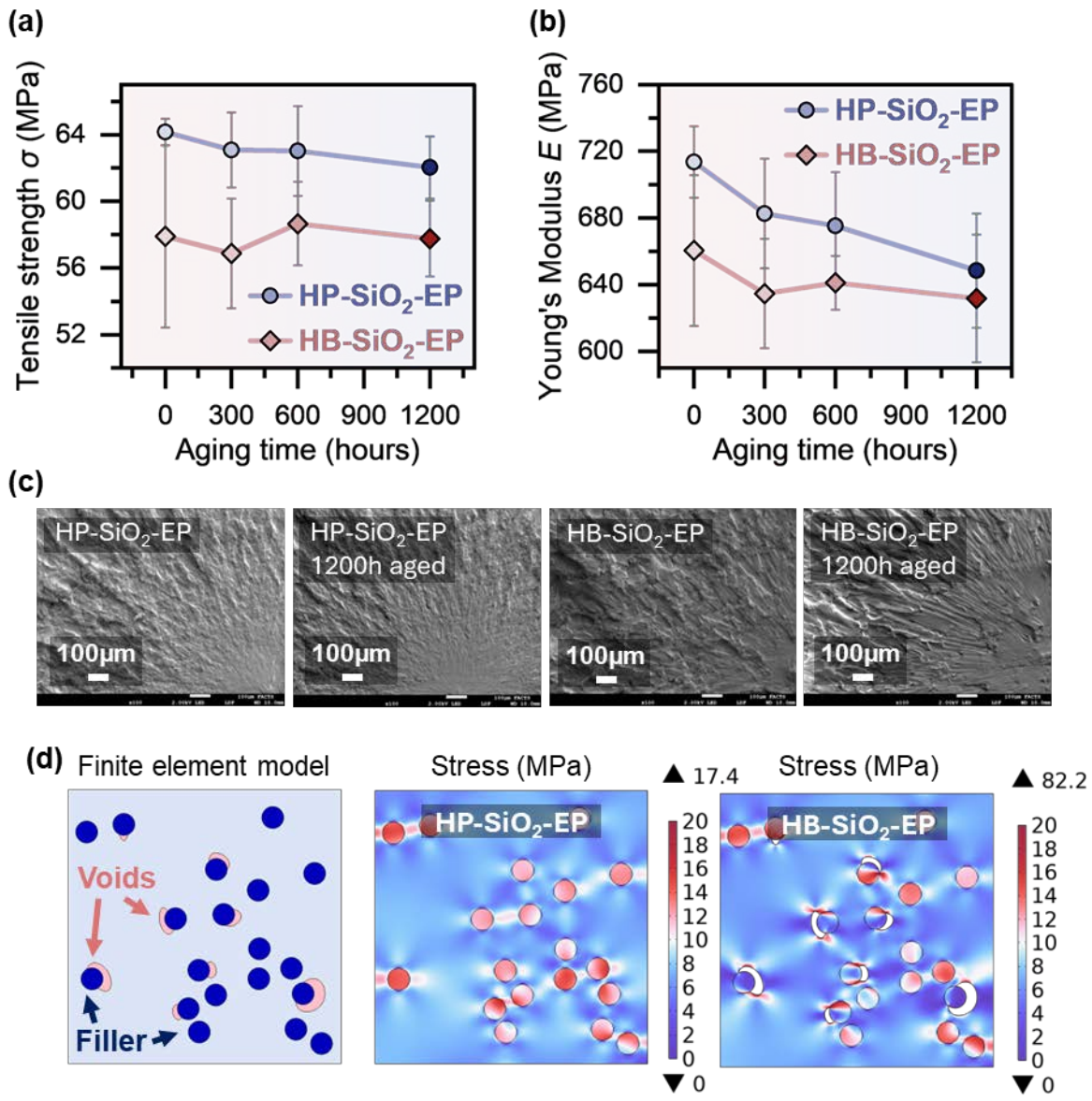


**Figure 5.5** Mechanical characteristics and fractographic analysis of EP-$SiO_2$ composites. **(a)** Tensile strength and **(b)** Young's modulus versus aging duration. **(c)** SEM graphs of fracture surfaces before and after 1200 hours of aging. **(d)** Finite element simulation of stress distribution in EP-$SiO_2$ composites.

### 5.3.5 Dielectric Breakdown Characteristics and Failure Analysis

The dielectric breakdown strength of modified epoxy resins was evaluated in insulating oil under ambient condition using an AC voltage source. Two-parameter Weibull analysis was

employed to characterize the failure probability of the EP composites under various electrical stresses. These two parameters are summarized in **Table 5.2**. **Figure 5.6(a,b)** illustrates the failure probability distributions of HB-$SiO_2$-EP and HP-$SiO_2$-EP as a function of hygrothermal aging duration. During the degradation process, the regression lines for both EP composites shift leftward, indicating a reduction in dielectric breakdown strength under harsh conditions. The characteristic breakdown strength ($\alpha$), defined as the strength at which the failure probability is at 63.2%, is summarized in **Figure 5.6(c)**. The characteristic breakdown strength, $\alpha$, for HP-$SiO_2$-EP decreases from 74 to 49 kV/mm, while for HB-$SiO_2$-EP, it drops from 51 to 37 kV/mm. This degradation can be attributed to enhanced charge transport due to water absorption, which may form a "shell" around individual particles, potentially creating percolating networks and adversely affecting the dielectric breakdown strength [235], [236]. Notably, the HP-$SiO_2$-EP consistently demonstrates superior dielectric reliability compared to HB-$SiO_2$-EP, both before and after hygrothermal aging. This observation underscores the significant influence of filler surface wettability on the dielectric resistance of EP composites. **Figure 5.6(d)** compares the electric field distributions in HP-$SiO_2$-EP and HB-$SiO_2$-EP using finite element analysis. When applying the same lateral externa electric field to both composites, the electric field in HB-$SiO_2$-EP is much higher than that in HP-$SiO_2$-EP due to electric field distortion caused by interfacial voids. Subsequently, the dielectric breakdown process was simulated using the phase field method. Based on the laws of thermodynamics, the phase field method uses a phase field variable which continuously changes from 0 to 1 to describe the evolution of breakdown damage, with 0 representing the intact material and 1 the fully broken-down material [237], [238]. Here, an increasing electric field in the horizontal direction was applied to both composites, and the breakdown damage evolution was shown in **Figure 5.6(e).** The results illustrate that the breakdown is initiated from the fillers in HP-$SiO_2$-EP and connects to each other with the increasing electric field, resulting in the final breakdown. The breakdown time of HP-$SiO_2$-EP is longer than that of HB-$SiO_2$-EP, showing a higher dielectric strength. For HB-$SiO_2$-EP, the air inside the interfacial voids is first broken down, then the damage propagates from the voids until they connect with each other and fully breakdown.

**Table 5.2** Scale parameter $\alpha$ *and* Shape parameter $\beta$ for epoxy resin composites throughout 1200-hour aging process.

| Specimen type | Aging time (h) | Scale parameter $\alpha$ (kV/mm) | Shape parameter $\beta$ |
|---|---|---|---|
| HP-$SiO_2$-EP | 0 | 74.1 | 4.6 |
| | 300 | 62.7 | 5.5 |
| | 600 | 56.8 | 7.5 |
| | 1200 | 49.1 | 7.3 |
| HB-$SiO_2$-EP | 0 | 51.1 | 8.3 |
| | 300 | 46.3 | 10.8 |
| | 600 | 43.4 | 9.3 |
| | 1200 | 36.7 | 5.9 |

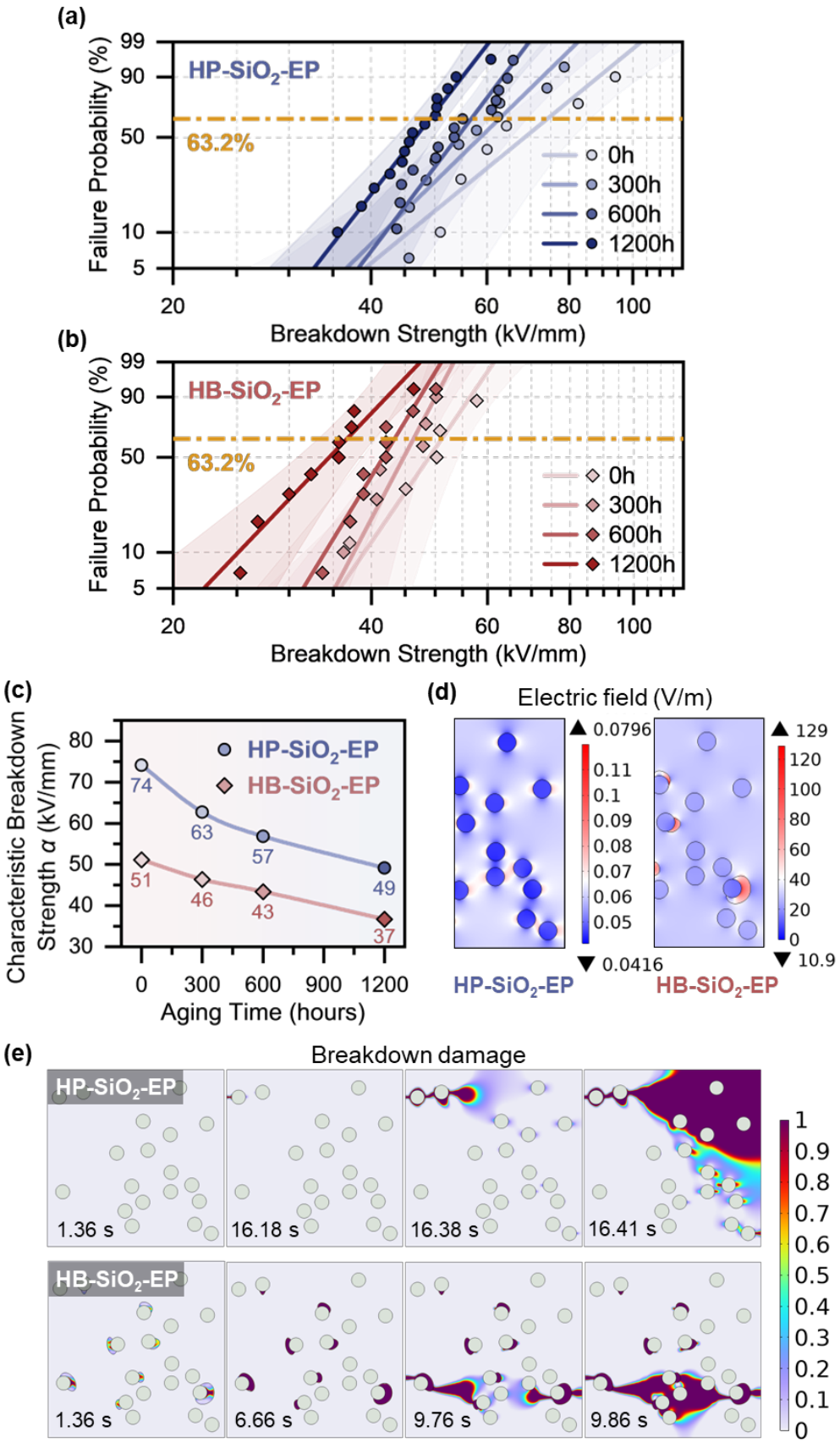
(a)
HP-SiO2-EP
63.2%
0h
300h
600h
1200h
Failure Probability (%)
Breakdown Strength (kV/mm)
(b)
HB-SiO2-EP
63.2%
0h
300h
600h
1200h
Failure Probability (%)
Breakdown Strength (kV/mm)
(c)
HP-SiO2-EP
HB-SiO2-EP
Characteristic Breakdown Strength α (kV/mm)
Aging Time (hours)
74
63
57
49
51
46
43
37
(d)
Electric field (V/m)
HP-SiO2-EP
HB-SiO2-EP
(e)
Breakdown damage
HP-SiO2-EP
1.36 s
16.18 s
16.38 s
16.41 s
HB-SiO2-EP
1.36 s
6.66 s
9.76 s
9.86 s

**Figure 5.6** Dielectric breakdown analysis of EP-$SiO_2$ composites. Failure probability of **(a)** HP-$SiO_2$-EP and **(b)** HB-$SiO_2$-EP under various electrical stress. **(c)** Characteristic AC breakdown strengths $\alpha$ at 63.2% failure probability as a function of aging duration. Simulation of **(d)** electrical field distortion and **(e)** the dielectric breakdown process in EP-SiO2 composites.

### 5.3.6 Dielectric Spectroscopy of HP-$SiO_2$-EP and HB-$SiO_2$-EP under Hygrothermal Aging

The dielectric spectra of epoxy resin incorporating $SiO_2$ with different surface wettability were obtained using the capacitance method at room temperature across multiple frequencies. **Figure 5.7** illustrates the dielectric spectra for **(a)** HP-$SiO_2$-EP and **(b)** HB-$SiO_2$-EP across multiple frequencies, with the color gradient transitioning from light to dark representing increasing aging durations from 0 to 1200 hours. Both HP-$SiO_2$-EP and HB-$SiO_2$-EP exhibit significant increases in dielectric constant and loss during hygrothermal aging, particularly in the low-frequency region. This indicates more severe ionic conduction caused by water uptake [239]. The relaxation of polymer structures is also evident in the dielectric spectra [231].

Notably, all specimens demonstrate decreasing dielectric constant and loss with increasing frequency. Differences between specimens are pronounced at frequencies below 100 Hz but converge at higher frequencies. This phenomenon is attributed to a shift in dominant effects: at low frequencies, the filler interface dominates the dielectric properties, and degraded impurities, including ionic species, also contribute to the increased dielectric constant and loss, while at high frequencies, frequency-dependent impacts such as electron hopping and Debye dielectric relaxation become more significant [240], [241].

Herein, to minimize the impact of loading frequency on dielectric properties, the dielectric constant and loss at a specific frequency 50 Hz are compared in **Figure 5.7(c-d)**. Initially, HB-$SiO_2$-EP exhibits a lower dielectric constant and loss than HP-$SiO_2$-EP, likely due to the introduction of fluorinated groups during filler surface treatment, which can decrease polymer polarizability [242]. However, as the aging duration increases, the dielectric

properties of HB-$SiO_2$-EP exhibit a more pronounced deterioration compared to HP-$SiO_2$-EP. Specifically, HB-$SiO_2$-EP exhibits a 28% increase in dielectric constant and a 311% rise in dielectric loss. In contrast, HP-$SiO_2$-EP shows more moderate changes, with a 13% increase in dielectric constant and a 234% rise in dielectric loss. Water significantly contributes to this rapid increase due to its stronger dipoles compared to epoxy resin and $SiO_2$ [146], [243]. Moreover, humidity can disrupt polymer chains and increase free volume, resulting in higher polymer polarization ability [244]. Consequently, despite its hydrophobic filler surface, HB-$SiO_2$-EP appears to absorb more water during the hygrothermal aging process, rendering its final dielectric properties more sensitive to humidity and heat than HP-$SiO_2$-EP.

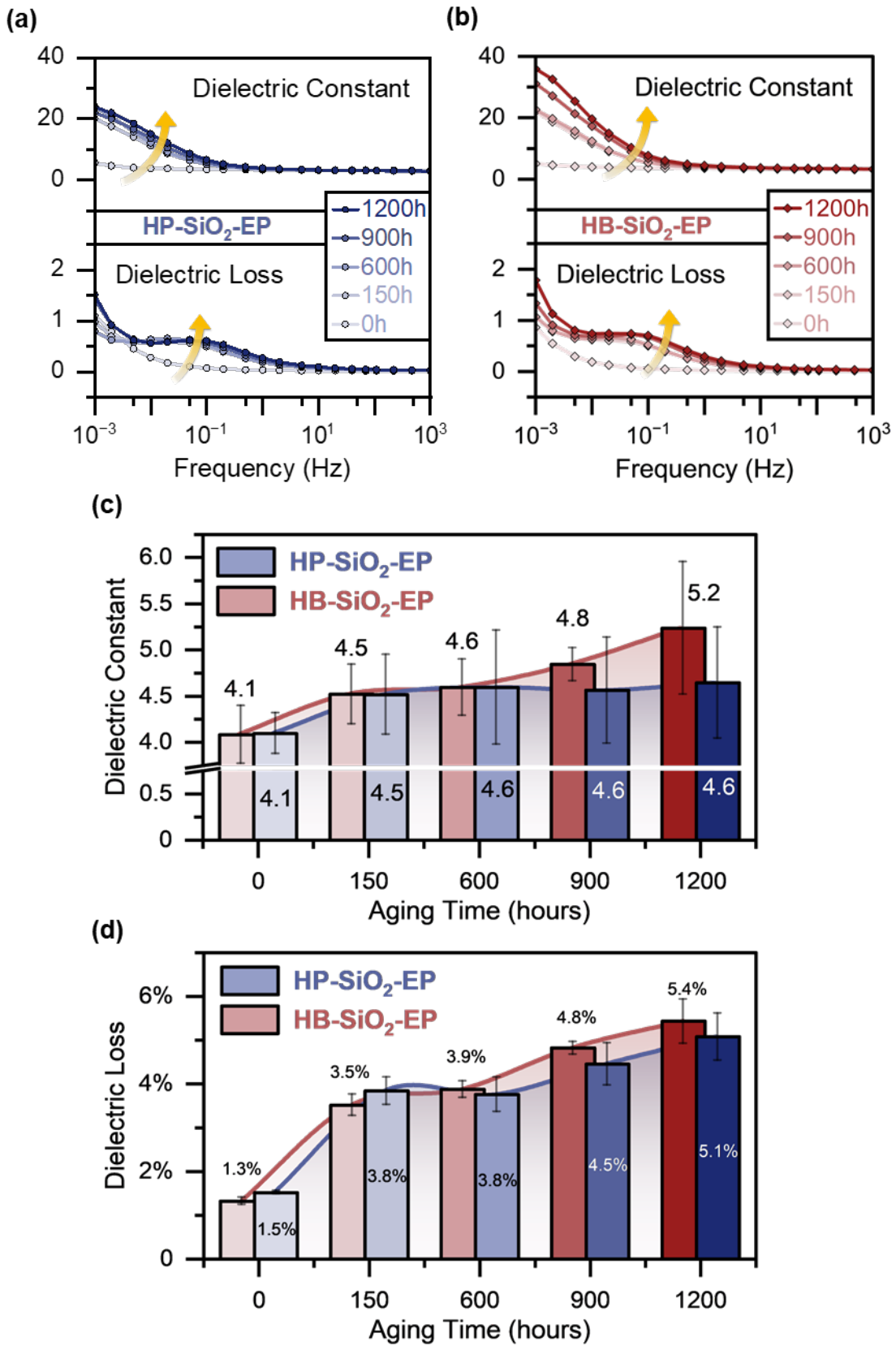
(a)
Dielectric Constant
HP-SiO2-EP
Dielectric Loss
1200h
900h
600h
150h
0h
Frequency (Hz)
(b)
Dielectric Constant
HB-SiO2-EP
Dielectric Loss
1200h
900h
600h
150h
0h
Frequency (Hz)
(c)
HP-SiO2-EP
HB-SiO2-EP
Dielectric Constant
4.1
4.5
4.6
4.8
5.2
Aging Time (hours)
(d)
HP-SiO2-EP
HB-SiO2-EP
Dielectric Loss
1.3%
3.5%
3.9%
4.8%
5.4%
1.5%
3.8%
3.8%
4.5%
5.1%
Aging Time (hours)

**Figure 5.7** Dielectric properties of $SiO_2$-EP composites throughout 1200-hour aging process. Dielectric spectra under multi-frequency for **(a)** HP-$SiO_2$-EP and **(b)** HB-$SiO_2$-EP with various aging durations. **(c)** Dielectric constant and **(d)** dielectric loss at 50 Hz for HP-$SiO_2$-EP and HB-$SiO_2$-EP with various aging durations.

### 5.3.7 Volume Resistivity

The volume resistivity of HB-$SiO_2$-EP and HP-$SiO_2$-EP was quantitatively assessed using an electrometer under ambient conditions following varying durations of hygrothermal aging. The results are illustrated in **Figure 5.8**, revealing a pronounced decrease in volume resistivity for both composite types with increasing aging duration, attributed to water uptake and material degradation [231]. The hygrothermal process facilitates ionic transport through absorbed water and epoxy hydrolysis, consequently diminishing volume resistivity [245].

Initially, HB-$SiO_2$-EP exhibits superior volume resistivity at $(3.1 \pm 0.35) \times 10^{14}$ Ω·cm, compared to HP-$SiO_2$-EP at $(2.9 \pm 0.65) \times 10^{14}$ Ω·cm. However, HB-$SiO_2$-EP subsequently demonstrates a more severe decline in resistivity. A critical crossover point is observed at 600 hours, beyond which the volume resistivity of HB-$SiO_2$-EP becomes inferior to that of HP-$SiO_2$-EP. This long-term aging behavior suggests that the poor interfacial adhesion between HB-$SiO_2$ and epoxy resin matrix exerts a more dominant influence than the hydrophobic nature of the filler surface. Consequently, this leads to increased moisture uptake at the filler-EP interface, ultimately compromising resistivity. The higher moisture absorption is a key factor contributing to the decline in resistivity.

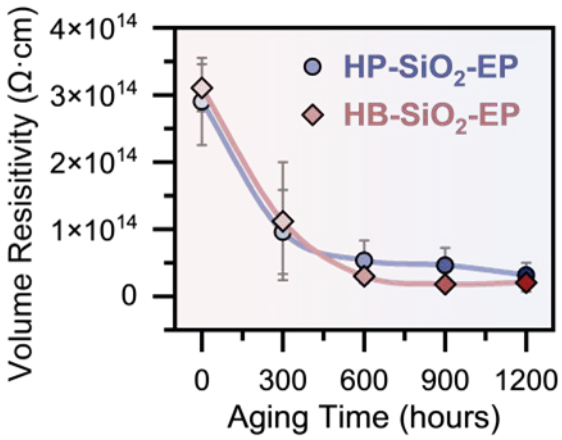


**Figure 5.8** Volume resistivity of $SiO_2$-EP composites throughout 1200-hour aging process.

## 5.4 Summary

In this research, $SiO_2$ micro-particles with hydrophilic (HP) and hydrophobic (HB) surfaces were prepared and incorporated into epoxy resin system. These composites were subjected to hygrothermal aging at 95ºC and 95% RH for durations up to 1200 hours. Comprehensive tests including the wettability, dielectric and mechanical characterizations were conducted to compare their performance. SEM and EDX, along with finite element simulations, were employed to reveal the degradation and failure mechanisms. The following conclusions can be drawn:

(1) HP-$SiO_2$-EP exhibits excellent filler dispersion and dense filler-matrix interface. Conversely, HB-$SiO_2$-EP displays poor filler dispersion and visible interfacial voids due to incompatibility between filler surface and epoxy resin matrix.

(2) HP-$SiO_2$-EP demonstrates higher tensile strength (64 ± 1 MPa), Young's modulus (714 ± 21 MPa) and characteristic dielectric breakdown strength (74 kV/mm) compared to HB-$SiO_2$-EP (58 ± 5 MPa, 660 ± 45 MPa and 51 kV/mm, respectively) due to the stronger interface. Despite significant degradation from hygrothermal aging, HP-$SiO_2$-EP maintains better durability after 1200 hours of aging.

(3) HP-$SiO_2$-EP presented lower sensitivity to hygrothermal aging than HB-$SiO_2$-EP, exhibiting less increases in dielectric constant (+13% vs. +28%) and loss (+234% vs. +311%), and a smaller decrease in volume resistivity (-89% vs. -93%), indicating the superior long-term stability of HP-$SiO_2$-EP.

(4) This study quantitatively evaluates the effects of filler surface wettability on the long-term performance of EP-$SiO_2$ composites, providing valuable insights for high-reliability material design in electrical and electronic application.

# Chapter 6

# Optimizing Dielectric, Mechanical, and Thermal Properties of Epoxy Resin through Molecular Design for Multifunctional Performance

*Current methods for enhancing epoxy resin (EP) properties, such as filler incorporation, often face challenges like particle agglomeration and interfacial defects, limiting performance improvements. In this study, a novel molecular design approach for EP is proposed, avoiding the dispersion issue in filler incorporation. Three molecular modifications are introduced to EP systems using facile synthesis procedures, including modifiers with bulky groups and crosslinking potential to reduce the dielectric constant while enhancing mechanical and thermal reliability, along with deep traps to increase breakdown strength. The modified epoxy resins exhibit significant improvements in electrical, mechanical and thermal properties. FTIR, SEM, and EDX confirm successful grafting and exceptional dispersion without agglomeration. This study demonstrates that small amounts of chemical modifiers can significantly enhance epoxy resin performance. The resulting materials can meet the requirements for next-generation dielectric materials while maintaining low production costs.*

---

* This section is published substantially in Materials Horizons, 2025. http://dx.doi.org/10.1039/d4mh01414f. 

## 6.1 Introduction

The utility of epoxy resin (EP) has been ubiquitous in industries that require high-performing materials due to its versatility from chemical and processing perspectives. The outstanding properties of EP, such as high modulus, high strength, good adhesion, and high chemical resistance, among others, are highly desirable in diverse applications, including construction, automotive sectors, and aerospace industries [232], [246], [247]. These exceptional qualities have made EP indispensable for a wide range of applications that demand robustness and durability. However, despite the numerous advantages of traditional EP, the continuing miniaturization of electronic devices and the increasing power output of electrical equipment have created new challenges that require materials with low dielectric constant, high breakdown strength, and high electrical resistivity [218], [237]. Traditional EP often fails to meet the stringent requirements of advanced dielectric materials for these emerging applications. As a result, the development of innovative modification approaches for EP has gained considerable interest within the scientific and industrial communities.

To address the need for improved dielectric properties in EP, researchers have devised strategies involving the incorporation of fillers [190], [238]. These particles, when dispersed within the epoxy matrix, introduce numerous deep traps capable of capturing injected charges and suppressing space charge accumulation. However, the effectiveness of this suppression mechanism heavily depends on achieving uniform nanoparticle dispersion throughout the polymer matrix [248]. While the addition of fillers can potentially enhance dielectric properties, it may adversely impact the processability and mechanical performance of the resulting polymer composites. Moreover, the presence of fillers can lead to a mismatch between the filler and polymer matrix, causing electric distortion and potentially degrading critical properties such as breakdown strength, dielectric loss, and electrical resistivity [128]. Consequently, increasing attention has been directed toward molecular modification techniques, which offer the advantage of being free from the agglomeration problems associated with filler incorporation.

The effects of modifications on the thermal stability of EP have been extensively studied. Lin and Pearce [166], [167] investigated the thermal properties of DGEBA (Diglycidyl Ether of bisphenol A)-DGEBF (Diglycidyl Ether of 9,9-bis(4-hydroxyphenyl)fluorene) and DGEBA-DGEPP (Diglycidyl Ether of Phenolphthalein) copolymers. Their findings revealed that the DGEBA-DGEBF copolymer exhibited superior heat and flame resistance compared to the DGEBA-DGEPP copolymer, attributable to its higher aromatic ring content. Fourier-transform infrared (FTIR) data suggested that the possible degradation mechanisms for these EP involve the Wieland rearrangement, Claisen rearrangement, and Norrish-type reactions. Chen et al. prepared five different EPs cured with TMB (trimethoxy boroxine) and DDS (diaminodiphenylsulfone) hardeners [168]. The results indicated that polymers with high aromaticity and/or cyclic ring structures in the chain backbone generally exhibited enhanced heat resistance. Furthermore, the morphology and structure of organosilicon polymer-modified EP were investigated by incorporating an organosilicon polymer (denoted as ETOP) as a modifier to blend with bisphenol A-type EP [169]. The study demonstrated that the cross-linked epoxy-rich matrix possessed a higher glass transition temperature ($T_g$) than pure EP at higher ETOP content. This observation was attributed to the participation of epoxide groups on ETOP molecules in the cross-linking reaction of the matrix, thereby increasing the cross-link density and enhancing the $T_g$.

Improving the toughness of EP is another active area of research, aimed at enhancing the ability of these materials to deform plastically and resist crack propagation. Misaki et al.[165] investigated the fracture properties of p,p'-diaminodiphenyl methane-cured EP modified with various aromatic and aliphatic glycidyl compounds. Their findings revealed that while most of these compounds promoted an increase in fracture toughness, the heat resistance of the modified EP was compromised to some extent by the incorporation of glycidyl compounds. Additionally, they observed an inverse relationship between cross-linked density of the resins and their impact strength and fracture toughness. Remarkably, the addition of 10 wt% of a terpolymer resulted in a substantial (140%) increase in the fracture toughness of the modified EP.

While extensive research efforts have been dedicated to modifying EP to improve their thermal and mechanical properties, relatively few studies are focused on enhancing their dielectric characteristics. With the rapid development in energy storage and conversion, flexible electronics, smart sensing, and 5G/6G communication, there is an urgent need for EP with tailorable dielectric properties [128]. Some research demonstrates that the introduction of polar groups in resin enhances the dielectric breakdown strength, which can be attributed to the formation of deep traps that capture charges [170], [171]. Meanwhile, the existence of bulky groups benefits the reduction of dielectric constants [172].

Inspired by these previous findings, this study synthesized three types of molecularly modified EP using various strategies, such as introducing polar groups to increase the breakdown voltage, incorporating bulky groups, and promoting crosslinking to reduce the dielectric constant and loss. Fourier-transform infrared spectroscopy (FTIR), scanning electron microscopy (SEM), and energy-dispersive X-ray spectroscopy (EDX) were employed to reveal the chemical structure of the modified EP and the distribution of modifiers. Dielectric, mechanical, and thermal stability tests were conducted to evaluate the performance of the modified EP. The findings of this study provide an efficient way to simultaneously enhance the dielectric, mechanical, and thermal properties of EP, making the molecularly modified EP a promising candidate for a new generation of dielectric materials applied in the electrical and electronic industry.

## 6.2 Experimental

### 6.2.1 Materials

EP solution ARALDITE® LY 5052 and amine hardener ARADUR® 5052 CH were provided by Huntsman Advanced Materials Americas LLC. The three modifiers, allyl chloroacetate (AC), 2-Amino-5-chloro-2’-fluorobenzophenone (ACF), and maleic anhydride (MA), were supplied by Sigma-Aldrich Pte Ltd. Their chemical structures and physical states are listed in **Table 6.1**. Methanol provided by Aik Moh Chemicals Pte Ltd was used as the solvent.

**Table 6.1** Modifier Properties and Pre-treatment Procedures

| Modifiers | Chemical Structure | Physical State at RT* | Improvement Strategy | Treatment Prior to Blending with Liquid EP |
|---|---|---|---|---|
| Allyl chloroacetate (**AC**) | 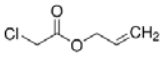 $C_5H_7ClO_2$ | Colourless liquid | Polar group | Premix with hardener |
| Maleic anhydride (**MA**) | 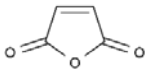 $C_4H_2O_3$ | White solid | Polar group+ crosslinking | Dissolve in methanol, mix with hardener, stir for 10 minutes to evaporate the solvent |
| 2-Amino-5-chloro-2'-fluorobenzophenone (**ACF**) | 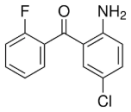 $C_{13}H_9ClFNO$ | Yellow powder | Polar group+ bulky group+ crosslinking | Grind to fine powder, then premix with hardener |

* RT = Room Temperature

### 6.2.2 Sample Preparation

#### 6.2.2.1 Preparation of Pure Epoxy Resin

Epoxy/amine resin specimens were prepared by mixing the uncured EP solution with the amine-containing hardener at a fixed weight ratio of 1:0.38. A Thinky Mixer ARE-310 was utilized for planetary mixing at 2000 rpm and centrifugal defoaming at 2200 rpm. The clear and bubble-free mixture was then gently poured into stainless-steel or silicone molds with specific cavities for curing. The EP was cured at room temperature for 24 hours, followed by post-curing at 100ºC for 4 hours. The specimens were stored in a dry box at 40% relative humidity. The detailed procedure including mold preparation can be seen in section **3.2**.

#### 6.2.2.2 Preparation of Chemically Modified Epoxy Resin with AC, ACF and MA

The three modifiers, AC, ACF, and MA, were incorporated into the EP at concentrations of 0.5, 1.0, and 1.5 wt.%. The preparation method was similar to that of the neat EP, except

that the modifier was pre-mixed with the low-viscosity hardener solution before blending with the liquid EP. This step ensured optimal dispersion and homogeneous grafting throughout the system. The pre-treatment of modifiers to facilitate dissolution into the hardener varied based on their physical state, as detailed in **Table 6.1**. Notably, for the hardener and MA-methanol solution, the methanol was fully evaporated before proceeding to the next step, as verified through weight checks and FTIR analysis. Once a homogeneous hardener-modifier mixture was obtained, the liquid EP was added, cast, and cured following the same procedure described in Section **6.2.2.1**.

### 6.2.3 Chemical Structure Analysis

Fourier-transform infrared (FTIR) spectroscopy was employed to identify chemical reactions occurring during the modification process and to confirm the successful grafting of modifiers onto the polymer chain. The FTIR Frontier from PerkinElmer, equipped with attenuated total reflectance (ATR), was used. The light source spanned wavelengths from 4000-600 $cm^{-1}$ (with ATR for solid samples) and 4000-500 $cm^{-1}$ (without ATR for liquid samples), using 32 scan accumulations with a resolution of 4 $cm^{-1}$. For solid specimens, the dimensions are a rectangular block with a length of 40 mm, width of 10 mm, and thickness of 2.5 mm.

To understand the chemical reactions during curing, changes in chemical bonds under different curing states were evaluated using FTIR. Specimens were analyzed after 24 hours of room temperature curing, representing an incomplete curing state (defined as pre cure), and after an additional 4 hours of curing at 100 °C, representing the complete curing state (defined as post cure).

### 6.2.4 Analysis of Curing Behavior

Differential Scanning Calorimetry (DSC) tests were conducted using DSC Q10 from TA Instruments. To assess the curing behavior, the uncured epoxy resin, hardener, and modifier were mixed following the pretreatment outlined in Section **6.2.2.2** with testing

initiated within 10 minutes of mixing. The heating rate was 10°C/min, from 0°C to 250°C, and the heat released during curing was recorded. Duplicate tests were performed for each specimen type, and the curing heat values for specimens ($H_1$ and $H_2$) were confirmed to meet the inequality specified in BS ISO 14322 [249].

$$\frac{|H_1 - H_2|}{(H_1 + H_2)/2} \times 100 \leq 10\% \qquad (Equation\ 6.1)$$

Cured specimens, prepared as described in Section **6.2.2.2** (24 hours at room temperature followed by 4 hours at 100°C), were also analyzed by DSC under the same conditions (0 °C to 250 °C at 10° C/min). A few milligrams of film fragments were used for this test. The DSC curves of the cured specimens were compared with those of the uncured specimens to determine the degree of curing.

### 6.2.5 Dielectric Spectroscopy and Volume Resistivity

Dielectric spectra of the EP were acquired using a Meggar IDAX 300 to assess the effects of chemical modifications on the dielectric constant and dielectric loss. Volume resistivity was measured with a 6517B Electrometer from Keithley Instruments, designed for high-resistivity samples. The tests were conducted using uniform plate samples with a thickness of 2 mm and cylindrical electrodes with a guard ring, in accordance with IEC 62631.

### 6.2.6 Dielectric Breakdown Strength

The dielectric breakdown strength was measured using an AC high-voltage tester (Hipotronics 700 Series). Thin film specimens with a thickness of 200 μm were used to minimize the impact of defects. Step voltage was applied to the films via copper electrodes, with the initial voltage determined by a short-time test using a constant speed. Details can be found in ASTM D90. The data was analysed using a two-parameter Weibull distribution, as described by Equation 6.2, to evaluate the dielectric breakdown behaviour:

$$F(E;\alpha,\beta) = 1 - \exp\left\{-\left(\frac{E}{\alpha}\right)^{\beta}\right\} \quad \text{(Equation 6.2)}$$

where $F$ is the probability of failure at a given electrical stress. $E$ is the measured breakdown strength. $\alpha$ is the scale parameter representing the characteristic breakdown strength at 63.2% failure probability, and $\beta$ is the shape parameter describing the data distribution. A higher $\alpha$ indicates stronger resistance to dielectric breakdown.

### 6.2.7 Mechanical Properties

Tensile properties were characterized using a Shimadzu AGS-X mechanical tester, following ASTM D638 standards. A 20 kN load cell and a strain rate of 1 mm/min were used. Dog-bone-shaped test samples with a thickness of 2.5 mm, a width of 3.18 mm, and a gauge length of 7.62 mm were used. Tensile strength and Young's modulus were determined from these tests. Hardness was measured using a MITECH MH180 Leeb Hardness Tester on the same specimen before tensile measurements.

### 6.2.8 Fractographic Analysis

The morphology and element dispersion on the fracture surfaces of EP samples were analysed using a field emission scanning electron microscope (SEM) and energy-dispersive X-ray analysis (EDX). JEOL JSM 7800F Prime, equipped with an Oxford Ultim Max EDS detector, was used for this analysis. A platinum coating, along with conductive tapes, was applied to the sample surface to obtain high-quality images of non-conductive polymers.

### 6.2.9 Thermal Stability

Dynamic mechanical analysis (DMA) was conducted to measure the glass transition temperature ($T_g$) of the EP. Rectangular specimen with a length of 40 mm, width of 10 mm,

and thickness of 2.5 mm were used in this test. The three-point bending mode was used, with the temperature range extending from room temperature to 200°C.

## 6.3 Results

### 6.3.1 Chemical Change During Modification Process

#### 6.3.1.1 Allyl Chloroacetate-Epoxy Resin (EP-AC)

The FTIR spectra of EP-AC are shown in **Figure 6.1(a)**. The right section displays the spectra for post-cured EP-AC with different AC contents. The characteristic C=O peak at 1743 $cm^{-1}$ [250] is observed in all EP-AC samples and increases with higher AC content, confirming the existence of AC in the EP system. To ensure that AC is chemically bonded to the polymer chain, further analysis was conducted. The chemical bonds in EP containing 1.5 wt.% AC (EP-AC-1.5) were characterized before and after heat curing, as illustrated in the left section of **Figure 6.1(a)**. The reduction in the intensity of the C=C peak at 1648 $cm^{-1}$[251] suggests the consumption of C=C bonds in AC and their integration into the EP chain. The consistent C=C intensities across different AC concentrations further support this conclusion. The proposed reaction mechanism, shown in **Figure 6.1(d)**, suggests that the C=C bond in AC reacts with -NH- groups in the epoxy/amine resin.

#### 6.3.1.2 2-Amino-5-Chloro-2'-Fluorobenzophenone-Epoxy Resin (EP-ACF)

ACF contains amine groups, which are similar to the curing sites of the amine hardener in this EP system. One ACF molecule can potentially bond with two epoxy rings, thereby enhancing crosslinking. The FTIR spectra of EP-ACF with varying ACF content are shown in **Figure 6.1(b)**. A decrease in the epoxide peak at 912 $cm^{-1}$ [29], [252] is observed as ACF content increases, indicating greater consumption of epoxy rings by ACF. Therefore, it can be concluded that the amine groups in ACF react with epoxy rings, as illustrated in the reaction mechanism in **Figure 6.1(d)**.

#### 6.3.1.3 Maleic Anhydride-Epoxy Resin (EP-MA)

As shown in **Figure 6.1(c)**, there is an increase in the ester bond peak at 1735cm$^{-1}$ and a decrease in the epoxide peak at 912cm$^{-1}$ [29], [250], [252] as MA content increases. This indicates the consumption of epoxide groups, along with the formation of ester bonds. The same trend is also evident in the comparison of specimens before and after heat curing, directly indicating the grafting process of MA onto the EP chain. The proposed chemical reaction mechanism is shown in **Figure 6.1(d)**. Each MA molecule contains two reactive sites that can react with epoxy groups, contributing to crosslinking.

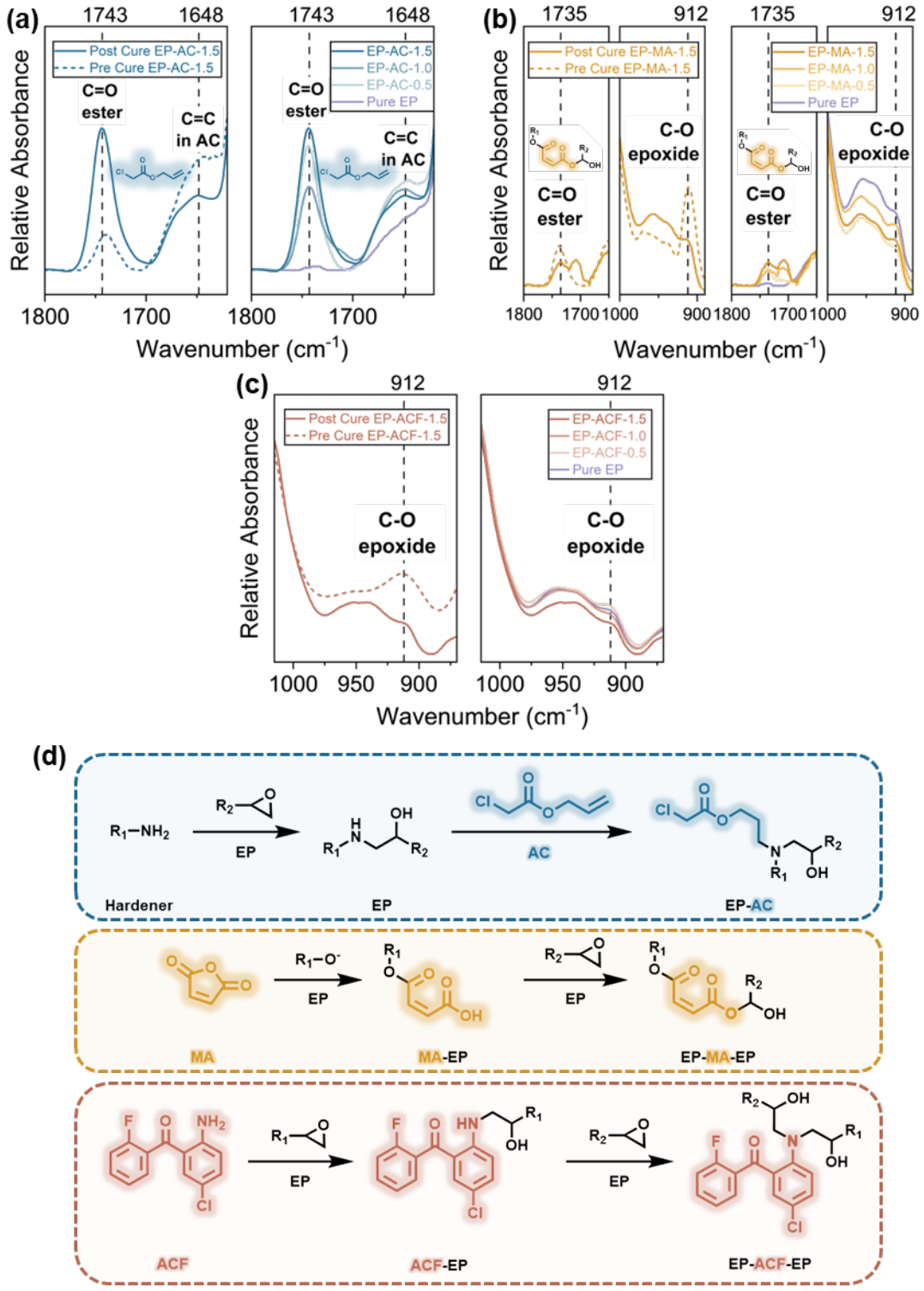


**Figure 6.1** Chemical changes during the molecular modification of EP. **(a-c)** FTIR spectra of EP modified with AC, MA, and ACF, respectively, before and after thermal post-curing, and with

varying modifier dosages after complete curing. **(d)** Proposed mechanisms for the chemical grafting of the three modifiers onto the EP chain.

#### 6.3.1.4 Curing Behavior of Modified EP

Differential Scanning Calorimetry (DSC) was used to investigate the degree of curing for all modified EP with the highest dosage of 1.5 wt.%. The DSC curve comparisons for uncured and cured EP with 1.5 wt.% modifiers are illustrated in **Figure 6.2**. The DSC curves for uncured specimens displayed distinct exothermic peaks, indicating ongoing curing. In contrast, the cured specimens (under the conditions described in Section **6.2.2.2**) showed flat curves with no exothermic activity, indicating that curing was effectively complete for all three modified epoxy resins.

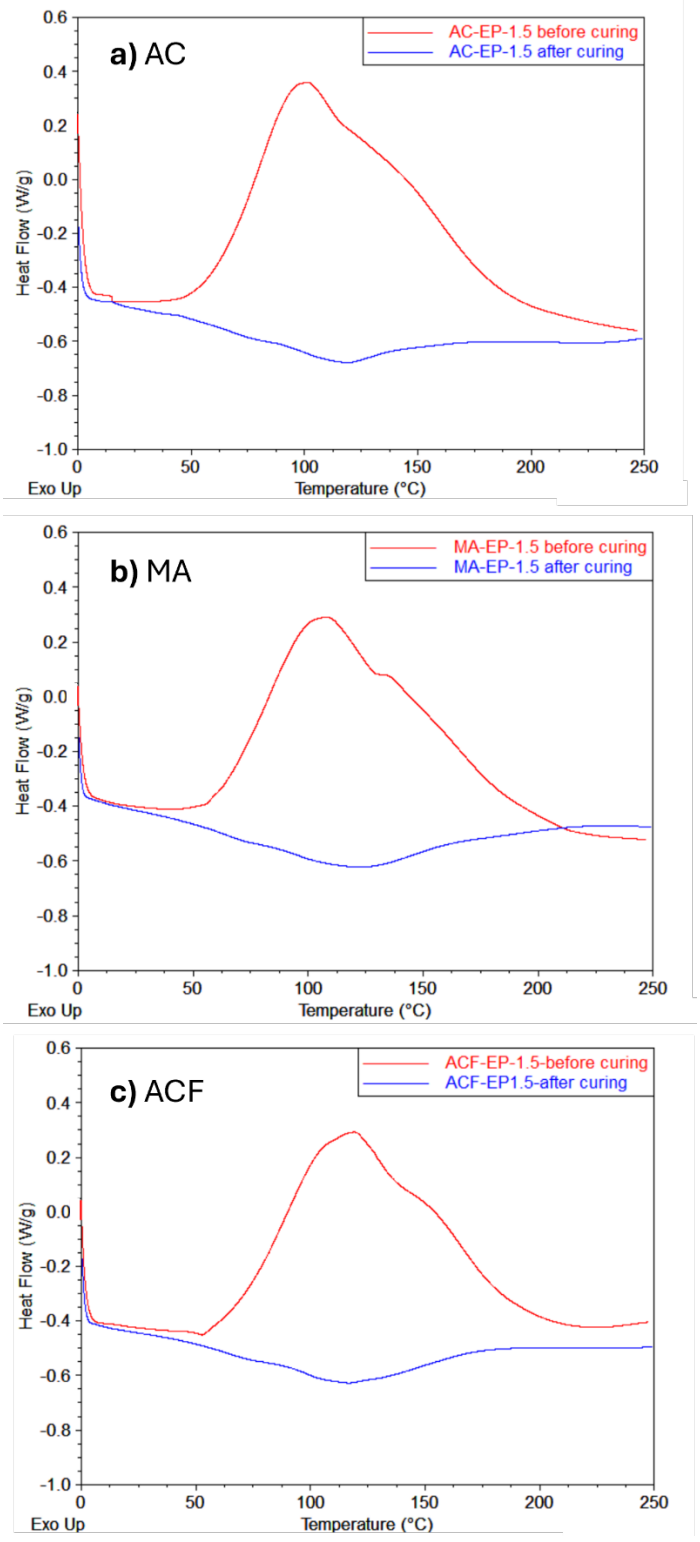


**Figure 6.2** DSC curves for uncured and cured **(a)** EP-AC-1.5, **(b)** EP-MA-1.5, and **(c)** EP-ACF-1.5.

### 6.3.2 Microstructural Analysis of Chemically Modified Epoxy Resin

EDX analysis was conducted to assess the dispersion of the modifiers. The elemental mappings for various elements in the modified EP with 1.5 wt.% modifier content are shown in **Figure 6.3(a-d)**. The mappings demonstrate a homogeneous distribution of elements, including those specific to the modifiers, confirming the uniform dispersion of the modifiers in the EP matrix. Specifically, **Figure 6.3 (b)** to **(d)** illustrate well-dispersed elemental signals for carbon (C), nitrogen (N), oxygen (O), and modifier-specific elements like chlorine (Cl) and fluorine (F). This indicates effective incorporation of the modifiers on molecular level without any agglomeration. It ensures a uniform composition throughout the EP matrix, addressing issues such as agglomeration and uneven dispersion commonly seen in filler-incorporated composites.

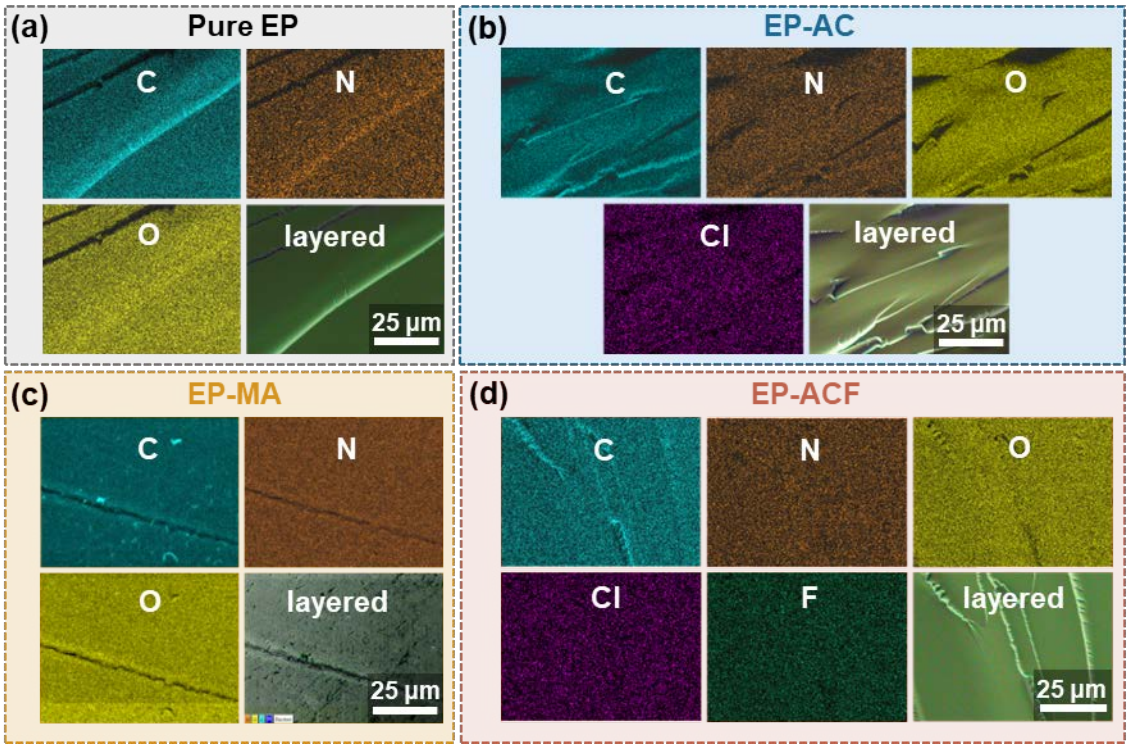


**Figure 6.3** EDX elemental mapping of the fracture surfaces for **(a)** Pure EP, and EP modified with 1.5 wt.% of **(b)** AC, **(c)** MA and **(d)** ACF.

### 6.3.3 Improvement in Dielectric Properties

#### 6.3.3.1 Dielectric Constant and Dielectric Loss

The dielectric spectra of EP modified with AC, MA, and ACF at varying concentrations were analyzed using the capacitance method at room temperature. **Figure 6.4(a-c)** illustrates the dielectric constant and dielectric loss spectra across multiple frequencies. **Figure 6.4(d)** compares the dielectric spectra of the three modified EP at their optimal modifier contents: 1.0 wt.% for EP-AC, 0.5 wt.% for EP-MA, and 1.5 wt.% for EP-ACF. Generally, all modified EP exhibit lower dielectric constants and dielectric losses compared to pure EP, primarily due to enhanced crosslinking density. Additionally, both the dielectric constant and loss decrease with increasing frequency.

The dielectric constant and loss at a fixed frequency of 50 Hz are compared in **Figure 6.4(e,f)**. All modified EP, regardless of the modifier concentration, exhibit a lower dielectric constant than pure EP. Each type of molecular modification has a distinct impact on the dielectric properties of the epoxy resin:

**1) EP-ACF**

ACF introduces bulky aromatic groups, which create steric hindrance and restrict dipole alignment under an electric field. In addition, ACF promotes crosslinking within the polymer matrix, forming a more rigid structure and limiting charge carrier movement. These combined effects lead to a 27% reduction in dielectric constant and a 42% reduction in dielectric loss for EP-ACF-1.5 compared to pure EP.

**2) EP-MA**

MA reacts with up to two epoxide groups, promoting crosslinking that limits dipole mobility and reduces polarization. Consequently, EP-MA-0.5 exhibits a dielectric constant up to 30% lower than pure EP. The increased crosslink density also reduces dielectric loss by limiting charge carrier movement, resulting in a 10% reduction compared to pure EP.

Due to competition with the hardener and the high molar concentration of MA, the optimal dosage by weight must be carefully selected.

**3) EP-AC**

The grafting of AC molecules onto the epoxy resin chain increases molecular weight, enhancing the rigidity of the polymer chain and hindering dipole movement. This results in a 20% reduction in the dielectric constant for EP-AC-1.0 compared to pure EP. The increased rigidity also contributes to a 12% reduction in dielectric loss.

In summary, all three modifications are able to reduce the dielectric constant and loss of epoxy resin through different strategies. Among them, ACF is the most effective, followed by MA and AC. These reductions in dielectric constant and loss significantly enhance the performance of EP in electrical and electronic applications by minimizing power dissipation and signal delays [253], [254].

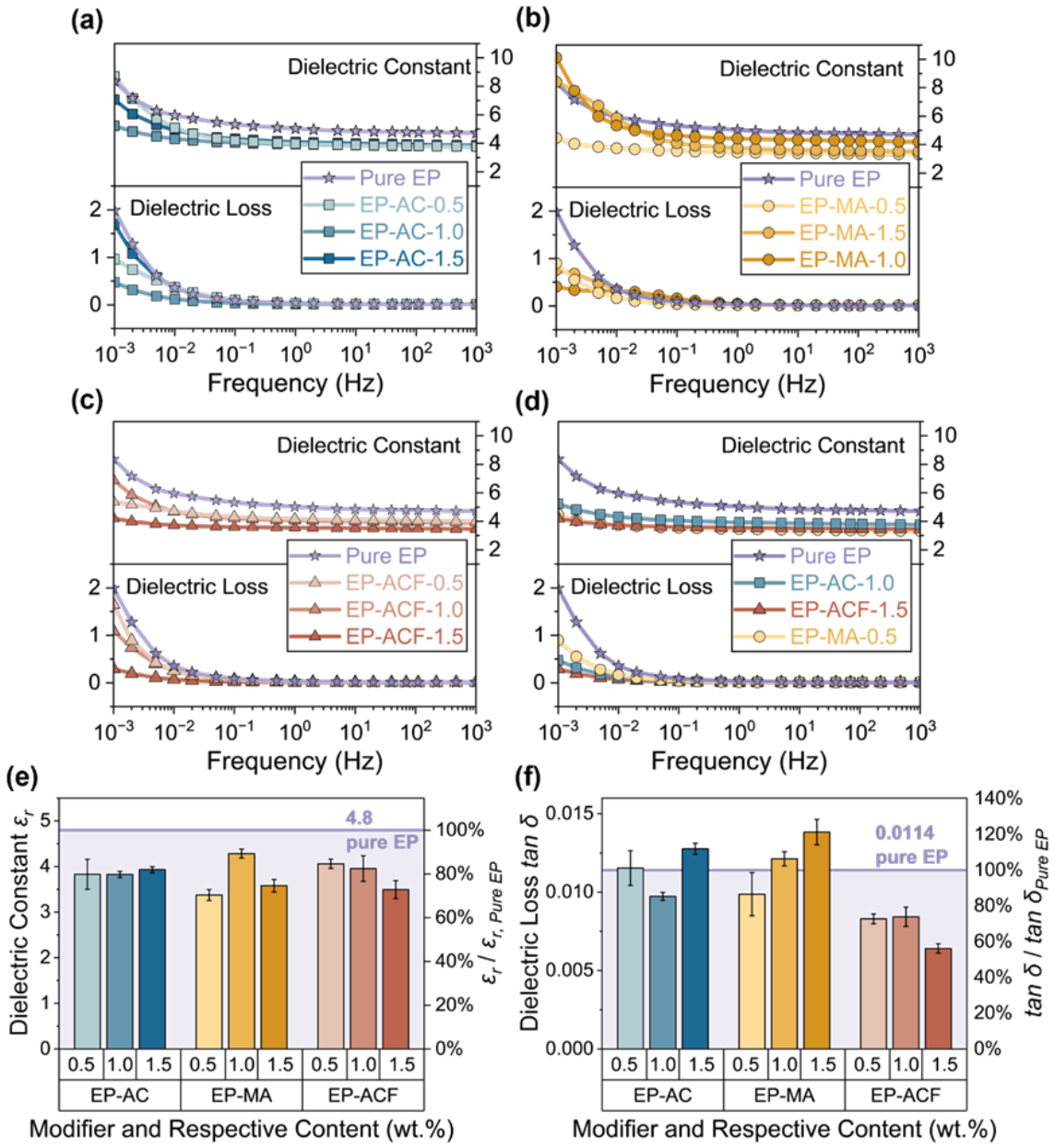


**Figure 6.4** Dielectric properties of modified EP. **(a-c)** Dielectric constant and dielectric loss spectra for EP modified with varying concentrations (0, 0.5, 1.0, and 1.5 wt.%) of **(a)** AC, **(b)** MA, and **(c)** ACF. **(d)** Comparison of dielectric constant and dielectric loss spectra for the three modifiers at their optimal concentrations. Comparison of **(e)** dielectric constant and **(f)** dielectric loss for AC, MA, and ACF-modified EP at various dosages tested under 50 Hz.

### 6.3.3.2 Volume Resistivity

Volume resistivity of the modified EP was measured using an electrometer at ambient temperature. As shown in **Figure 6.5(a)**, all modified EP exhibit significant improvement in resistivity compared to pure epoxy. This enhancement is attributed to the polar groups in the modifiers, which form deep traps that capture charge carriers and reduce their mobility [255], [256]. Notably, EP-MA-0.5 achieves the highest resistivity at $1.1\times10^{15}$ Ω·cm, which is 17 times higher than that of pure EP, as shown in **Figure 6.5(b)**. EP-AC-1.5 follows with a resistivity of $4.7\times10^{14}$ Ω·cm, a 7-fold increase compared to pure EP. EP-ACF-1.0 shows a smaller improvement, with a 5-fold increase in resistivity, due to the lower density of polar groups in ACF. Interestingly, peak resistivity values are observed in both EP-ACF and EP-MA systems. When excessive ACF or MA is present, they compete with the hardener for epoxy rings, resulting in defects that reduce electrical durability. These defects are primarily structural irregularities caused by incomplete or disrupted crosslinking, leading to shorter or more branched polymer chains and microstructural heterogeneities [22], [257]. Additionally, excess modifier and unreacted hardener act as impurities within the thermoset network, increasing the polymer free volume, compromising uniformity and creating localized weak points that further degrade performance [258]. Therefore, identifying the optimal modifier content is crucial.

#### 6.3.3.3 Dielectric Breakdown Strength

The dielectric breakdown strength of the modified EP was tested under AC voltage in insulating oil at ambient temperature. Two-parameter Weibull statistical analysis was employed to determine the failure probability of specimens under varying electrical stress.

The characteristic dielectric breakdown strength ($\alpha$) for each group is summarized in **Figure 6.5(c)**, indicating that all modifiers can effectively improve dielectric durability. **Figure 6.5(d)** illustrates the failure probability of pure EP and all modified EP at optimal concentrations. EP-MA-0.5 shows the highest breakdown strength at 73.9 kV/mm, which is 120% of that of pure EP (61.5 kV/mm). The ester bond in MA, particularly the carbonyl (C=O) groups, introduces charge traps in the polymer [259], [260]. Due to the high concentration of C=O groups in MA, the density of charge traps is significantly increased

in EP-MA. These deep traps effectively reduce charge mobility and impede space charge accumulation, thereby enhancing the dielectric properties and electrical resistivity of the modified polymer. Improved breakdown strength can also be seen in EP-AC-1.5 at 73.4 kV/mm and EP-ACF-1.0 at 64.0 kV/mm.

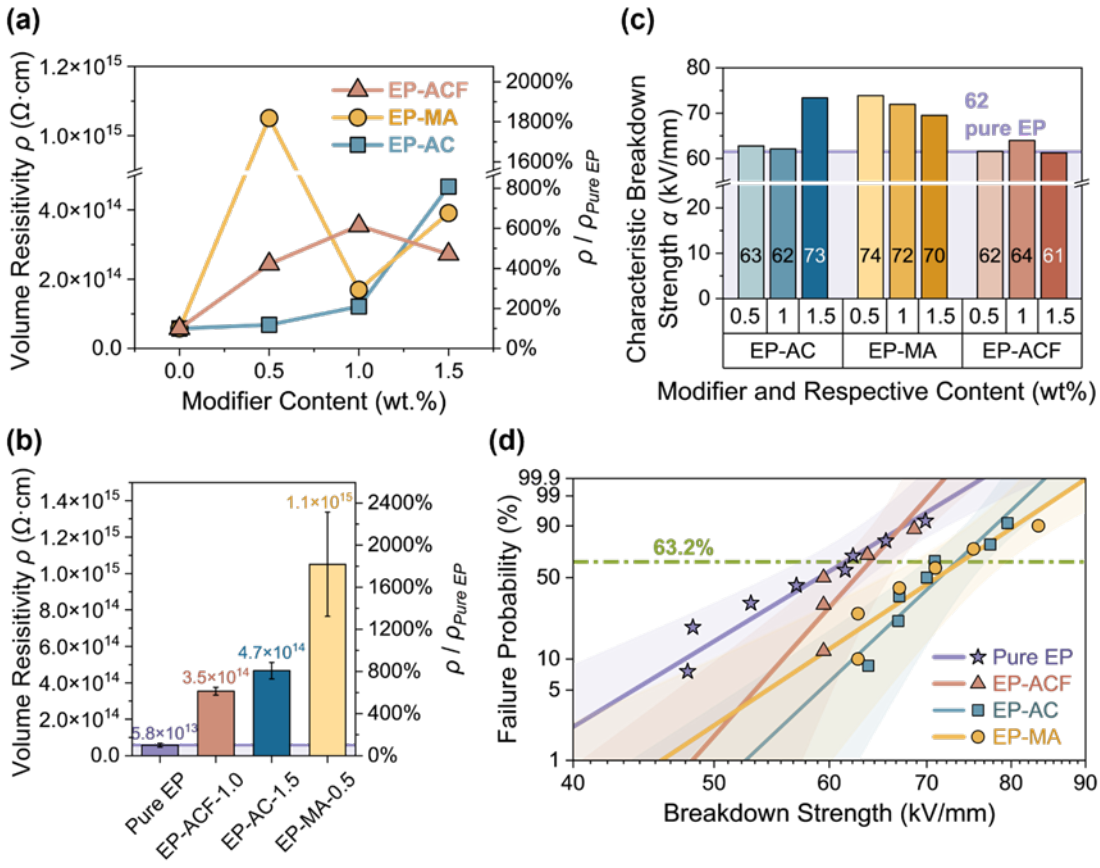


**Figure 6.5** Volume resistivity and dielectric breakdown. **(a)** Volume resistivity for pure EP and AC, MA, and ACF modified EP with various concentrations. **(b)** Comparison of volume resistivity for the modified EP with the optimal modifier concentrations. **(c)** Characteristic AC breakdown strengths when failure probability is at 63.2%. **(d)** Failure probability of pure and modified EP at optimal concentrations under various electrical stresses, analyzed using Weibull statistics.

### 6.3.4 Mechanical Properties

The mechanical properties of the modified EP including tensile strength, Young's modulus, and hardness, were characterized. Tensile strengths for all groups are shown in **Figure**

**6.6(a)**. Among the modifiers, AC is the most effective, increasing the tensile strength of EP-AC-1.5 from 69.7 MPa (pure EP) to 77.7 MPa. The tensile strength improves with increasing AC content, which can be attributed to the high concentration of ester bonds in AC, leading to a more stable mechanical structure [232], [233], [261]. ACF and MA modifications also enhance the mechanical strength, with both achieving the tensile strength of 75.4 MPa at their optimal concentrations. The Young's modulus values are displayed in **Figure 6.6(b)**, revealing significant improvements due to these molecular modifications. Specifically, EP-AC-1.5 demonstrates the highest modulus at 787 MPa, followed by EP-ACF-1.5 at 735 MPa and EP-MA-1.5 at 695 MPa, while the modulus for pure EP is 618 MPa. The hardness of the modified EP was also evaluated and illustrated in **Figure 6.6(c)**. All three modifications benefit the hardness of the EP due to the enhanced crosslinking within the polymer network. MA produces the greatest improvement in hardness, followed by ACF and AC.

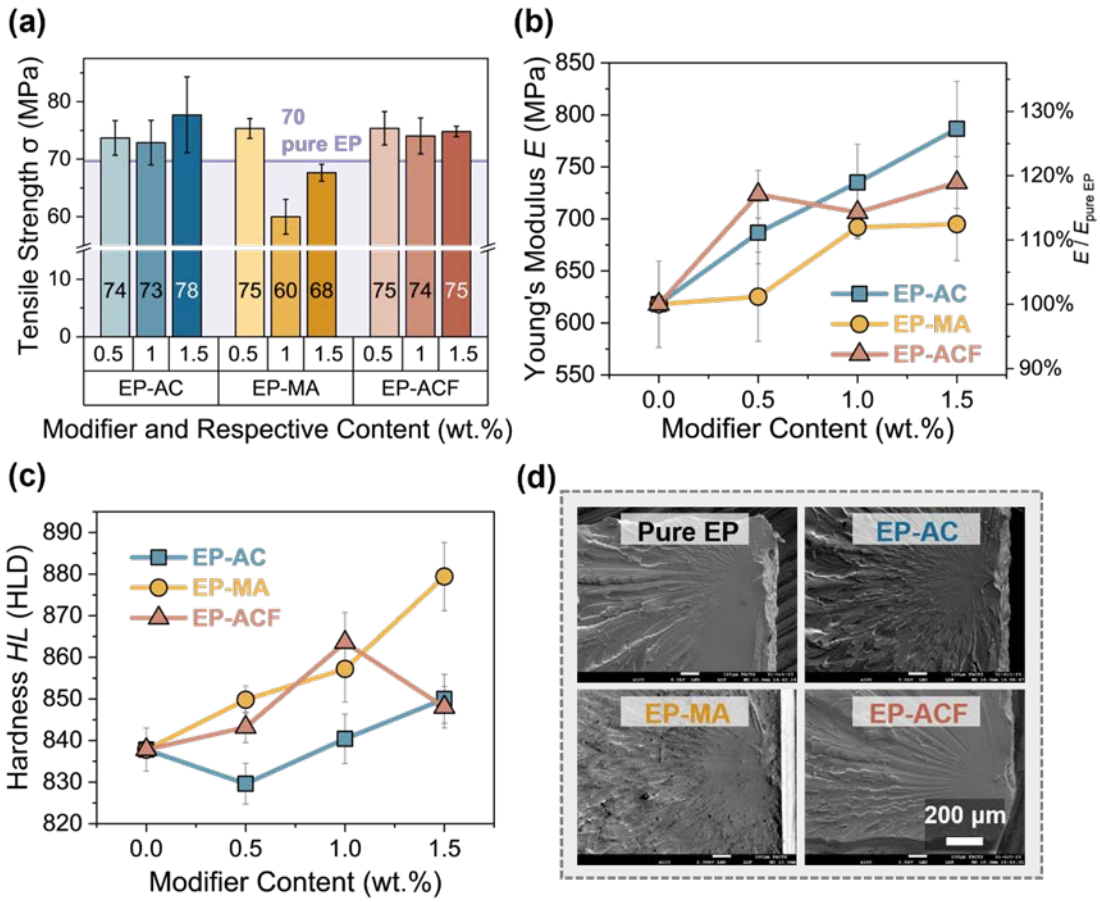

**Figure 6.6** Mechanical properties of modified EP. **(a)** Tensile strength, **(b)** Young's modulus, and **(c)** hardness for modified EP at various modifier concentration. **(d)** SEM images of fracture surfaces for pure and modified EP.

### 6.3.5 Thermal Properties

The $T_g$ of the modified epoxy resins was measured via DMA to assess the thermal properties. As shown in **Figure 6.7(a)**, all three types of modifications result in increased $T_g$ at their optimal modifier content. EP-AC-1.5 exhibits the highest $T_g$ at 140 °C, while the $T_g$ of pure EP is 130 °C. The next one is EP-ACF-1.5 with a $T_g$ at 136 °C, followed by EP-MA-0.5 at 131 °C. The increase in $T_g$ can be attributed to the enhanced crosslinking within the polymer network [262] and extended chain length [263]. Additionally, the rigid benzene rings in ACF also contribute to the increased $T_g$ due to the steric hindrance effect [264], [265]. The increased crosslinking density is the main factor driving the improvement in resistivity and breakdown strength.

Notably, $T_g$ for EP-MA decreases as MA content increases. This weakening effect, due to excessive MA, is also observed in tensile strength and dielectric durability. This is caused by competition between MA and the amine hardener, reducing crosslinking efficiency and increasing the polymer free volume [257]. Reduced crosslinking is confirmed by the curing dynamics study. The released heat during the curing reaction decreases with increasing MA concentration. Therefore, the optimal dosage of modifiers must be carefully selected.

### 6.3.6 Water Absorption

Water absorption behavior is critical for dielectric materials if the equipment is designed to operate in humid environments, as moisture can adversely affect dielectric properties due to the high polarity of water molecules [266].

While the introduction of polar groups into epoxy resins benefits properties such as resistivity and dielectric breakdown strength, these same polar groups also increase water

absorption [267], which is adverse to the dielectric performance of the material. Accelerated water absorption tests were conducted in boiling water for all three types of modified resins with the highest modifier dosage (1.5 wt.%). As illustrated in **Figure 6.7(b)**, EP-MA-1.5 shows higher water absorption than pure EP due to the incorporation of ester bonds. This highlights the trade-off between enhanced dielectric properties and reduced hydrophobicity. Bulky groups such as benzene and fluorinated groups incorporated by ACF are expected to mitigate this adverse impact. The addition of benzene helps hinder water diffusion, while fluorinated groups reduce the polarizability of the polymer [242]. As a result, EP-ACF not only shows lower water absorption than pure epoxy resin but also maintains high resistivity and strong dielectric properties. These combined benefits make EP-ACF an ideal candidate for dielectric applications in humid environments.

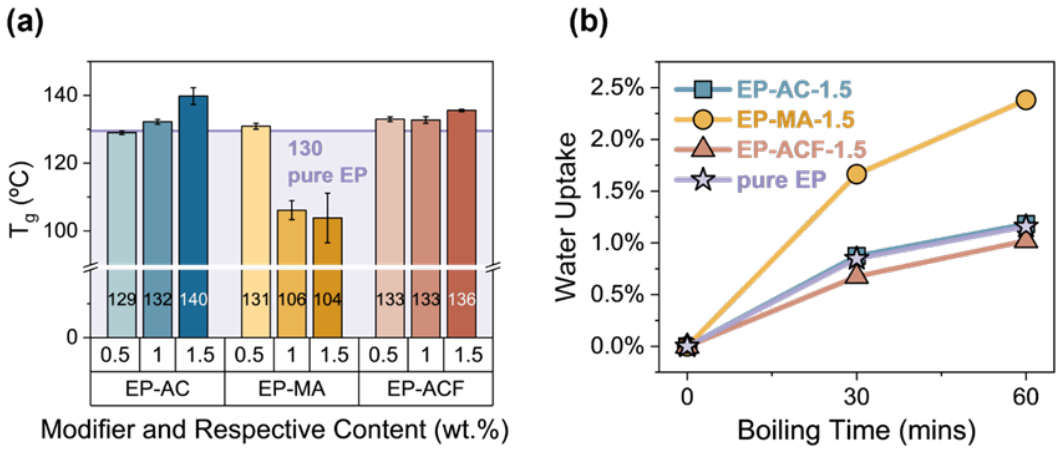


**Figure 6.7** **(a)** $T_g$ of modified EP at various modifier concentrations. **(b)** Water absorption of modified epoxy resins with 1.5 wt.% modifier content.

### 6.3.7 Long-Term Aging Performance

Long term hygrothermal aging behavior is critical for dielectric materials if the equipment is designed to operate in humid environments, as moisture can adversely affect dielectric properties due to the high polarity of water molecules [266].

While the introduction of polar groups into epoxy resins benefits properties such as resistivity and dielectric breakdown strength, these same polar groups also increase water

absorption [267], which is adverse to the dielectric performance of the material. Hygrothermal aging tests were conducted for all three types of modified resins with the highest modifier dosage (1.5 wt.%). As illustrated in **Figure 6.8(a)** and **Figure 6.8(b)**, EP-AC shows the most unstable performance in dielectric constant/loss and resistivity after 1200 hours aging, followed by EP-MA. Due to the incorporation of ester bonds, the modified EPs tend to absorb more water, which significantly impacts the electrical properties due to the strong dipoles [243]. Additionally, humidity can cause the disruption of polymer chains and increase in free volume [244]. This highlights the trade-off between enhanced dielectric properties and reduced hydrophobicity. Bulky groups such as benzene rings and fluorinated groups incorporated by ACF are expected to mitigate this adverse impact. The addition of benzene helps hinder water diffusion, while fluorinated groups reduce the polarizability of the polymer [242]. As a result, EP-ACF shows the most stable long-term dielectric properties (+24% in dielectric constant and +6.7 times in dielectric loss). Notably, EP-ACF presents the lowest initial resistivity among the three modifications but maintains the highest resistivity after 1200 hours of hygrothermal aging. These stable properties under extreme hydrothermal conditions make EP-ACF an ideal candidate for dielectric applications in humid and hot environments.

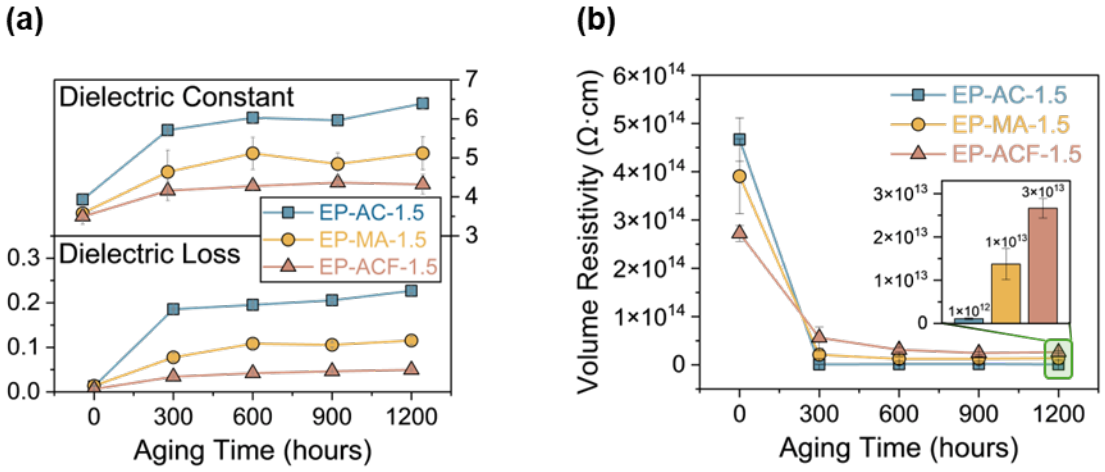


**Figure 6.8** **(a)** Dielectric constant/loss and **(b)** volume resistivity of modified EP with 1.5 wt.% modifier content at 50 Hz with various aging durations.

## 6.4 Summary

In this study, epoxy/amine resin was successfully modified at the molecular level using strategies such as incorporating charge traps, adding bulky groups, and promoting crosslinking to enhance its dielectric, mechanical, and thermal properties.

Molecular modification offers a simple and effective way to enhance epoxy resin durability by directly strengthening its polymer network. Unlike nano/micro filler incorporation, which faces challenges such as dispersion issues and interfacial defects, molecular modification ensures uniform property improvement without introducing weak points. It is also easier to implement, avoiding complex dispersion processes while still enhancing mechanical, thermal, and dielectric properties. Additionally, it requires only a low dosage of modifiers, reducing costs, and maintains low viscosity, ensuring good processability.

Based on the results from FTIR, dielectric spectroscopy, resistivity, breakdown tests, mechanical characterizations, DMA, SEM, and EDX, the following conclusions are drawn:

(1) All modified EP show reduced dielectric constant and loss compared to pure EP, primarily due to the introduction of bulky groups and crosslinking effects, minimizing dielectric polarization and molecular mobility. ACF is the most effective due to both bulky groups and crosslinking potential, followed by MA and AC.

(2) Volume resistivity and dielectric breakdown strength improve significantly in modified EPs, with EP-MA achieving $1.1\times10^{15}$ Ω·cm for resistivity and 74 kV/mm for breakdown strength. These improvements are due to deep traps formed by functional groups and increased crosslink density, hindering charge carrier movement and preventing electrical failure.

(3) Mechanical and thermal properties are enhanced, particularly in EP-AC-1.5, which shows increased tensile strength (78 MPa), Young's modulus (787 MPa), and $T_g$ (140°C). MA and ACF also demonstrate improved tensile strength, modulus, and

thermal stability at optimal dosage.

(4) EP-ACF shows reduced water uptake compared to pure EP, due to bulky benzene and fluorinated groups that hinder water diffusion, making it suitable for humid environments.

(5) FTIR confirms the structural modification, with bulky groups and crosslinking sites to enhance dielectric, mechanical and thermal properties and polar groups to form charge traps, improving dielectric durability. SEM and EDX confirm homogeneous distribution.

(6) Optimizing modifier dosage is crucial for achieving desired properties. The uniform distribution and effectiveness of these modifications make the properties highly sensitive to modifier concentration. The recommended dosages are 0.5 wt.% for MA and 1.5 wt.% for AC and ACF.

# Chapter 7

# Conclusions and Recommendations

*This chapter summarizes the contributions of this research and provides recommendations for future development and improvement.*

## 7.1 Conclusions

This thesis investigates the degradation mechanisms and develops strategies to improve the durability of epoxy-based insulation materials for high-stress electrical applications. By examining the roles of void formation, interfacial bonding in composites, and improvement through molecular modifications, this research advance understanding of degradation mechanism and offer practical directions for improving epoxy insulation reliability.

The study initially focused on evaluating the impact of voids and thermal aging on pure epoxy resin. Voids formed during manufacturing were found to act as stress concentrators that accelerate material breakdown, especially under thermal stress. Weibull statistics incorporated with defect density parameter quantitively described the impact of aging and voids on the mechanical performance, showing that specimens with lower void content demonstrated improved resistance, highlighting the importance of void removal or minimizing void formation during manufacturing. By improving processing methods to reduce void content, the long-term reliability of electrical insulation materials can be substantially enhanced, particularly in switchgear components that experience thermal and mechanical stresses. The heterogeneous degradation mechanism driven by oxidation diffusion from the surface to its core was revealed by chemical investigation, compromising mechanical stability over time. These results support the hypothesis that a more precise evaluation of void and thermal aging impacts can be achieved by using Weibull analysis and accelerated thermal testing.

Further investigation into interfacial defects in epoxy composites focused on filler-matrix interactions. By incorporating fillers with different surface wettability, the study assessed their impact on the stability of the composites under hygrothermal conditions. It was observed that hydrophilic fillers, due to their stronger bonding with the epoxy, provide better durability in both mechanical and dielectric properties compared to hydrophobic fillers. This highlights the importance of proper filler surface that enhances interfacial bonding, which helps mitigate the formation of interfacial defects, thereby enhancing the material reliability. In industrial applications, incorporating hydrophilic fillers can lead to

more durable composites, especially in environments where moisture and thermal resistance are critical, such as in tropical or other extreme conditions. These findings confirm the hypothesis that the interfacial defects impact on long-term performance, and the current study has deepened the understanding by analyzing the effects of fillers with varying degree of surface wetting states.

Additionally, the research explored molecular modifications aimed at strengthening epoxy resin at a molecular level, avoiding interfacial defects issue in epoxy composites. By introducing polar, bulky groups, and extra crosslinking sites, the study achieved simultaneous improvements in dielectric strength, mechanical resilience and thermal stability. Importantly, the preparation process for these modifications was both simple and efficient, requiring ultra-low dosage (≤ 1.5 wt.%) of modifiers to achieve substantial performance gains. The modified epoxy resin displayed a lower dielectric loss and enhanced mechanical and dielectric durability, validating the hypothesis that properly designed molecular-level modifications can provide substantial improvements. These enhancements allow the resins to withstand elevated temperatures, electric fields, and environmental stresses, making them ideal for use in power systems. This facile, cost-effective preparation approach offers a practical, scalable solution for enhancing epoxy durability, providing a strong foundation for future material development in demanding electrical environments.

While the molecular modification of epoxy resins enhances multiple properties simultaneously, its effectiveness may vary depending on the chemical structure of the epoxy resin used. For resins that lack the necessary reactive sites, the modifiers may not yield optimal results. To overcome this limitation, it is crucial to select the corresponding modifier that contains the functional groups required to react with the epoxy resin's specific chemical structure. Strategies such as promoting crosslinking, introducing deep traps, and adding bulky groups have been confirmed to be effective in improving the properties of epoxy resins with appropriate reactive sites. Therefore, understanding the chemical structure of the epoxy resin is essential in selecting the right modifier. Future work should

focus on developing and testing modifiers that are specifically tailored to different epoxy resins, ensuring better compatibility and improved performance.

Overall, this thesis enhances the understanding of degradation mechanisms in epoxy-based insulation materials and presents strategies to improve their durability, offering practical recommendations for the electrical industry. Through targeted experiments and analyses, the findings validate the initial hypotheses and provide valuable insights for future material design, aligning closely with the original aim of improving the durability and reliability of epoxy-based insulation materials.

## 7.2 Future Work

Building on the findings and contributions of this research, several opportunities for future work are identified. These recommendations aim to further enhance the performance, durability, and application range of epoxy-based insulation materials in demanding electrical environments.

### 1) Self-Healing Strategies in Insulating Materials

Recently, the self-healing strategy for dielectric damage is also reported. Microcapsules containing UV-sensitive healing agent, which flows into tree channels and are cured by the electroluminescence from electrical treeing, were dispersed in the polymer matrix to obtain the self-healing ability, as shown in **Figure 7.1** [43]. Moreover, the capsules can be magnetically directed to the high-failure probability region, reducing the concentration of the capsules, as shown in **Figure 7.2**. While these strategies demonstrate healing potential, they present challenges, such as disruption to the polymer structure and interfacial defects introduced by the microcapsules, which can weaken overall performance, particularly over the long term. Therefore, further investigation in this area is essential, with a focus on addressing interfacial issues and developing novel strategies to mitigate these limitations.

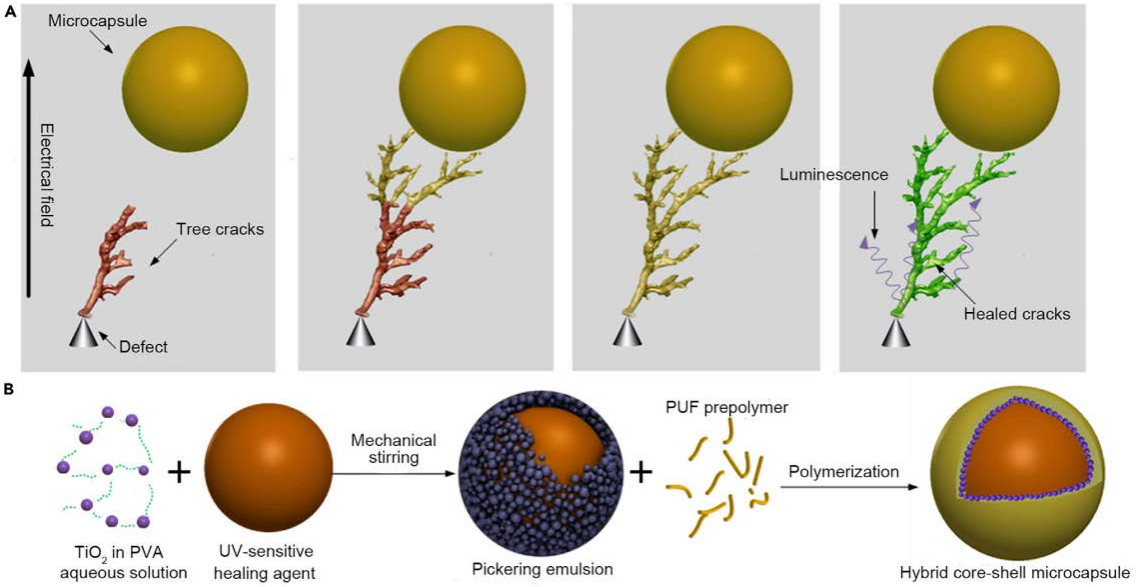


**Figure 7.1** Design of the Healing Strategy and Preparation of the Microcapsules [43]. *Open access, no permission is required.*

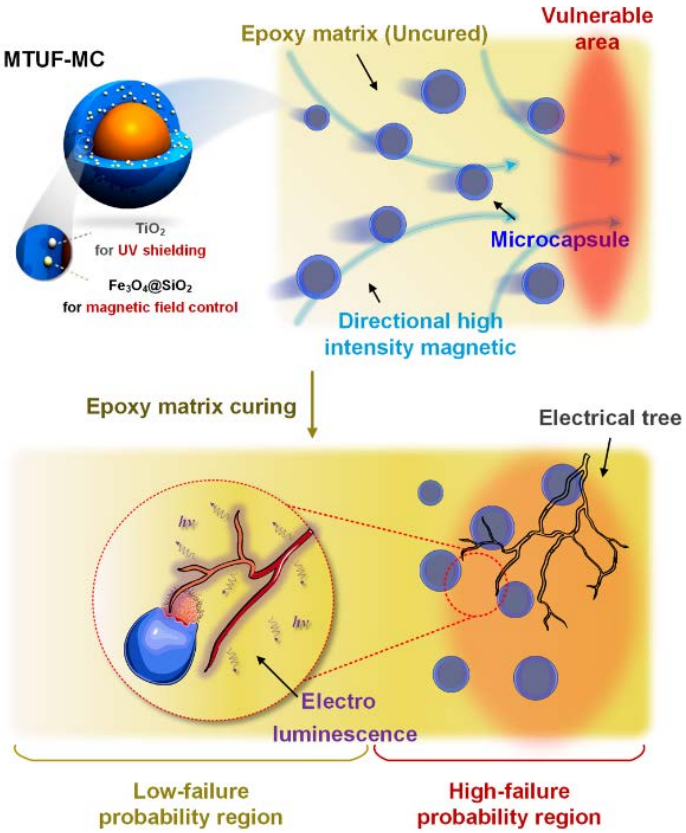


**Figure 7.2** Schematic of Magnetically Targeted Self-Healing. Reprinted with permission from [268].

**2) Simultaneous Improvement in Thermal Conductivity and Dielectric Breakdown**

To satisfy the requirement of the emerging power system with high densification, the improvement in the dielectric and thermal performance of polymeric insulating materials is still urgent. However, the improvement of thermal conductivity is always accompanied by the loss of electrical insulation ability. A significant challenge is to improve the dielectric ability and thermal conductivity of polymer insulations simultaneously [150].

Wang et al. prepared an epoxy composite with 200 nm $Al_2O_3$ microsphere(A) and 1 μm BN nanosheet (B), as shown in **Figure 7.3** [269]. At low loading of fillers, A6+B2(epoxy resin with 6 %wt. $Al_2O_3$ and 2 %wt. BN) shows 3 times increase in thermal conductivity, low dielectric loss (0.022, while neat epoxy resin EP is 0.05), higher $T_g$ than neat EP and maintains a close dielectric breakdown strength compared to neat epoxy resin. Other strategies introducing magnetic directed fillers achieve the simultaneous improvement at specific directions. Ruan et al. proposed a 2d ordinal filler structure by doping $Fe_3O_4$ on BN microparticles (plate) and applying a rotating magnetic field during curing, as shown in **Figure 7.4**[270]. The dielectric breakdown strength of the composite is improved to 127% of BN/EP and 118% of neat epoxy resin. The researchers reported that large current density was mainly concentrated in the region of BN bridging along the electric field direction. And there is no need to reach the completely ideal tiling, which can reduce the amount of $Fe_3O_4$ used and minimize the impact of adding $Fe_3O_4$. This strategy improves the thermal conductivity and dielectric breakdown strength simultaneously in specific directions. While this strategy enhances thermal conductivity and dielectric breakdown strength directionally, further research is needed to achieve simultaneous improvements in multiple directions, as well as simplify preparation procedure and reduce costs.

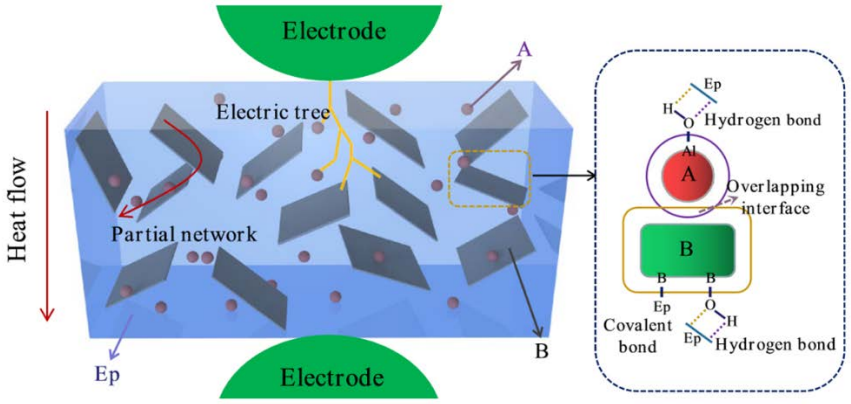


**Figure 7.3** Thermal conductive network and hindrance to electrical tree [269]. *Open access, no permission is required.*

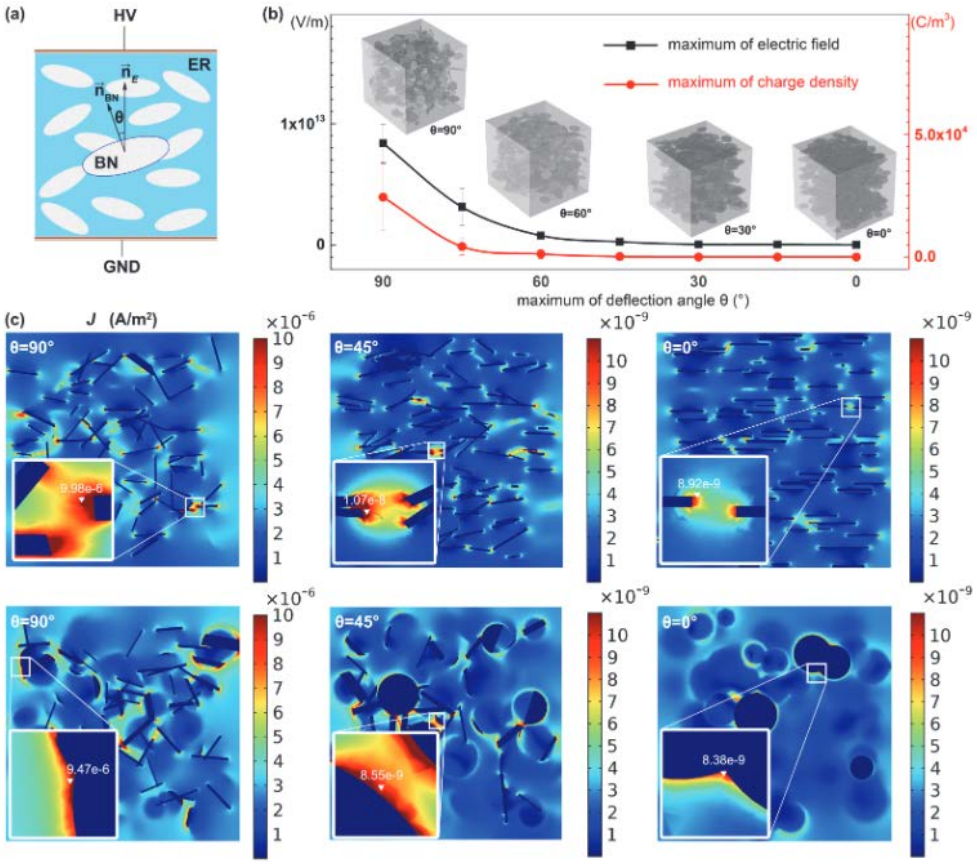


**Figure 7.4** **(a)** Scheme of model settings. **(b)** The variation of max electric field and max charge density (in resin matrix) as a function of deflection angle θ. **(c)** Current density distributions for models in 90, 45 and 0°deflection angles (the upper side view, the lower the vertical view) [270]. *No permission is required for thesis purposes.*

# REFERENCES

**Reference**

[1] B. Du, Ed., *Polymer Insulation Applied for HVDC Transmission*. Singapore: Springer Singapore, 2021. doi: 10.1007/978-981-15-9731-2.

[2] S. Sundhar, A. Bernstorf, W. Goch, D. Linson, and L. Huntsman, 'Polymer insulating materials and insulators for high voltage outdoor applications', in *Conference Record of the 1992 IEEE International Symposium on Electrical Insulation*, Baltimore, MD, USA: IEEE, 1992, pp. 222–228. doi: 10.1109/ELINSL.1992.247015.

[3] C. W. Reed, 'An assessment of material selection for high voltage DC extruded polymer cables', *IEEE Electrical Insulation Magazine*, vol. 33, no. 4, pp. 22–26, Jul. 2017, doi: 10.1109/MEI.2017.7956629.

[4] Y. Liu and X. Cao, 'Electrical tree growth characteristics in XLPE cable insulation under DC voltage conditions', *IEEE Transactions on Dielectrics and Electrical Insulation*, vol. 22, no. 6, pp. 3676–3684, Dec. 2015, doi: 10.1109/TDEI.2015.005222.

[5] G. Chen, M. Hao, Z. Xu, A. Vaughan, J. Cao, and H. Wang, 'Review of high voltage direct current cables', *CSEE Journal of Power and Energy Systems*, vol. 1, no. 2, pp. 9–21, Jun. 2015, doi: 10.17775/CSEEJPES.2015.00015.

[6] S. K. Angalane and E. Kasinathan, 'A review on polymeric insulation for high-voltage application under various stress conditions', *Polymer Composites*, vol. 43, no. 8, pp. 4803–4834, 2022, doi: 10.1002/pc.26793.

[7] J. S. Ho and S. G. Greenbaum, 'Polymer Capacitor Dielectrics for High Temperature Applications', *ACS Appl. Mater. Interfaces*, vol. 10, no. 35, pp. 29189–29218, Sep. 2018, doi: 10.1021/acsami.8b07705.

[8] S. Tandon and R. J. Farris, 'Metalized Polypropylene Film in Capacitors: Characterization and the Effect of Interfacial Pressure on the Dielectric Strength', *MRS Online Proceedings Library*, vol. 476, no. 1, pp. 147–153, Dec. 1997, doi: 10.1557/PROC-476-147.

[9] 'Electrical Insulation for Rotating Machines: Design, Evaluation, Aging, Testing, and Repair | IEEE eBooks | IEEE Xplore'. Accessed: Sep. 05, 2022. [Online]. Available: https://ieeexplore.ieee.org.remotexs.ntu.edu.sg/book/5201844

[10] P. Li *et al.*, 'Wormholes effect in flashover process of alumina filled epoxy resin surfaces in SF6', *IEEE Transactions on Dielectrics and Electrical Insulation*, vol. 22, no. 4, pp. 2142–2147, Aug. 2015, doi: 10.1109/TDEI.2015.004809.

[11] G. Ueta, S. Okabe, T. Utsumi, and J. Nukaga, 'Electric conductivity characteristics of FRP and epoxy insulators for GIS under DC voltage', *IEEE Transactions on Dielectrics and Electrical Insulation*, vol. 22, no. 4, pp. 2320–2328, Aug. 2015, doi: 10.1109/TDEI.2015.005030.

[12] P. Mohan, 'A Critical Review: The Modification, Properties, and Applications of Epoxy Resins', *Polymer-Plastics Technology and Engineering*, vol. 52, no. 2, pp. 107–125, 2013, doi: 10.1080/03602559.2012.727057.

[13] B. Ellis, Ed., *Chemistry and Technology of Epoxy Resins*. Dordrecht: Springer Netherlands, 1993. doi: 10.1007/978-94-011-2932-9.

[14] A. Toldy, B. Szolnoki, and G. Marosi, 'Flame retardancy of fibre-reinforced epoxy resin composites for aerospace applications', *Polymer degradation and stability*, vol. 96, no. 3, pp. 371–376, 2011.

[15] H. S. Kim, K. Y. Park, and D. G. Lee, 'A study on the epoxy resin concrete for the ultra-precision machine tool bed', *Journal of Materials Processing Technology*, vol. 48, no. 1, pp. 649–655, Jan. 1995, doi: 10.1016/0924-0136(94)01705-6.

[16] T. Dakin, 'Application of Epoxy Resins in Electrical Apparatus', *IEEE Trans. Elect. Insul.*, vol. EI-9, no. 4, pp. 121–128, Dec. 1974, doi: 10.1109/TEI.1974.299321.

[17] N. Andraschek, A. J. Wanner, C. Ebner, and G. Riess, 'Mica/Epoxy-Composites in the Electrical Industry: Applications, Composites for Insulation, and Investigations on Failure Mechanisms for Prospective Optimizations', *Polymers*, vol. 8, no. 5, Art. no. 5, May 2016, doi: 10.3390/polym8050201.

[18] C. A. Finch, 'Encyclopedia of polymer science and engineering, volume 6: Editor-in-Chief Jacqueline I. Kroschwitz, John Wiley & Sons, New York and Chichester, 1986. pp. xxiv + 839, price £145.00. ISBN 0-471-80050-3', *British Polymer Journal*, vol. 19, no. 5, pp. 483–483, 1987, doi: 10.1002/pi.4980190510.

[19] T. K. Kwei, 'Epoxy resin chemistry, ACS symposium series 114, Ronald S. Bauer, American Chemical Society, Washington, DC, 1979, 271 pp.', *Journal of Polymer Science:*

*Polymer Letters Edition*, vol. 18, no. 5, pp. 395–395, 1980, doi: 10.1002/pol.1980.130180514.

[20] D. Ratna, *Handbook of thermoset resins*. Shawbury: iSmithers, 2009.

[21] C. May, *Epoxy Resins: Chemistry and Technology, Second Edition,*. Routledge, 2018.

[22] L. Wu, S. V. Hoa, Minh-Tan, and Ton-That, 'Effects of composition of hardener on the curing and aging for an epoxy resin system', *Journal of Applied Polymer Science*, vol. 99, no. 2, pp. 580–588, 2006, doi: 10.1002/app.22493.

[23] H. A. Al-Turaif, 'Relationship between tensile properties and film formation kinetics of epoxy resin reinforced with nanofibrillated cellulose', *Progress in Organic Coatings*, p. 5, 2013.

[24] I.-K. Hong, Y. S. Yoon, and S.-B. Lee, 'Selection of thinner for epoxy type resins for neon transformer housing', *Journal of Industrial and Engineering Chemistry*, vol. 18, no. 6, pp. 1997–2003, Nov. 2012, doi: 10.1016/j.jiec.2012.05.018.

[25] F.-L. Jin, S.-Y. Lee, and S.-J. Park, 'Polymer matrices for carbon fiber-reinforced polymer composites', *Carbon letters*, vol. 14, no. 2, pp. 76–88, 2013, doi: 10.5714/CL.2013.14.2.076.

[26] S.-J. Park, H.-J. Jeong, and C. Nah, 'A study of oxyfluorination of multi-walled carbon nanotubes on mechanical interfacial properties of epoxy matrix nanocomposites', *Materials Science and Engineering A*, p. 4, 2004.

[27] C. C. Riccardi, H. E. Adabbo, and R. J. J. Williams, 'Curing reaction of epoxy resins with diamines', *Journal of Applied Polymer Science*, vol. 29, no. 8, pp. 2481–2492, Aug. 1984, doi: 10.1002/app.1984.070290805.

[28] F. Seniha Güner, Y. Yağcı, and A. Tuncer Erciyes, 'Polymers from triglyceride oils', *Progress in Polymer Science*, vol. 31, no. 7, pp. 633–670, Jul. 2006, doi: 10.1016/j.progpolymsci.2006.07.001.

[29] M. G. González, J. C. Cabanelas, and J. Baselga, 'Applications of FTIR on Epoxy Resins - Identification, Monitoring the Curing Process, Phase Separation and Water Uptake', in *Infrared Spectroscopy - Materials Science, Engineering and Technology*, T. Theophanides, Ed., InTech, 2012. doi: 10.5772/36323.

[30] I. E. C. Standard, ‘Evaluation and qualification of electrical insulation systems’, *IEC Std*, vol. 60505, 2011.

[31] X. Yang *et al.*, ‘High-efficiency improvement of thermal conductivities for epoxy composites from synthesized liquid crystal epoxy followed by doping BN fillers’, *Composites Part B: Engineering*, vol. 185, 2020, doi: 10.1016/j.compositesb.2020.107784.

[32] Z. Wang *et al.*, ‘Dielectric properties and thermal conductivity of epoxy composites using quantum-sized silver decorated core/shell structured alumina/polydopamine’, *Composites Part A: Applied Science and Manufacturing*, vol. 118, pp. 302–311, Mar. 2019, doi: 10.1016/j.compositesa.2018.12.022.

[33] I. Jeong *et al.*, ‘Liquid crystalline epoxy resin with improved thermal conductivity by intermolecular dipole–dipole interactions’, *Journal of Polymer Science Part A: Polymer Chemistry*, vol. 57, no. 6, pp. 708–715, 2019, doi: 10.1002/pola.29315.

[34] P. Siedlaczek *et al.*, ‘Hygrothermal aging of particle-filled epoxy-based composites’, *Polymer Degradation and Stability*, vol. 208, p. 110248, Feb. 2023, doi: 10.1016/j.polymdegradstab.2022.110248.

[35] M. Liang and K. L. Wong, ‘Study of Mechanical and Thermal Performances of Epoxy Resin Filled with Micro Particles and Nanoparticles’, *Energy Procedia*, vol. 110, pp. 156–161, 2017, doi: 10.1016/j.egypro.2017.03.121.

[36] Y. Yang, G. Xian, H. Li, and L. Sui, ‘Thermal aging of an anhydride-cured epoxy resin’, *Polymer Degradation and Stability*, vol. 118, pp. 111–119, Aug. 2015, doi: 10.1016/j.polymdegradstab.2015.04.017.

[37] M. C. Celina, ‘Review of polymer oxidation and its relationship with materials performance and lifetime prediction’, *Polymer Degradation and Stability*, vol. 98, no. 12, pp. 2419–2429, Dec. 2013, doi: 10.1016/j.polymdegradstab.2013.06.024.

[38] J. Middleton, B. Burks, T. Wells, A. M. Setters, I. Jasiuk, and M. Kumosa, ‘The effect of ozone and high temperature on polymer degradation in polymer core composite conductors’, *Polym. Degrad. Stab.*, vol. 98, no. 11, pp. 2282–2290, Nov. 2013, doi: 10.1016/j.polymdegradstab.2013.08.013.

[39] A. Tcharkhtchi, S. Farzaneh, S. Abdallah-Elhirtsi, B. Esmaeillou, F. Nony, and A. Baron, ‘Thermal Aging Effect on Mechanical Properties of Polyurethane’, *International*

*Journal of Polymer Analysis and Characterization*, vol. 19, no. 7, pp. 571–584, Oct. 2014, doi: 10.1080/1023666X.2014.932644.

[40] Y. Long *et al.*, 'Skin-core structure of thermally aged epoxy resin: Roles of oxidation and re-crosslinking', *Polymer Degradation and Stability*, vol. 193, p. 109743, Nov. 2021, doi: 10.1016/j.polymdegradstab.2021.109743.

[41] D. Ghosh and D. Khastgir, 'Degradation and Stability of Polymeric High-Voltage Insulators and Prediction of Their Service Life through Environmental and Accelerated Aging Processes', *ACS Omega*, vol. 3, no. 9, pp. 11317–11330, Sep. 2018, doi: 10.1021/acsomega.8b01560.

[42] L. A. Dissado, *Electrical Degradation and Breakdown in Polymers [electronic resource] / L.A. Dissado & J.C. Fothergill*. in Materials, Circuits & Devices. Stevenage: IET, 1992.

[43] L. Gao *et al.*, 'Autonomous Self-Healing of Electrical Degradation in Dielectric Polymers Using In Situ Electroluminescence', *Matter*, vol. 2, no. 2, pp. 451–463, Feb. 2020, doi: 10.1016/j.matt.2019.11.012.

[44] G. Teyssedre and C. Laurent, 'Advances in high-field insulating polymeric materials over the past 50 years', *IEEE Electrical Insulation Magazine*, vol. 29, no. 5, pp. 26–36, Sep. 2013, doi: 10.1109/MEI.2013.6585854.

[45] N. Shimizu and C. Laurent, 'Electrical tree initiation', *IEEE Transactions on Dielectrics and Electrical Insulation*, vol. 5, no. 5, pp. 651–659, 1998, doi: 10.1109/94.729688.

[46] L. A. Dissado, S. J. Dodd, J. V. Champion, P. I. Williams, and J. M. Alison, 'Propagation of electrical tree structures in solid polymeric insulation', *IEEE Transactions on Dielectrics and Electrical Insulation*, vol. 4, no. 3, pp. 259–279, Jun. 1997, doi: 10.1109/94.598282.

[47] I. Iddrissu, Z. Lv, and S. M. Rowland, 'The dynamic character of partial discharge in epoxy resin at different stages of treeing', in *2016 IEEE International Conference on Dielectrics (ICD)*, Jul. 2016, pp. 728–731. doi: 10.1109/ICD.2016.7547719.

[48] X. Chen, Y. Xu, X. Cao, S. J. Dodd, and L. A. Dissado, 'Effect of tree channel conductivity on electrical tree shape and breakdown in XLPE cable insulation samples',

*IEEE Transactions on Dielectrics and Electrical Insulation*, vol. 18, no. 3, pp. 847–860, Jun. 2011, doi: 10.1109/TDEI.2011.5931074.

[49] Z. Lv, S. M. Rowland, S. Chen, H. Zheng, and K. Wu, 'Modelling of partial discharge characteristics in electrical tree channels: Estimating the PD inception and extinction voltages', *IEEE Transactions on Dielectrics and Electrical Insulation*, vol. 25, no. 5, pp. 1999–2010, 2018, doi: 10.1109/tdei.2018.007175.

[50] Z. Lv, S. M. Rowland, S. Chen, H. Zheng, and I. Iddrissu, 'Evolution of partial discharges during early tree propagation in epoxy resin', *IEEE Trans. Dielect. Electr. Insul.*, vol. 24, no. 5, pp. 2995–3003, Oct. 2017, doi: 10.1109/TDEI.2017.006731.

[51] V. A. Zakrevskii, N. T. Sudar, A. Zaopo, and Yu. A. Dubitsky, 'Mechanism of electrical degradation and breakdown of insulating polymers', *Journal of Applied Physics*, vol. 93, no. 4, pp. 2135–2139, Feb. 2003, doi: 10.1063/1.1531820.

[52] G. Blaise, 'Space-charge physics and the breakdown process', *Journal of Applied Physics*, vol. 77, no. 7, pp. 2916–2927, 1995, doi: 10.1063/1.358707.

[53] X. Wang, Z. Lv, K. Wu, X. Chen, D. Tu, and L. A. Dissado, 'Study of the factors that suppress space charge accumulation in LDPE nanocomposites', *IEEE Transactions on Dielectrics and Electrical Insulation*, vol. 21, no. 4, pp. 1670–1679, 2014, doi: 10.1109/tdei.2014.004292.

[54] Q. Wang, T. Li, B. Wang, C. Liu, Q. Huang, and M. Ren, 'Prediction of void growth and fiber volume fraction based on filament winding process mechanics', *Composite Structures*, vol. 246, 2020, doi: 10.1016/j.compstruct.2020.112432.

[55] L. Liu, B.-M. Zhang, D.-F. Wang, and Z.-J. Wu, 'Effects of cure cycles on void content and mechanical properties of composite laminates', *Composite Structures*, vol. 73, no. 3, pp. 303–309, Jun. 2006, doi: 10.1016/j.compstruct.2005.02.001.

[56] B. Madsen, A. Thygesen, and H. Lilholt, 'Plant fibre composites – porosity and volumetric interaction', *Composites Science and Technology*, vol. 67, no. 7, pp. 1584–1600, Jun. 2007, doi: 10.1016/j.compscitech.2006.07.009.

[57] Y. Li, Q. Li, and H. Ma, 'The voids formation mechanisms and their effects on the mechanical properties of flax fiber reinforced epoxy composites', *Composites Part A: Applied Science and Manufacturing*, vol. 72, pp. 40–48, 2015, doi: 10.1016/j.compositesa.2015.01.029.

[58] E. M. Odom and D. F. Adams, ‘Specimen size effect during tensile testing of an unreinforced polymer’, *J Mater Sci*, vol. 27, no. 7, pp. 1767–1771, Apr. 1992, doi: 10.1007/BF01107202.

[59] M. Turk, I. Hamerton, and D. S. Ivanov, ‘Ductility potential of brittle epoxies: Thermomechanical behaviour of plastically-deformed fully-cured composite resins’, *Polymer*, vol. 120, pp. 43–51, Jun. 2017, doi: 10.1016/j.polymer.2017.05.052.

[60] A. H. Korayem, M. R. Barati, G. P. Simon, X. L. Zhao, and W. H. Duan, ‘Reinforcing brittle and ductile epoxy matrices using carbon nanotubes masterbatch’, *Composites Part A: Applied Science and Manufacturing*, vol. 61, pp. 126–133, Jun. 2014, doi: 10.1016/j.compositesa.2014.02.016.

[61] J. Ke *et al.*, ‘incorporating CO2-sourced cyclic carbonate’, p. 12, 2018.

[62] A. M. Petrudi, K. Vahedi, M. Rahmani, and M. M. Petrudi, ‘Numerical and analytical simulation of ballistic projectile penetration due to high velocity impact on ceramic target’, *Fracture and Structural Integrity*, vol. 14, no. 54, Art. no. 54, Sep. 2020, doi: 10.3221/IGF-ESIS.54.17.

[63] Y. Huang and A. J. Kinloch, ‘The toughness of epoxy polymers containing microvoids’, *Polymer*, vol. 33, no. 6, pp. 1330–1332, 1992, doi: 10.1016/0032-3861(92)90785-u.

[64] I. M. McAninch, G. R. Palmese, J. L. Lenhart, and J. J. La Scala, ‘DMA testing of epoxy resins: The importance of dimensions’, *Polymer Engineering & Science*, vol. 55, no. 12, pp. 2761–2774, 2015, doi: 10.1002/pen.24167.

[65] A. Krivda *et al.*, ‘Characterization of epoxy microcomposite and nanocomposite materials for power engineering applications’, *IEEE Electrical Insulation Magazine*, vol. 28, no. 2, pp. 38–51, 2012, doi: 10.1109/mei.2012.6159180.

[66] G. C. Montanari, R. Hebner, P. Morshuis, and P. Seri, ‘An Approach to Insulation Condition Monitoring and Life Assessment in Emerging Electrical Environments’, *IEEE Transactions on Power Delivery*, vol. 34, no. 4, pp. 1357–1364, 2019, doi: 10.1109/tpwrd.2019.2897905.

[67] G. C. Montanari, D. Fabiani, P. Morshuis, and L. Dissado, ‘Why residual life estimation and maintenance strategies for electrical insulation systems have to rely upon

condition monitoring', *IEEE Transactions on Dielectrics and Electrical Insulation*, vol. 23, no. 3, pp. 1375–1385, Jun. 2016, doi: 10.1109/TDEI.2015.005613.

[68] W. Weibull, 'A statistical distribution function of wide applicability', *Journal of applied mechanics*, vol. 18, no. 3, pp. 293–297, 1951.

[69] D. Davies, 'The statistical approach to engineering design in ceramics', presented at the Proceedings of the British Ceramic Society, 1973, pp. 429–452.

[70] G. D. Quinn and R. Morrell, 'Design Data for Engineering Ceramics: A Review of the Flexure Test', *Journal of the American Ceramic Society*, vol. 74, no. 9, pp. 2037–2066, 1991, doi: 10.1111/j.1151-2916.1991.tb08259.x.

[71] C. Neusel, H. Jelitto, D. Schmidt, R. Janßen, F. Felten, and G. A. Schneider, 'Thickness-dependence of the breakdown strength: Analysis of the dielectric and mechanical failure', *Journal of the European Ceramic Society*, vol. 35, no. 1, pp. 113–123, 2015.

[72] T. Zhang, Y. Lei, J. Yin, J. Du, and P. Yu, 'Effects of pores on dielectric breakdown of alumina ceramics under AC electric field', *Ceramics International*, vol. 45, no. 11, pp. 13951–13957, 2019.

[73] B. Mieller, 'Influence of test procedure on dielectric breakdown strength of alumina', p. 9, 2019.

[74] R. Bermejo, P. Supancic, I. Kraleva, R. Morrell, and R. Danzer, 'Strength reliability of 3D low temperature co-fired multilayer ceramics under biaxial loading', *Journal of the European Ceramic Society*, vol. 31, no. 5, pp. 745–753, May 2011, doi: 10.1016/j.jeurceramsoc.2010.11.031.

[75] L. Collini and G. R. Carfagni, 'Flexural strength of glass–ceramic for structural applications', *Journal of the European Ceramic Society*, vol. 34, no. 11, pp. 2675–2685, Sep. 2014, doi: 10.1016/j.jeurceramsoc.2013.10.032.

[76] Y. Lu *et al.*, 'Flexural strength and Weibull analysis of Y-TZP fabricated by stereolithographic additive manufacturing and subtractive manufacturing', *Journal of the European Ceramic Society*, vol. 40, no. 3, pp. 826–834, 2020.

[77] E. B. Callaway and F. W. Zok, 'Strengths of ceramic fiber bundles: Theory and practice', *Journal of the American Ceramic Society*, vol. 100, no. 11, pp. 5306–5317, 2017, doi: 10.1111/jace.15062.

[78] L. A. Bicalho, C. A. R. P. Baptista, R. C. Souza, C. Santos, K. Strecker, and M. J. R. Barboza, 'Fatigue and subcritical crack growth in ZrO2–bioglass ceramics', *Ceramics International*, vol. 39, no. 3, pp. 2405–2414, Apr. 2013, doi: 10.1016/j.ceramint.2012.08.093.

[79] A. Dey, A. K. Mukhopadhyay, S. Gangadharan, M. K. Sinha, and D. Basu, 'Weibull modulus of nano-hardness and elastic modulus of hydroxyapatite coating', *J Mater Sci*, vol. 44, no. 18, pp. 4911–4918, Sep. 2009, doi: 10.1007/s10853-009-3750-y.

[80] H.-S. Nam, 'Statistical analysis of Vickers hardness and fracture toughness of repeated crack-healing SiC composite ceramics considering economics', *Journal of Ceramic Processing Research*, vol. 20, no. 4, pp. 379–387, 2019.

[81] J. Gong, 'Indentation toughness of ceramics: a statistical analysis', *Ceramics international*, vol. 28, no. 7, pp. 767–772, 2002.

[82] D. N. Boccaccini *et al.*, 'Influence of porosity on mechanical properties of tetragonal stabilized zirconia', *Journal of the European Ceramic Society*, vol. 38, no. 4, pp. 1720–1735, 2018.

[83] E. Barbero, J. Fernández-Sáez, and C. Navarro, 'Statistical analysis of the mechanical properties of composite materials', *Composites Part B: Engineering*, vol. 31, no. 5, pp. 375–381, Jul. 2000, doi: 10.1016/S1359-8368(00)00027-5.

[84] K. Naresh, K. Shankar, and R. Velmurugan, 'Reliability analysis of tensile strengths using Weibull distribution in glass/epoxy and carbon/epoxy composites', *Composites Part B: Engineering*, vol. 133, pp. 129–144, Jan. 2018, doi: 10.1016/j.compositesb.2017.09.002.

[85] C. Yeung and A. S. Vaughan, 'On the Effect of Nanoparticle Surface Chemistry on the Electrical Characteristics of Epoxy-Based Nanocomposites', *Polymers*, vol. 8, no. 4, Art. no. 4, Apr. 2016, doi: 10.3390/polym8040126.

[86] S. Singha and M. J. Thomas, 'Dielectric properties of epoxy nanocomposites', *IEEE Transactions on Dielectrics and Electrical Insulation*, vol. 15, no. 1, pp. 12–23, Feb. 2008, doi: 10.1109/T-DEI.2008.4446732.

[87] R. Kochetov, T. Andritsch, P. H. F. Morshuis, and J. J. Smit, 'Anomalous behaviour of the dielectric spectroscopy response of nanocomposites', *IEEE Transactions on Dielectrics and Electrical Insulation*, vol. 19, no. 1, pp. 107–117, Feb. 2012, doi: 10.1109/TDEI.2012.6148508.

[88] S. Siddabattuni, T. P. Schuman, and F. Dogan, ‘Dielectric Properties of Polymer–Particle Nanocomposites Influenced by Electronic Nature of Filler Surfaces’, *ACS Appl. Mater. Interfaces*, vol. 5, no. 6, pp. 1917–1927, Mar. 2013, doi: 10.1021/am3030239.

[89] R. Kochetov, A. V. Korobko, T. Andritsch, P. H. F. Morshuis, S. J. Picken, and J. J. Smit, ‘Modelling of the thermal conductivity in polymer nanocomposites and the impact of the interface between filler and matrix’, *Journal of Physics D: Applied Physics*, vol. 44, no. 39, p. 395401, Sep. 2011, doi: 10.1088/0022-3727/44/39/395401.

[90] Q. Xie, Y. Cheng, S. Chen, G. Wu, Z. Wang, and Z. Jia, ‘Dielectric and thermal properties of epoxy resins with TiO2 nanowires’, *J Mater Sci: Mater Electron*, vol. 28, no. 23, pp. 17871–17880, Dec. 2017, doi: 10.1007/s10854-017-7728-2.

[91] J. K. Nelson, Ed., *Dielectric Polymer Nanocomposites*. Boston, MA: Springer US, 2010. doi: 10.1007/978-1-4419-1591-7.

[92] B. El-Kareh and L. N. Hutter, *Fundamentals of Semiconductor Processing Technology*. Springer Science & Business Media, 2012.

[93] J. F. Shackelford and W. Alexander, Eds., *CRC materials science and engineering handbook*, 3rd ed. Boca Raton, FL: CRC Press, 2001.

[94] T. H. DiStefano and D. E. Eastman, ‘The band edge of amorphous SiO2 by photoinjection and photoconductivity measurements’, *Solid State Communications*, vol. 9, no. 24, pp. 2259–2261, Dec. 1971, doi: 10.1016/0038-1098(71)90643-0.

[95] A. Laturia, M. L. Van de Put, and W. G. Vandenberghe, ‘Dielectric properties of hexagonal boron nitride and transition metal dichalcogenides: from monolayer to bulk’, *npj 2D Mater Appl*, vol. 2, no. 1, Art. no. 1, Mar. 2018, doi: 10.1038/s41699-018-0050-x.

[96] Y. Hattori, K. Watanabe, T. Taniguchi, and K. Nagashio, ‘Layer-by-Layer Dielectric Breakdown of Hexagonal Boron Nitride’, Oct. 07, 2015, *arXiv*: arXiv:1510.01930. doi: 10.48550/arXiv.1510.01930.

[97] Q. Cai *et al.*, ‘High thermal conductivity of high-quality monolayer boron nitride and its thermal expansion’, *Science Advances*, vol. 5, no. 6, p. eaav0129, Jun. 2019, doi: 10.1126/sciadv.aav0129.

[98] C. Yuan *et al.*, ‘Modulating the thermal conductivity in hexagonal boron nitride via controlled boron isotope concentration’, *Commun Phys*, vol. 2, no. 1, Art. no. 1, May 2019, doi: 10.1038/s42005-019-0145-5.

[99] G. Cassabois, P. Valvin, and B. Gil, ‘Hexagonal boron nitride is an indirect bandgap semiconductor’, *Nature Photon*, vol. 10, no. 4, Art. no. 4, Apr. 2016, doi: 10.1038/nphoton.2015.277.

[100] T. Ruemenapp and D. Peier, ‘Dielectric breakdown in aluminium nitride’, in *1999 Eleventh International Symposium on High Voltage Engineering*, Aug. 1999, pp. 373–376 vol.4. doi: 10.1049/cp:19990870.

[101] J. H. Edgar, Z. J. Yu, A. U. Ahmed, and A. Rys, ‘Low temperature metal-organic chemical vapor deposition of aluminum nitride with nitrogen trifluoride as the nitrogen source’, *Thin Solid Films*, vol. 189, no. 2, pp. L11–L14, Aug. 1990, doi: 10.1016/0040-6090(90)90469-T.

[102] R. A. Parker, ‘Static Dielectric Constant of Rutile (Ti${\mathrm{O}}_{2}$), 1.6-1060\ifmmode^\circ\else\textdegree\fi{}K’, *Phys. Rev.*, vol. 124, no. 6, pp. 1719–1722, Dec. 1961, doi: 10.1103/PhysRev.124.1719.

[103] ‘What is silicon carbide? | TechWeb’. Accessed: Jan. 31, 2023. [Online]. Available: https://techweb.rohm.com/product/power-device/sic/sic-basic/3669/

[104] ‘Silicon Carbide SiC Material Properties’. Accessed: Jan. 31, 2023. [Online]. Available: http://accuratus.com/silicar.html

[105] G. L. Zhao and D. Bagayoko, ‘Electronic structure and charge transfer in 3C- and 4H-SiC’, *New J. Phys.*, vol. 2, pp. 16–16, Jul. 2000, doi: 10.1088/1367-2630/2/1/316.

[106] M. C. says, ‘Titanium Dioxide - Titania ( TiO2)’, AZoM.com. Accessed: Jan. 30, 2023. [Online]. Available: https://www.azom.com/article.aspx?ArticleID=1179

[107] T. Gao and B. P. Jelle, ‘Thermal Conductivity of TiO 2 Nanotubes’, *J. Phys. Chem. C*, vol. 117, no. 3, pp. 1401–1408, Jan. 2013, doi: 10.1021/jp3108655.

[108] D. O. Scanlon *et al.*, ‘Band alignment of rutile and anatase TiO2’, *Nature Mater*, vol. 12, no. 9, Art. no. 9, Sep. 2013, doi: 10.1038/nmat3697.

[109] R. J. Gonzalez, R. Zallen, and H. Berger, ‘Infrared reflectivity and lattice fundamentals in anatase TiO2’, . . ..

[110] ‘Overview - Alumina, 96%, Al 2 O 3’. Accessed: Jan. 30, 2023. [Online]. Available: https://www.matweb.com/search/datasheet.aspx?matguid=204094cb0fd34c099b8a52c9c7df1d5c&n=1&ckck=1

[111] ‘Aluminum Oxide | Al2O3 Material Properties’. Accessed: Jan. 30, 2023. [Online]. Available: https://accuratus.com/alumox.html

[112] J. L. Lauer, J. L. Shohet, C. Cismaru, R. W. Hansen, M. Y. Foo, and T. J. Henn, ‘Photoemission and conduction currents in vacuum ultraviolet irradiated aluminum oxide’, *Journal of Applied Physics*, vol. 91, no. 3, pp. 1242–1246, Feb. 2002, doi: 10.1063/1.1428790.

[113] E. O. Filatova and A. S. Konashuk, ‘Interpretation of the Changing the Band Gap of Al2O3 Depending on Its Crystalline Form: Connection with Different Local Symmetries’, *J. Phys. Chem. C*, vol. 119, no. 35, pp. 20755–20761, Sep. 2015, doi: 10.1021/acs.jpcc.5b06843.

[114] I. Costina and R. Franchy, ‘Band gap of amorphous and well-ordered Al2O3 on Ni3Al(100)’, *Appl. Phys. Lett.*, vol. 78, no. 26, pp. 4139–4141, Jun. 2001, doi: 10.1063/1.1380403.

[115] J. D. Hwang and C.-Y. Chang, ‘Post-annealing treatment in improving high dielectric constant MgO-based metal-oxide-semiconductor diodes’, *Appl. Phys. Lett.*, vol. 120, no. 25, p. 252902, Jun. 2022, doi: 10.1063/5.0094513.

[116] D. M. Roessler and W. C. Walker, ‘Electronic Spectrum and Ultraviolet Optical Properties of Crystalline MgO’, *Phys. Rev.*, vol. 159, no. 3, pp. 733–738, Jul. 1967, doi: 10.1103/PhysRev.159.733.

[117] Y. He, ‘Heat capacity, thermal conductivity, and thermal expansion of barium titanate-based ceramics’, *Thermochimica Acta*, vol. 419, no. 1, pp. 135–141, Sep. 2004, doi: 10.1016/j.tca.2004.02.008.

[118] S. Ramakanth and K. C. James Raju, ‘Band gap narrowing in BaTiO3 nanoparticles facilitated by multiple mechanisms’, *Journal of Applied Physics*, vol. 115, no. 17, p. 173507, May 2014, doi: 10.1063/1.4871776.

[119] M. Kurimoto *et al.*, ‘Permittivity characteristics of epoxy/alumina nanocomposite with high particle dispersibility by combining ultrasonic wave and centrifugal force’, *IEEE Transactions on Dielectrics and Electrical Insulation*, vol. 17, no. 4, pp. 1268–1275, Aug. 2010, doi: 10.1109/TDEI.2010.5539699.

[120] J. K. Nelson and J. C. Fothergill, ‘Internal charge behaviour of nanocomposites’, *Nanotechnology*, vol. 15, no. 5, p. 586, Mar. 2004, doi: 10.1088/0957-4484/15/5/032.

[121] S. Singha and M. J. Thomas, ‘Permittivity and tan delta characteristics of epoxy nanocomposites in the frequency range of 1 MHz-1 GHz’, *IEEE Transactions on Dielectrics and Electrical Insulation*, vol. 15, no. 1, pp. 2–11, Feb. 2008, doi: 10.1109/T-DEI.2008.4446731.

[122] R. Kochetov, T. Andritsch, P. H. F. Morshuis, and J. J. Smit, ‘Effect of filler size on complex permittivity and thermal conductivity of epoxy-based composites filled with BN particles’, presented at the 2010 Annual Report Conference on Electrical Insulation and Dielectic Phenomena, Oct. 2010, pp. 1–4. doi: 10.1109/CEIDP.2010.5723962.

[123] T. Tanaka, M. Kozako, N. Fuse, and Y. Ohki, ‘Proposal of a multi-core model for polymer nanocomposite dielectrics’, *IEEE Transactions on Dielectrics and Electrical Insulation*, vol. 12, no. 4, pp. 669–681, Aug. 2005, doi: 10.1109/TDEI.2005.1511092.

[124] M. G. Danikas and T. Tanaka, ‘Nanocomposites-a review of electrical treeing and breakdown’, *IEEE Electr. Insul. Mag.*, vol. 25, no. 4, pp. 19–25, Jul. 2009, doi: 10.1109/MEI.2009.5191413.

[125] T. Imai *et al.*, ‘Effects of nano- and micro-filler mixture on electrical insulation properties of epoxy based composites’, *IEEE Transactions on Dielectrics and Electrical Insulation*, vol. 13, no. 2, pp. 319–326, Apr. 2006, doi: 10.1109/TDEI.2006.1624276.

[126] M. M. Adnan *et al.*, ‘Epoxy-Based Nanocomposites for High-Voltage Insulation: A Review’, *Advanced Electronic Materials*, vol. 5, no. 2, p. 1800505, 2019, doi: 10.1002/aelm.201800505.

[127] T. Andritsch, R. Kochetov, Y. T. Gebrekiros, U. Lafont, P. H. F. Morshuis, and J. J. Smit, ‘Synthesis and dielectric properties of epoxy based nanocomposites’, IEEE, 2009. doi: 10.1109/ceidp.2009.5377771.

[128] J. Chen *et al.*, ‘Engineering the Dielectric Constants of Polymers: From Molecular to Mesoscopic Scales’, *Advanced Materials*, p. 2308670, Dec. 2023, doi: 10.1002/adma.202308670.

[129] A. Syakur, Hermawan, and H. Sutanto, ‘Determination of Hydrophobic Contact Angle of Epoxy Resin Compound Silicon Rubber and Silica’, *IOP Conf. Ser.: Mater. Sci. Eng.*, vol. 190, no. 1, p. 012025, Apr. 2017, doi: 10.1088/1757-899X/190/1/012025.

[130] J. Zheng *et al.*, 'Behavior of epoxy resin filled with nano-SiO treated with a Eugenol epoxy silane', *Journal of Applied Polymer Science*, vol. 138, no. 14, p. 50138, 2021, doi: 10.1002/app.50138.

[131] H. Xu *et al.*, 'Synergetic optimization of charge transport and breakdown strength of epoxy nanocomposites: Realizing sandwich topological structure through constructing a SiC@SiO2/EP surface layer and m-BNNS/EP insert layer', *Materials Science in Semiconductor Processing*, vol. 141, p. 106430, Apr. 2022, doi: 10.1016/j.mssp.2021.106430.

[132] X. Chen *et al.*, 'Salt Template Assisted BN Scaffold Fabrication toward Highly Thermally Conductive Epoxy Composites', *ACS Appl. Mater. Interfaces*, vol. 12, no. 14, pp. 16987–16996, Apr. 2020, doi: 10.1021/acsami.0c04882.

[133] W. Wang, Q. Li, Y. Liu, H. Wang, R. Wang, and H. Jin, 'Enhanced Thermal Properties of Epoxy Resin Composites: The role of Tailoring Surface Chemistry of Nano-SiO2', in *2021 IEEE Conference on Electrical Insulation and Dielectric Phenomena (CEIDP)*, Dec. 2021, pp. 403–406. doi: 10.1109/CEIDP50766.2021.9705392.

[134] R. Kochetov, T. Andritsch, U. Lafont, P. H. F. Morshuis, and J. J. Smit, 'Thermal conductivity of nano-filled epoxy systems', IEEE, 2009. doi: 10.1109/ceidp.2009.5377801.

[135] '3D boron nitride foam filled epoxy composites with significantly enhanced thermal conductivity by a facial and scalable approach', *Chemical Engineering Journal*, vol. 397, p. 125447, Oct. 2020, doi: 10.1016/j.cej.2020.125447.

[136] I. A. Tsekmes *et al.*, 'How different fillers affect the thermal conductivity of epoxy composites', IEEE, 2014. doi: 10.1109/ceidp.2014.6995843.

[137] I. A. Tsekmes, R. Kochetov, P. H. F. Morshuis, and J. J. Smit, 'Thermal conductivity of polymeric composites: A review', IEEE, 2013. doi: 10.1109/icsd.2013.6619698.

[138] H. Fischer, 'Polymer nanocomposites: from fundamental research to specific applications', *Materials Science and Engineering: C*, vol. 23, no. 6, pp. 763–772, Dec. 2003, doi: 10.1016/j.msec.2003.09.148.

[139] E. Thostenson, C. Li, and T. Chou, 'Nanocomposites in context', *Composites Science and Technology*, vol. 65, no. 3–4, pp. 491–516, Mar. 2005, doi: 10.1016/j.compscitech.2004.11.003.

[140] B. Fiedler, F. H. Gojny, M. H. G. Wichmann, M. C. M. Nolte, and K. Schulte, 'Fundamental aspects of nano-reinforced composites', *Composites Science and Technology*, vol. 66, no. 16, pp. 3115–3125, Dec. 2006, doi: 10.1016/j.compscitech.2005.01.014.

[141] M. H. G. Wichmann, M. Cascione, B. Fiedler, M. Quaresimin, and K. Schulte, 'Influence of surface treatment on mechanical behaviour of fumed silica/epoxy resin nanocomposites', *Composite Interfaces*, vol. 13, no. 8–9, pp. 699–715, Jan. 2006, doi: 10.1163/156855406779366723.

[142] O. Becker, R. Varley, and G. Simon, 'Morphology, thermal relaxations and mechanical properties of layered silicate nanocomposites based upon high-functionality epoxy resins', *Polymer*, vol. 43, no. 16, pp. 4365–4373, Jul. 2002, doi: 10.1016/S0032-3861(02)00269-0.

[143] M. Chan, K. Lau, T. Wong, M. Ho, and D. Hui, 'Mechanism of reinforcement in a nanoclay/polymer composite', *Composites Part B: Engineering*, vol. 42, no. 6, pp. 1708–1712, Sep. 2011, doi: 10.1016/j.compositesb.2011.03.011.

[144] T. Andritsch, R. Kochetov, Y. T. Gebrekiros, P. H. F. Morshuis, and J. J. Smit, 'Short term DC breakdown strength in epoxy based BN nano- and microcomposites', IEEE, 2010. doi: 10.1109/icsd.2010.5568098.

[145] T. Soulestin, V. Ladmiral, F. D. Dos Santos, and B. Améduri, 'Vinylidene fluoride- and trifluoroethylene-containing fluorinated electroactive copolymers. How does chemistry impact properties?', *Progress in Polymer Science*, vol. 72, pp. 16–60, Sep. 2017, doi: 10.1016/j.progpolymsci.2017.04.004.

[146] H. Zhao and R. K. Y. Li, 'Effect of water absorption on the mechanical and dielectric properties of nano-alumina filled epoxy nanocomposites', *Composites Part A: Applied Science and Manufacturing*, vol. 39, no. 4, pp. 602–611, Apr. 2008, doi: 10.1016/j.compositesa.2007.07.006.

[147] S. Khandelwal and K. Y. Rhee, 'Recent advances in basalt-fiber-reinforced composites: Tailoring the fiber-matrix interface', *Composites Part B: Engineering*, vol. 192, p. 108011, Jul. 2020, doi: 10.1016/j.compositesb.2020.108011.

[148] J. Thomas *et al.*, 'Recent Advances in Cross-linked Polyethylene-based Nanocomposites for High Voltage Engineering Applications: A Critical Review',

*Industrial & Engineering Chemistry Research*, vol. 58, no. 46, pp. 20863–20879, 2019, doi: 10.1021/acs.iecr.9b02172.

[149] I. A. Tsekmes, R. Kochetov, P. H. F. Morshuis, and J. J. Smit, 'AC breakdown strength of epoxy-boron nitride nanocomposites: Trend & reproducibility', IEEE, 2015. doi: 10.1109/icacact.2014.7223609.

[150] Z. Li, K. Okamoto, Y. Ohki, and T. Tanaka, 'The role of nano and micro particles on partial discharge and breakdown strength in epoxy composites', *IEEE Transactions on Dielectrics and Electrical Insulation*, vol. 18, no. 3, pp. 675–681, Jun. 2011, doi: 10.1109/TDEI.2011.5931052.

[151] M. Bell *et al.*, 'Investigation of dielectric breakdown in silica-epoxy nanocomposites using designed interfaces', *J Colloid Interface Sci*, vol. 495, pp. 130–139, Jun. 2017, doi: 10.1016/j.jcis.2017.02.001.

[152] B. Wetzel, F. Haupert, and M. Qiu Zhang, 'Epoxy nanocomposites with high mechanical and tribological performance', *Composites Science and Technology*, vol. 63, no. 14, pp. 2055–2067, Nov. 2003, doi: 10.1016/S0266-3538(03)00115-5.

[153] M. Zhi Rong, M. Qiu Zhang, H. Liu, H. Zeng, B. Wetzel, and K. Friedrich, 'Microstructure and tribological behavior of polymeric nanocomposites', *Ind Lubrication and Tribology*, vol. 53, no. 2, pp. 72–77, Apr. 2001, doi: 10.1108/00368790110383993.

[154] E. Lizundia, I. Serna, E. Axpe, and J. L. Vilas, 'Free-volume effects on the thermomechanical performance of epoxy–SiO2 nanocomposites', *Journal of Applied Polymer Science*, vol. 134, no. 34, p. 45216, 2017, doi: 10.1002/app.45216.

[155] S. Zhao, L. S. Schadler, R. Duncan, H. Hillborg, and T. Auletta, 'Mechanisms leading to improved mechanical performance in nanoscale alumina filled epoxy', *Composites Science and Technology*, vol. 68, no. 14, pp. 2965–2975, Nov. 2008, doi: 10.1016/j.compscitech.2008.01.009.

[156] S. Sinha, S. Roy, A. Singh, V. Srivastava, and P. Bhati, 'Surface Wettability Prediction using ML/AI', in *2022 4th International Conference on Artificial Intelligence and Speech Technology (AIST)*, Dec. 2022, pp. 1–6. doi: 10.1109/AIST55798.2022.10064943.

[157] I. Noda, ‘Surface-hydrophilic elastomers’, in *Studies in Polymer Science*, vol. 11, I. Noda and D. N. Rubingh, Eds., in Polymer Solutions, Blends, and Interfaces, vol. 11. , Elsevier, 1992, pp. 1–21. doi: 10.1016/B978-0-444-89397-0.50006-3.

[158] L. Wang *et al.*, ‘Modelling for effects of surface chemical composition on contact angle and applications in membrane flux control’, *Chemical Engineering Science*, vol. 267, p. 118319, Mar. 2023, doi: 10.1016/j.ces.2022.118319.

[159] V. K. Raghavendran and L. T. Drzal, ‘Fiber-Matrix Interfacial Adhesion Improvement in Carbon Fiber-Bisphenol-A Polycarbonate Composites by Polymer Grafting’, *The Journal of Adhesion*, vol. 78, no. 10, pp. 895–922, Oct. 2002, doi: 10.1080/00218460214096.

[160] K. Tanaka, S. Ogata, R. Kobayashi, T. Tamura, M. Kitsunezuka, and A. Shinma, ‘Enhanced heat transfer through filler-polymer interface by surface-coupling agent in heat-dissipation material: A non-equilibrium molecular dynamics study’, *Journal of Applied Physics*, vol. 114, no. 19, p. 193512, Nov. 2013, doi: 10.1063/1.4831946.

[161] B. Xu and Q. Zhang, ‘Preparation and Properties of Hydrophobically Modified Nano-SiO2 with Hexadecyltrimethoxysilane’, *ACS Omega*, vol. 6, no. 14, pp. 9764–9770, Apr. 2021, doi: 10.1021/acsomega.1c00381.

[162] W. Li, L. Zhang, M. Zhang, W. Dou, X. Zhang, and S. Chen, ‘The effects of interfacial water and SiO2 surface wettability on the adhesion properties of SiO2 in epoxy nanocomposites’, *Applied Surface Science*, vol. 502, p. 144151, Feb. 2020, doi: 10.1016/j.apsusc.2019.144151.

[163] Y. Yan, Y. Cai, X. Liu, G. Ma, W. Lv, and M. Wang, ‘Hydrophobic Modification on the Surface of SiO2 Nanoparticle: Wettability Control’, *Langmuir*, vol. 36, no. 49, pp. 14924–14932, Dec. 2020, doi: 10.1021/acs.langmuir.0c02118.

[164] J. Hu, Z. Fang, Y. Huang, and J. Lu, ‘Fabrication of superhydrophobic surfaces based on fluorosilane and TiO2/SiO2 nanocomposites’, *Surface Engineering*, vol. 37, no. 3, pp. 271–277, Mar. 2021, doi: 10.1080/02670844.2020.1730059.

[165] T. Misaki, T. Hirohata, M. Yoshii, and T. Hamasaki, ‘Properties of networks obtained by internal plasticization of epoxy resin with aromatic and aliphatic glycidyl compounds’, *Journal of Applied Polymer Science*, vol. 37, no. 9, pp. 2617–2625, 1989, doi: 10.1002/app.1989.070370913.

[166] S. C. Lin and E. M. Pearce, ‘Epoxy resins. II. The preparation, characterization, and curing of epoxy resins and their copolymers’, *Journal of Polymer Science: Polymer Chemistry Edition*, vol. 17, no. 10, pp. 3095–3119, 1979, doi: 10.1002/pol.1979.170171005.

[167] S. C. Lin, B. J. Bulkin, and E. M. Pearce, ‘Epoxy resins. III. Application of fourier transform IR to degradation studies of epoxy systems’, *Journal of Polymer Science: Polymer Chemistry Edition*, vol. 17, no. 10, pp. 3121–3148, 1979, doi: 10.1002/pol.1979.170171006.

[168] C. S. Chen, B. J. Bulkin, and E. M. Pearce, ‘New epoxy resins. II. The preparation, characterization, and curing of epoxy resins and their copolymers’, *Journal of Applied Polymer Science*, vol. 27, no. 9, pp. 3289–3312, 1982, doi: 10.1002/app.1982.070270909.

[169] T.-M. Lee, C.-C. M. Ma, C.-W. Hsu, and H.-L. Wu, ‘Syntheses of epoxy-bridged polyorganosiloxanes and the effects of terminated alkoxysilanes on cured thermal properties’, *Journal of Applied Polymer Science*, vol. 99, no. 6, pp. 3491–3499, 2006, doi: 10.1002/app.22973.

[170] X.-D. Zhao, H. Zhao, and W.-F. Sun, ‘Significantly Improved Electrical Properties of Crosslinked Polyethylene Modified by UV-Initiated Grafting MAH’, *Polymers*, vol. 12, no. 1, p. 62, 2020, doi: 10.3390/polym12010062.

[171] Y. Song, Y. Shen, H. Liu, Y. Lin, M. Li, and C.-W. Nan, ‘Improving the dielectric constants and breakdown strength of polymer composites: effects of the shape of the BaTiO3 nanoinclusions, surface modification and polymer matrix’, *J. Mater. Chem.*, vol. 22, no. 32, pp. 16491–16498, Jul. 2012, doi: 10.1039/C2JM32579A.

[172] F. Fu *et al.*, ‘Preparation of Hydrophobic Low- *k* Epoxy Resins with High Adhesion Using a Benzocyclobutene-Rosin Modifier’, *ACS Sustainable Chem. Eng.*, vol. 11, no. 15, pp. 5973–5985, Apr. 2023, doi: 10.1021/acssuschemeng.2c07698.

[173] Z. Wei *et al.*, ‘Graphene Enhanced Electrical Properties of Polyethylene Blends for High-Voltage Insulation’, *Electronic Materials Letters*, vol. 15, no. 5, pp. 582–594, 2019, doi: 10.1007/s13391-019-00158-3.

[174] S. J. Han, H.-I. Lee, H. M. Jeong, B. K. Kim, A. V. Raghu, and K. R. Reddy, ‘Graphene Modified Lipophilically by Stearic Acid and its Composite With Low Density

Polyethylene', *Journal of Macromolecular Science, Part B*, vol. 53, no. 7, pp. 1193–1204, Jul. 2014, doi: 10.1080/00222348.2013.879804.

[175] B. Li *et al.*, 'A rubber-modified epoxy composite with very high toughness and heat resistance', *Polymers and Polymer Composites*, vol. 27, no. 9, pp. 582–586, 2019, doi: 10.1177/0967391119854649.

[176] Z. Li *et al.*, 'Solution-shearing of dielectric polymer with high thermal conductivity and electric insulation', *Science Advances*, vol. 7, no. 40, p. eabi7410, 2021, doi: 10.1126/sciadv.abi7410.

[177] '2425-79-8 Substance Detail | CAS SciFinder$^n$'. Accessed: Sep. 12, 2022. [Online]. Available: https://scifinder-n.cas.org.remotexs.ntu.edu.sg/searchDetail/substance/631eec38c4e8722cd43c0da3/substanceDetails

[178] 'CAS # 28064-14-4, Phenol polymer with formaldehyde glycidyl ether, Phenol-formaldehyde polymer glycidyl ether, Phenol-formaldehyde polymer oxiranylmethyl ether'. Accessed: Sep. 12, 2022. [Online]. Available: https://www.chemblink.com/products/28064-14-4.htm

[179] '6864-37-5 Substance Detail | CAS SciFinder$^n$'. Accessed: Sep. 12, 2022. [Online]. Available: https://scifinder-n.cas.org.remotexs.ntu.edu.sg/searchDetail/substance/631eed7cc4e8722cd43c2193/substanceDetails

[180] '2855-13-2 Substance Detail | CAS SciFinder$^n$'. Accessed: Sep. 12, 2022. [Online]. Available: https://scifinder-n.cas.org.remotexs.ntu.edu.sg/searchDetail/substance/631eee01c4e8722cd43c2a4a/substanceDetails

[181] '90-72-2 Substance Detail | CAS SciFinder$^n$'. Accessed: Sep. 12, 2022. [Online]. Available: https://scifinder-n.cas.org.remotexs.ntu.edu.sg/searchDetail/substance/631eee4ac4e8722cd43c2f71/substanceDetails

[182] '69-72-7 Substance Detail | CAS SciFinder$^n$'. Accessed: Sep. 12, 2022. [Online]. Available: https://scifinder-

n.cas.org.remotexs.ntu.edu.sg/searchDetail/substance/631eee4dc4e8722cd43c2fc8/substanceDetails

[183] R. Ramsdale-Capper and J. P. Foreman, 'Internal antiplasticisation in highly crosslinked amine cured multifunctional epoxy resins', *Polymer*, vol. 146, pp. 321–330, Jun. 2018, doi: 10.1016/j.polymer.2018.05.048.

[184] M. Ezzahmouly *et al.*, 'Micro-computed tomographic and SEM study of porous bioceramics using an adaptive method based on the mathematical morphological operations', *Heliyon*, vol. 5, no. 12, Dec. 2019, doi: 10.1016/j.heliyon.2019.e02557.

[185] A. Bieberle-Hütter, A. C. Bronneberg, K. George, and M. C. M. van de Sanden, 'Operando attenuated total reflection Fourier-transform infrared (ATR-FTIR) spectroscopy for water splitting', *J. Phys. D: Appl. Phys.*, vol. 54, no. 13, p. 133001, Jan. 2021, doi: 10.1088/1361-6463/abd435.

[186] *Dielectric and resistive properties of solid insulating materials Relative permittivity and dissipation factor. Technical frequencies (0,1 Hz to 10 MHz). AC Methods*, Under Review. 2018.

[187] D09 Committee, 'Test Method for Dielectric Breakdown Voltage and Dielectric Strength of Solid Electrical Insulating Materials at Commercial Power Frequencies', ASTM International. doi: 10.1520/D0149-20.

[188] D20 Committee, 'Test Method for Tensile Properties of Plastics', ASTM International. doi: 10.1520/D0638-14.

[189] Q. Li *et al.*, 'Flexible high-temperature dielectric materials from polymer nanocomposites', *Nature*, vol. 523, no. 7562, pp. 576–579, 2015, doi: 10.1038/nature14647.

[190] D. Q. Tan, 'Review of Polymer-Based Nanodielectric Exploration and Film Scale-Up for Advanced Capacitors', *Adv. Funct. Mater.*, vol. 30, no. 18, p. 1808567, May 2020, doi: 10.1002/adfm.201808567.

[191] X. Huang, B. Sun, Y. Zhu, S. Li, and P. Jiang, 'High-k polymer nanocomposites with 1D filler for dielectric and energy storage applications', *Progress in Materials Science*, vol. 100, pp. 187–225, Feb. 2019, doi: 10.1016/j.pmatsci.2018.10.003.

[192] Y. Wang *et al.*, 'Gradient-layered polymer nanocomposites with significantly improved insulation performance for dielectric energy storage', *Energy Storage Materials*, vol. 24, pp. 626–634, 2020, doi: 10.1016/j.ensm.2019.06.013.

[193] X. Huang and P. Jiang, 'Core–Shell Structured High-k Polymer Nanocomposites for Energy Storage and Dielectric Applications', *Advanced Materials*, vol. 27, no. 3, pp. 546–554, 2015, doi: 10.1002/adma.201401310.

[194] Y. Liu *et al.*, 'D−π−A Strategy to boost dielectric breakdown strength of polyimide insulation', *Polymer Degradation and Stability*, vol. 209, p. 110264, Mar. 2023, doi: 10.1016/j.polymdegradstab.2023.110264.

[195] W. Bian, T. Yao, M. Chen, C. Zhang, T. Shao, and Y. Yang, 'The synergistic effects of the micro-BN and nano-Al2O3 in micro-nano composites on enhancing the thermal conductivity for insulating epoxy resin', *Composites Science and Technology*, vol. 168, pp. 420–428, 2018, doi: 10.1016/j.compscitech.2018.10.002.

[196] J. Jiao, P. Liu, L. Wang, and Y. Cai, 'One-step synthesis of improved silica/epoxy nanocomposites with inorganic-organic hybrid network', *J Polym Res*, vol. 20, no. 8, pp. 1–8, Aug. 2013, doi: 10.1007/s10965-013-0202-9.

[197] L. Zhao *et al.*, 'Synchronously improved thermal conductivity and dielectric constant for epoxy composites by introducing functionalized silicon carbide nanoparticles and boron nitride microspheres', *Journal of Colloid and Interface Science*, vol. 627, pp. 205–214, Dec. 2022, doi: 10.1016/j.jcis.2022.07.058.

[198] J.-P. Chen *et al.*, 'SiC whiskers nucleated on rGO and its potential role in thermal conductivity and electronic insulation', *Chemical Engineering Journal*, vol. 423, 2021, doi: 10.1016/j.cej.2021.130181.

[199] Y. Ouyang, L. Bai, H. Tian, X. Li, and F. Yuan, 'Recent progress of thermal conductive ploymer composites: Al2O3 fillers, properties and applications', *Composites Part A: Applied Science and Manufacturing*, vol. 152, 2022, doi: 10.1016/j.compositesa.2021.106685.

[200] G. Yang *et al.*, 'Highly thermally conductive, electrically insulating, thermal resistance polyimide-base composites with fibrillated carbon networks for thermal management applications', *Composites Communications*, vol. 37, p. 101450, Jan. 2023, doi: 10.1016/j.coco.2022.101450.

[201] M. Hao *et al.*, 'Thermal conductivity enhancement of carbon fiber/epoxy composites via constructing three-dimensionally aligned hybrid thermal conductive structures on fiber surfaces', *Composites Science and Technology*, vol. 231, p. 109800, Jan. 2023, doi: 10.1016/j.compscitech.2022.109800.

[202] Y. Ni, T. T. Bisel, M. P. Spencer, W. K. Fuchs, M. Reddy Pallaka, and L. S. Fifield, 'Color Change During Thermal Degradation of Polyolefin Electric Cable Insulations', in *2021 IEEE Conference on Electrical Insulation and Dielectric Phenomena (CEIDP)*, Dec. 2021, pp. 129–132. doi: 10.1109/CEIDP50766.2021.9705427.

[203] Y. Ni, A. Sriraman, D. Li, I. Ellis, and L. S. Fifield, 'Investigation of Inverse Temperature Effects During Thermal-Radiation Aging of Semicrystalline Cable Insulation', in *2022 IEEE Conference on Electrical Insulation and Dielectric Phenomena (CEIDP)*, Oct. 2022, pp. 368–371. doi: 10.1109/CEIDP55452.2022.9985318.

[204] S. R. Mousavi *et al.*, 'A review of recent progress in improving the fracture toughness of epoxy-based composites using carbonaceous nanofillers', *Polymer Composites*, vol. 43, no. 4, pp. 1871–1886, 2022, doi: 10.1002/pc.26518.

[205] J. Yang, H. Wang, X. Liu, S. Fu, and P. Song, 'A nano-TiO2/regenerated cellulose biohybrid enables simultaneously improved strength and toughness of solid epoxy resins', *Composites Science and Technology*, vol. 212, p. 108884, Aug. 2021, doi: 10.1016/j.compscitech.2021.108884.

[206] J. Yi *et al.*, 'Improved tribological and thermo-mechanical properties of epoxy resin with micro-nano structured ZrO2/Ti3C2 particles', *Journal of Applied Polymer Science*, vol. 138, no. 41, p. 51209, 2021, doi: 10.1002/app.51209.

[207] S.-H. Kim, S.-J. Park, S.-Y. Lee, and S.-J. Park, 'Amine functionalization on thermal and mechanical behaviors of graphite nanofibers-loaded epoxy composites', *Journal of Materials Science & Technology*, vol. 151, pp. 80–88, Jul. 2023, doi: 10.1016/j.jmst.2022.12.038.

[208] P. Wang, H. Lei, X. Zhu, H. Chen, and D. Fang, 'Investigation on the mechanical properties of epoxy resin with void defects using digital image correlation and image-based finite element method', *Polymer Testing*, vol. 72, pp. 223–231, Dec. 2018, doi: 10.1016/j.polymertesting.2018.10.025.

[209] L. Di Landro, A. Montalto, P. Bettini, S. Guerra, F. Montagnoli, and M. Rigamonti, 'Detection of Voids in Carbon/Epoxy Laminates and Their Influence on Mechanical Properties', *Polymers and Polymer Composites*, vol. 25, no. 5, pp. 371–380, 2017, doi: 10.1177/096739111702500506.

[210] C. H. Park, A. Lebel, A. Saouab, J. Bréard, and W. I. Lee, 'Modeling and simulation of voids and saturation in liquid composite molding processes', *Composites Part A: Applied Science and Manufacturing*, vol. 42, no. 6, pp. 658–668, Jun. 2011, doi: 10.1016/j.compositesa.2011.02.005.

[211] J. Wood and M. Bader, 'Modelling the behaviour of gas bubbles in an epoxy resin: Evaluating the input parameters for a diffusion model using a free-volume approach', *Journal of Materials Science*, vol. 30, pp. 916–922, Feb. 1995, doi: 10.1007/BF01178425.

[212] Y.-B. Yin, Q.-S. Yang, S.-L. Wang, H.-D. Gao, Y.-W. He, and X.-L. Li, 'Formation of CO2 bubbles in epoxy resin coatings: A DFT study', *J Mol Graph Model*, vol. 86, pp. 192–198, Jan. 2019, doi: 10.1016/j.jmgm.2018.10.018.

[213] D. Saenz-Castillo, M. I. Martín, S. Calvo, F. Rodriguez-Lence, and A. Güemes, 'Effect of processing parameters and void content on mechanical properties and NDI of thermoplastic composites', *Composites Part A: Applied Science and Manufacturing*, vol. 121, pp. 308–320, Jun. 2019, doi: 10.1016/j.compositesa.2019.03.035.

[214] G. H. Michler and H.-H. K.-B. von Schmeling, 'The physics and micro-mechanics of nano-voids and nano-particles in polymer combinations', *Polymer*, vol. 54, no. 13, pp. 3131–3144, Jun. 2013, doi: 10.1016/j.polymer.2013.03.035.

[215] R. Protz, N. Kosmann, M. Gude, W. Hufenbach, K. Schulte, and B. Fiedler, 'Voids and their effect on the strain rate dependent material properties and fatigue behaviour of non-crimp fabric composites materials', *Composites Part B: Engineering*, vol. 83, pp. 346–351, Dec. 2015, doi: 10.1016/j.compositesb.2015.08.018.

[216] G. A. George, P. Cole-Clarke, N. St. John, and G. Friend, 'Real-time monitoring of the cure reaction of a TGDDM/DDS epoxy resin using fiber optic FT-IR', *Journal of Applied Polymer Science*, vol. 42, no. 3, pp. 643–657, 1991, doi: 10.1002/app.1991.070420310.

[217] B. Mailhot, S. Morlat-Thérias, M. Ouahioune, and J.-L. Gardette, 'Study of the Degradation of an Epoxy/Amine Resin, 1', *Macromolecular Chemistry and Physics*, vol. 206, no. 5, pp. 575–584, 2005, doi: 10.1002/macp.200400395.

[218] X. Huang, P. Jiang, and T. Tanaka, 'A review of dielectric polymer composites with high thermal conductivity', *IEEE Electr. Insul. Mag.*, vol. 27, no. 4, pp. 8–16, 2011, doi: 10.1109/MEI.2011.5954064.

[219] Q. Wang, Y. Yang, M. Yap, W. K. Chern, and Z. Chen, 'Simulating dielectric breakdown based on Maxwell's equations with inhomogeneous conductivity', in *2022 IEEE Conference on Electrical Insulation and Dielectric Phenomena (CEIDP)*, Oct. 2022, pp. 115–118. doi: 10.1109/CEIDP55452.2022.9985246.

[220] T. Zhang *et al.*, 'Recent progress in polymer dielectric energy storage: From film fabrication and modification to capacitor performance and application', *Progress in Materials Science*, vol. 140, p. 101207, Dec. 2023, doi: 10.1016/j.pmatsci.2023.101207.

[221] J. Zhou *et al.*, 'Recent advances in dispersion and alignment of fillers in PVDF-based composites for high-performance dielectric energy storage', *Materials Today Energy*, vol. 31, p. 101208, Jan. 2023, doi: 10.1016/j.mtener.2022.101208.

[222] L. Zeng, X. Liu, X. Chen, and C. Soutis, 'π - π interaction between carbon fibre and epoxy resin for interface improvement in composites', *Composites Part B: Engineering*, vol. 220, p. 108983, Sep. 2021, doi: 10.1016/j.compositesb.2021.108983.

[223] Z. Sun *et al.*, 'Nanocomposites for future electronics device Packaging: A fundamental study of interfacial connecting mechanisms and optimal conditions of silane coupling agents for Polydopamine-Graphene fillers in epoxy polymers', *Chemical Engineering Journal*, vol. 439, p. 135621, Jul. 2022, doi: 10.1016/j.cej.2022.135621.

[224] S. Mandal, Y. Hou, M. Wang, T. D. Anthopoulos, and K. L. Choy, 'Surface Modification of Hetero-phase Nanoparticles for Low-Cost Solution-Processable High-k Dielectric Polymer Nanocomposites', *ACS Appl. Mater. Interfaces*, vol. 15, no. 5, pp. 7371–7379, Feb. 2023, doi: 10.1021/acsami.2c19559.

[225] H.-A. Cha *et al.*, 'Nanocrystalline Composite Layer Realized by Simple Sintering Without Surface Treatment, Reducing Hydrophilicity and Increasing Thermal Conductivity', *Small Methods*, vol. 8, no. 7, p. 2300969, 2024, doi: 10.1002/smtd.202300969.

[226] B. J. Ryan and K. M. Poduska, ‘Roughness effects on contact angle measurements’, *American Journal of Physics*, vol. 76, no. 11, pp. 1074–1077, Nov. 2008, doi: 10.1119/1.2952446.

[227] Y. Rabbani, H. Shayesteh, N. Haghshenas, and M. Safarzadeh Khosrowshahi, ‘Investigation of grafting silane coupling agents on superhydrophobicity of carbonyl iron/SiO2 particles for efficient oil/water mixture and emulsion separation’, *Sci Rep*, vol. 13, no. 1, p. 788, Jan. 2023, doi: 10.1038/s41598-023-28131-z.

[228] Q. Fu *et al.*, ‘Development of Sol–Gel Icephobic Coatings: Effect of Surface Roughness and Surface Energy’, *ACS Appl. Mater. Interfaces*, vol. 6, no. 23, pp. 20685–20692, Dec. 2014, doi: 10.1021/am504348x.

[229] H. Liu, Y. Wang, J. Huang, Z. Chen, G. Chen, and Y. Lai, ‘Bioinspired Surfaces with Superamphiphobic Properties: Concepts, Synthesis, and Applications’, *Adv Funct Materials*, vol. 28, no. 19, p. 1707415, May 2018, doi: 10.1002/adfm.201707415.

[230] M. Harsch, J. Karger-Kocsis, and M. Holst, ‘Influence of fillers and additives on the cure kinetics of an epoxy/anhydride resin’, *European Polymer Journal*, vol. 43, no. 4, pp. 1168–1178, Apr. 2007, doi: 10.1016/j.eurpolymj.2007.01.025.

[231] Y. Yang *et al.*, ‘Electrical Properties of Epoxy Resin after Thermal Aging under High Humidity’, in *2022 IEEE Conference on Electrical Insulation and Dielectric Phenomena (CEIDP)*, Oct. 2022, pp. 171–174. doi: 10.1109/CEIDP55452.2022.9985334.

[232] Y. Deng, Q. Wang, J. Ma, J. T. Oh, and Z. Chen, ‘The combined impact of voids and thermal aging on the mechanical reliability of epoxy resin evaluated by statistical analysis’, *Polymer Degradation and Stability*, vol. 215, p. 110455, Sep. 2023, doi: 10.1016/j.polymdegradstab.2023.110455.

[233] Y. Deng *et al.*, ‘The Impact of Thermal Aging on Mechanical and Electrical Properties of Epoxy/Amine Resin’, in *2023 International Symposium on Electrical Insulating Materials (ISEIM)*, Sep. 2023, pp. 1–4. doi: 10.23919/ISEIM60444.2023.10329098.

[234] T. Cui, P. Verberne, and S. A. Meguid, ‘Characterization and atomistic modeling of the effect of water absorption on the mechanical properties of thermoset polymers’, *Acta Mech*, vol. 229, no. 2, pp. 745–761, Feb. 2018, doi: 10.1007/s00707-017-1997-y.

[235] D. Qiang, G. Chen, and T. Andritsch, ‘Influence of water absorption on dielectric properties of epoxy SiO2 and BN nanocomposites’, in *2015 IEEE Conference on Electrical Insulation and Dielectric Phenomena (CEIDP)*, Oct. 2015, pp. 439–442. doi: 10.1109/CEIDP.2015.7352130.

[236] L. Hui, L. S. Schadler, and J. K. Nelson, ‘The influence of moisture on the electrical properties of crosslinked polyethylene/silica nanocomposites’, *IEEE Transactions on Dielectrics and Electrical Insulation*, vol. 20, no. 2, pp. 641–653, Apr. 2013, doi: 10.1109/TDEI.2013.6508768.

[237] Q. Wang *et al.*, ‘Electrical tree modelling in dielectric polymers using a phase-field regularized cohesive zone model’, *Materials & Design*, vol. 235, p. 112409, Nov. 2023, doi: 10.1016/j.matdes.2023.112409.

[238] Q. Wang *et al.*, ‘Modeling the Dielectric Breakdown of Nanocomposites Using a Novel Phase-Field Model’, in *2023 International Symposium on Electrical Insulating Materials (ISEIM)*, Sep. 2023, pp. 01–04. doi: 10.23919/ISEIM60444.2023.10329100.

[239] M. Cotinaud, P. Bonniau, and A. R. Bunsell, ‘The effect of water absorption on the electrical properties of glass-fibre reinforced epoxy composites’, *J Mater Sci*, vol. 17, no. 3, pp. 867–877, Mar. 1982, doi: 10.1007/BF00540386.

[240] X. Xia, Y. Wang, Z. Zhong, and G. J. Weng, ‘A frequency-dependent theory of electrical conductivity and dielectric permittivity for graphene-polymer nanocomposites’, *Carbon*, vol. 111, pp. 221–230, Jan. 2017, doi: 10.1016/j.carbon.2016.09.078.

[241] F. He, S. Lau, H. L. Chan, and J. Fan, ‘High Dielectric Permittivity and Low Percolation Threshold in Nanocomposites Based on Poly(vinylidene fluoride) and Exfoliated Graphite Nanoplates’, *Advanced Materials*, vol. 21, no. 6, pp. 710–715, Feb. 2009, doi: 10.1002/adma.200801758.

[242] N. Song *et al.*, ‘Decreasing the dielectric constant and water uptake of co-polyimide films by introducing hydrophobic cross-linked networks’, *European Polymer Journal*, vol. 101, pp. 105–112, Apr. 2018, doi: 10.1016/j.eurpolymj.2018.02.024.

[243] D. B. Singh, A. Kumar, V. P. Tayal, and B. Sanyal, ‘Dielectric behaviour of epoxy and polyester laminates in moisture and electronic packaging exhalates’, *J Mater Sci*, vol. 23, no. 2, pp. 528–534, Feb. 1988, doi: 10.1007/BF01174680.

[244] M. Urbakh and J. Klafter, ‘Boundary Effects on Dipole-Dipole Interactions and Molecular Relaxation’, in *Disorder Effects on Relaxational Processes: Glasses, Polymers, Proteins*, R. Richert and A. Blumen, Eds., Berlin, Heidelberg: Springer, 1994, pp. 279–305. doi: 10.1007/978-3-642-78576-4_9.

[245] H. Suzuki, H. Shimakawa, A. Kumada, and M. Sato, ‘Molecular Dynamics Study of Ionic Conduction in Epoxy Resin’, *IEEE Transactions on Dielectrics and Electrical Insulation*, vol. 29, no. 1, pp. 170–177, Feb. 2022, doi: 10.1109/TDEI.2022.3148462.

[246] J. C. Capricho, B. Fox, and N. Hameed, ‘Multifunctionality in Epoxy Resins’, *Polymer Reviews*, vol. 60, no. 1, pp. 1–41, Jan. 2020, doi: 10.1080/15583724.2019.1650063.

[247] N. R. Paluvai, S. Mohanty, and S. K. Nayak, ‘Synthesis and Modifications of Epoxy Resins and Their Composites: A Review’, *Polymer-Plastics Technology and Engineering*, vol. 53, no. 16, pp. 1723–1758, Nov. 2014, doi: 10.1080/03602559.2014.919658.

[248] X.-D. Zhao, W.-F. Sun, and H. Zhao, ‘Enhanced Insulation Performances of Crosslinked Polyethylene Modified by Chemically Grafting Chloroacetic Acid Allyl Ester’, *Polymers*, vol. 11, no. 4, p. 592, 2019, doi: 10.3390/polym11040592.

[249] *Plastics. Epoxy resins. Determination of degree of crosslinking of crosslinked epoxy resins by differential scanning calorimetry (DSC)*, Confirmed. 2018.

[250] T. H. Ha, J. Y. Jang, Y. B. Cho, H. M. Jeong, and B. K. Kim, ‘Maleic anhydride grafted polyethylene powder coated with epoxy resin: A novel reactive hot melt adhesive’, *Journal of Applied Polymer Science*, vol. 116, no. 1, pp. 328–332, 2010, doi: 10.1002/app.31576.

[251] R. A. Nyquist, Ed., ‘Chapter 4 - Alkenes and Other Compounds Containing C=C Double Bonds’, in *Interpreting Infrared, Raman, and Nuclear Magnetic Resonance Spectra*, San Diego: Academic Press, 2001, pp. 55–91. doi: 10.1016/B978-012523475-7/50168-6.

[252] G. Nikolic, S. Zlatkovic, M. Cakic, S. Cakic, C. Lacnjevac, and Z. Rajic, ‘Fast Fourier transform IR characterization of epoxy GY systems crosslinked with aliphatic and cycloaliphatic EH polyamine adducts’, *Sensors (Basel)*, vol. 10, no. 1, pp. 684–696, 2010, doi: 10.3390/s100100684.

[253] M. Zahidul Islam, Y. Fu, H. Deb, M. Khalid Hasan, Y. Dong, and S. Shi, 'Polymer-based low dielectric constant and loss materials for high-speed communication network: Dielectric constants and challenges', *European Polymer Journal*, vol. 200, p. 112543, Nov. 2023, doi: 10.1016/j.eurpolymj.2023.112543.

[254] H. Sun *et al.*, 'Materials with low dielectric constant and loss and good thermal properties prepared by introducing perfluorononenyl pendant groups onto poly(ether ether ketone)', *RSC Adv.*, vol. 8, no. 14, pp. 7753–7760, Feb. 2018, doi: 10.1039/C7RA13600E.

[255] S. Hu *et al.*, 'Dielectric Properties Improvement of Grafting-Modified Polypropylene by Silane for HVDC Cable Insulation', *IEEE Transactions on Dielectrics and Electrical Insulation*, vol. 28, no. 6, pp. 2004–2010, Dec. 2021, doi: 10.1109/TDEI.2021.009776.

[256] C. Zhang, J. Chang, H. Zhang, C. Li, and H. Zhao, 'Improved Direct Current Electrical Properties of Crosslinked Polyethylene Modified with the Polar Group Compound', *Polymers*, vol. 11, no. 10, Art. no. 10, Oct. 2019, doi: 10.3390/polym11101624.

[257] C. Wang, H. Zhang, Y. Wang, C. Chen, Z. Zhang, and Y. Wang, 'Effect of Hardener Stoichiometry on the Dielectric Properties of Epoxy Resin/Liquid Nitrile Rubber Composite Materials', *IEEE Transactions on Dielectrics and Electrical Insulation*, vol. 30, no. 3, pp. 1178–1187, Jun. 2023, doi: 10.1109/TDEI.2022.3232586.

[258] R. F. Minty, L. Yang, and J. L. Thomason, 'The influence of hardener-to-epoxy ratio on the interfacial strength in glass fibre reinforced epoxy composites', *Composites Part A: Applied Science and Manufacturing*, vol. 112, pp. 64–70, Sep. 2018, doi: 10.1016/j.compositesa.2018.05.033.

[259] C. Yuan *et al.*, 'Improved High-Temperature Electrical Properties of Polymeric Material by Grafting Modification', *ACS Sustainable Chem. Eng.*, vol. 10, no. 27, pp. 8685–8693, Jul. 2022, doi: 10.1021/acssuschemeng.1c08417.

[260] J.-G. Gao, L.-W. Liu, and W.-F. Sun, 'Dielectric Characteristics of Crosslinked Polyethylene Modified by Grafting Polar-Group Molecules', *Polymers*, vol. 15, no. 1, Art. no. 1, Jan. 2023, doi: 10.3390/polym15010231.

[261] H. Lei *et al.*, 'Ester Bond: Chemically Labile Yet Mechanically Stable', *ACS Nano*, vol. 17, no. 17, pp. 16870–16878, Sep. 2023, doi: 10.1021/acsnano.3c03807.

[262] M. A. Sharaf and J. E. Mark, ‘The Effects of Cross-Linking and Strain on the Glass Transition Temperature of a Polymer Network’, *Rubber Chemistry and Technology*, vol. 53, no. 4, pp. 982–987, Sep. 1980, doi: 10.5254/1.3535073.

[263] K. O’Driscoll and R. A. Sanayei, ‘Chain-length dependence of the glass transition temperature’, *Macromolecules*, vol. 24, no. 15, pp. 4479–4480, Jul. 1991, doi: 10.1021/ma00015a038.

[264] C. Zhang *et al.*, ‘Renewable Castor-Oil-based Waterborne Polyurethane Networks: Simultaneously Showing High Strength, Self-Healing, Processability and Tunable Multishape Memory’, *Angewandte Chemie International Edition*, vol. 60, no. 8, pp. 4289–4299, 2021, doi: 10.1002/anie.202014299.

[265] F. Dong *et al.*, ‘Self-healing polyurethane with high strength and toughness based on a dynamic chemical strategy’, *J. Mater. Chem. A*, vol. 10, no. 18, pp. 10139–10149, May 2022, doi: 10.1039/D2TA00802E.

[266] O. Teschke, G. Ceotto, and E. F. de Souza, ‘Dielectric exchange force: a convenient technique for measuring the interfacial water relative permittivity profile’, *Phys. Chem. Chem. Phys.*, vol. 3, no. 17, pp. 3761–3768, Jan. 2001, doi: 10.1039/B009744F.

[267] M. Jia, Y. Li, C. He, and X. Huang, ‘Soluble Perfluorocyclobutyl Aryl Ether-Based Polyimide for High-Performance Dielectric Material’, *ACS Appl. Mater. Interfaces*, vol. 8, no. 39, pp. 26352–26358, Oct. 2016, doi: 10.1021/acsami.6b09383.

[268] W. Sima *et al.*, ‘Novel Smart Insulating Materials Achieving Targeting Self-Healing of Electrical Trees: High Performance, Low Cost, and Eco-Friendliness’, *ACS Applied Materials & Interfaces*, vol. 13, no. 28, pp. 33485–33495, 2021, doi: 10.1021/acsami.1c07469.

[269] Z. Wang *et al.*, ‘Simultaneously enhanced dielectric properties and through-plane thermal conductivity of epoxy composites with alumina and boron nitride nanosheets’, *Sci Rep*, vol. 11, no. 1, Art. no. 1, Jan. 2021, doi: 10.1038/s41598-021-81925-x.

[270] H. Ruan *et al.*, ‘Enhanced Breakdown Strength of BN/ER by the 2D Ordinal Tiled Structure of Fillers’, *IEEE Trans. Dielect. Electr. Insul.*, vol. 28, no. 2, pp. 423–430, Apr. 2021, doi: 10.1109/TDEI.2020.009184.